



173(2), 2018



**COMBUSTION ENGINES**



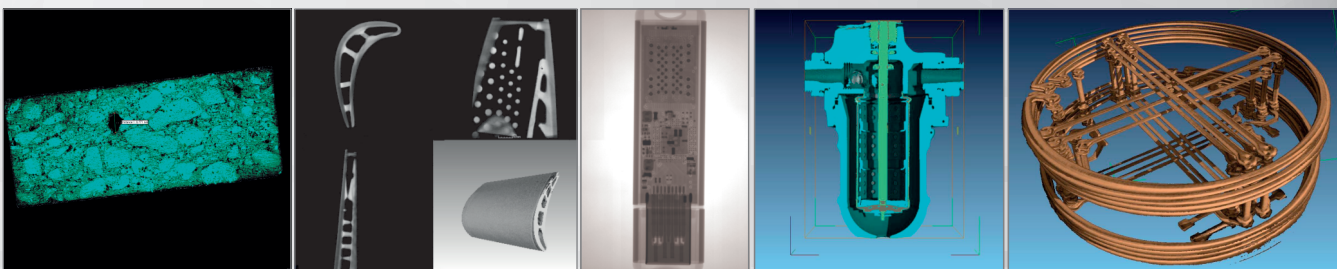


## INSTYTUT TECHNICZNY WOJSK LOTNICZYCH

ul. Księcia Bolesława 6, 01-494 Warszawa, skr. poczt. 96  
tel.: 261 851 300; tel./faks: 261 851 313  
www.itwl.pl e-mail: poczta@itwl.pl

### Tomograf komputerowy (CT) – badanie nieniszczące NDT

Instytut Techniczny Wojsk Lotniczych oferuje usługi z zakresu badań tomografem komputerowym. Badania prowadzone są na tomografie typu v/tome/x m 300 firmy GE o max. mocy lampy 300kV/500W. Urządzenie posiada również lampę do nanotomografii o mocy 80kV/15W.

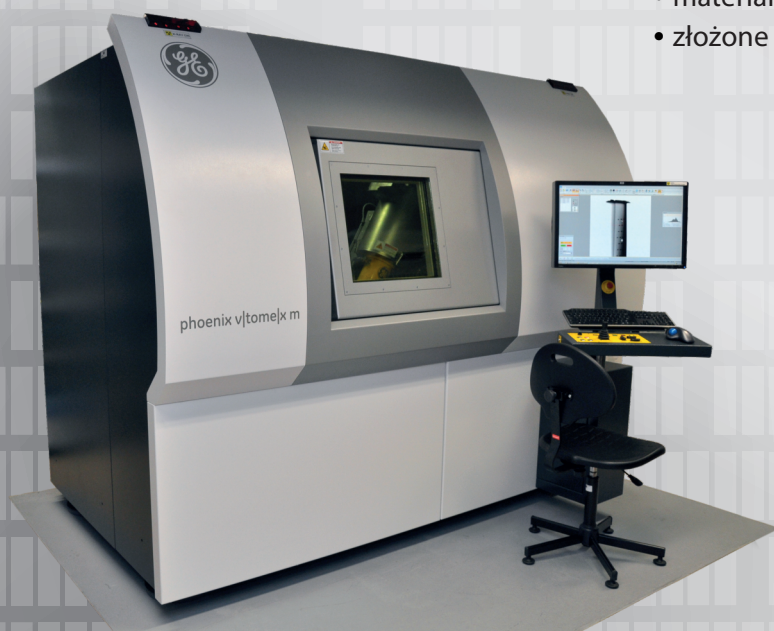


Prowadzimy prace badawcze obejmujące swym zakresem materiały takie jak:

- stopy tytanu
- stale
- materiały kompozytowe
- beton
- guma

Urządzenie umożliwia prowadzenie badań z zakresu:

- wykrywania defektów o rozmiarach powyżej  $0,5 \mu\text{m}$  z wykorzystaniem lampy 180kV
- materiałów o bardzo dużej gęstości (np. łopatki turbin silników lotniczych) z wykorzystaniem lampy o mocy 300 kV
- układy elektroniczne (scalone)
- materiały pirotechniczne
- złożone agregaty lotnicze



Masa badanych elementów do 50 kg.  
Wymiary orientacyjne 50×50×60 cm.

Posiadamy wysoko wykwalifikowany,  
certyfikowany personel.

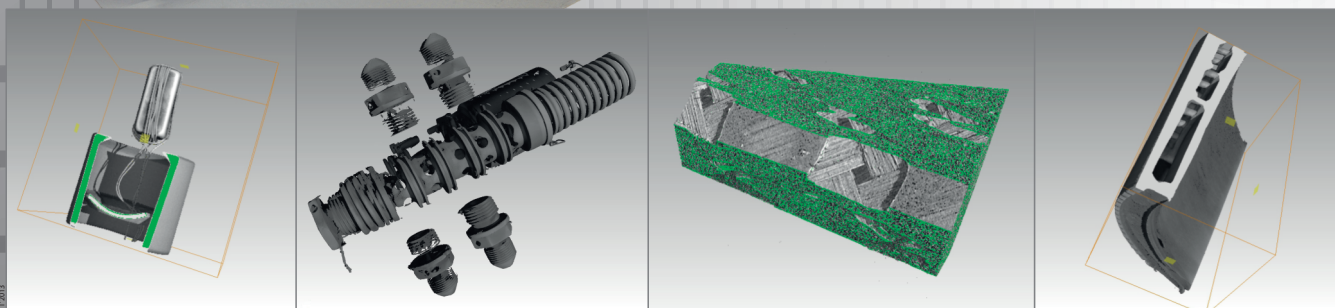
Kontakt bezpośredni:

**Zakład Silników Lotniczych**

tel.: +48 261 851 334; fax: +48 261 851 338

e-mail: jaroslaw.spychala@itwl.pl

***Zapraszamy do współpracy!***



## PTNSS Supporting Members Członkowie wspierający PTNSS

**BOSMAL Automotive Research and Development  
Institute Ltd**

Instytut Badań i Rozwoju  
Motoryzacji BOSMAL Sp. z o.o

**Motor Transport Institute**

Instytut Transportu Samochodowego

**The Institute for Sustainable Technologies**

Instytut Technologii Eksploatacji

**Institute of Aviation**

Instytut Lotnictwa

**Automotive Industry Institute**

Przemysłowy Instytut Motoryzacji

**The Rail Vehicles Institute TABOR**

Instytut Pojazdów Szynowych TABOR

**Institute of Mechanised**

**Construction and Rock Mining**

Instytut Mechanizacji Budownictwa  
i Górnictwa Skalnego

**Institute of Logistics and Warehousing**

Instytut Logistyki i Magazynowania

**Industrial Institute of Agricultural Engineering**

Przemysłowy Instytut Maszyn Rolniczych

**AVL List GmbH**

**Solaris Bus & Coach S.A.**

**Air Force Institute of Technology**

Instytut Techniczny Wojsk Lotniczych



## COMBUSTION ENGINES

A Scientific Magazine

2018, 173(2)

Year LVII

PL ISSN 2300-9896

Editor:

**Polskie Towarzystwo Naukowe Silników Spalinowych**

43-300 Bielsko-Biała, Sarni Stok 93 Street, Poland

tel.: +48 33 8130402, fax: +48 33 8125038

E-mail: [sekretariat@ptnss.pl](mailto:sekretariat@ptnss.pl)

WebSite: <http://www.ptnss.pl>

Papers available on-line: <http://combustion-engines.eu>

### Scientific Board:

Prof. Krzysztof Wisłocki – Chairman, Poland

Prof. Ewa Bardasz – USA

Prof. Bernard Challen – UK

Prof. Zdzisław Chłopek – Poland

Prof. Giovanni Cipolla – Italy

Prof. Jan Czerwiński – Switzerland

Prof. Vladimír Hlavna – Slovakia

Prof. Kazimierz Lejda – Poland

Prof. Hans Peter Lenz – Austria

Prof. Helmut List – Austria

Prof. Jan Macek – Czech Republic

Prof. Elena R. Magaril – Russia

Prof. Janusz Mysłowski – Poland

Prof. Andrzej Niewczas – Poland

Prof. Marek Orkisz – Poland

Prof. Dieter Peitsch – Germany

Prof. Stefan Pischinger – Germany

Prof. Roger Sierens – Belgium

Prof. Andrzej Sobiesiak – Canada

Prof. Richard Stobart – UK

Prof. Robin Vanhaelst – Germany

Prof. Michael P. Walsh – USA

Prof. Piotr Wolański – Poland

Prof. Mirosław Wyszynski – UK

### Editorial:

Institute of Combustion Engines and Transport

Poznań University of Technology

60-965 Poznań, Piotrowo 3 Street

tel.: +48 61 2244505, +48 61 2244502

E-mail: [papers@ptnss.pl](mailto:papers@ptnss.pl)

Prof. Jerzy Merksiz, DSc., DEng. (Editor-in-chief)

Miłosław Kozak, DSc., DEng. (Editorial Secretary for Science)

– [papers@ptnss.pl](mailto:papers@ptnss.pl)

Prof. Ireneusz Pielecha, DSc., DEng. (Technical Editor)

Krystyna Bubacz, MSc. (Proofreading Editor)

Wojciech Serdecki, DSc., DEng. (Statistical Editor)

and Associate Editors

# Contents

<i>Karczewski M., Koliński K.</i> Diagnostics of common rail components based on pressure curves in the fuel rail (CE-2018-201).....	3
<i>Krzesicki M., Boruc Ł., Kapusta Ł.J.</i> Evaluation of the possibilities of adapting a constant volume combustion chamber for research on ignition of hypergolic propellants under low and high-pressure conditions (CE-2018-202).....	9
<i>Pielecha I., Cieślik W., Fluder K.</i> Analysis of energy management strategies for hybrid electric vehicles in urban driving conditions (CE-2018-203).....	14
<i>Sidorowicz M., Pielecha I.</i> The injector location impact on the fuel combustion process in a direct gasoline injection system (CE-2018-204).....	19
<i>Chachurski R., Trzeciak A., Jędrówiak B.</i> Comparison of the results of mathematical modeling of a GTM 120 miniature turbine jet engine with the research results (CE-2018-205).....	30
<i>Wolak A., Zajac G., Żółty M.</i> Changes of properties of engine oils diluted with diesel oil under real operating conditions (CE-2018-206).....	34
<i>Szymlet N., Rymaniak Ł., Lijewski P., Sokolnicka B., Siedlecki M.</i> Research and analysis of harmful road emission from a two-wheel vehicle engine in laboratory conditions (CE-2018-207).....	41
<i>Fiedkiewicz Ł., Pielecha I.</i> Optical analysis of the gas flame development in a RCM using a high-power ignition system (CE-2018-208).....	47
<i>Pawlak M., Majka A., Kuźniar M., Pawluczy J.</i> Analysis of wind impact on emission of selected exhaust compounds in jet engines of a business jet aircraft in cruise phase (CE-2018-209).....	55
<i>Sroka Z.J., Walkowiak W., Reksa M., Kolanek C., Pillai C.T.</i> Solving the problem of air quality in Indian cities by retrofitting the EGR (CE-2018-210).....	61
<i>Pawlak M., Majka A., Kuźniar M., Pawluczy J.</i> Emission of selected exhaust compounds in jet engines of a jet aircraft in cruise phase (CE-2018-211) .....	67

Papers published in the  
**Combustion Engines**  
quarterly receive 13 points as stated  
by the Notification of the Minister of Science  
and Higher Education dated 31 December 2015.

**Editor**  
**Polish Scientific Society  
of Combustion Engines**  
43-300 Bielsko-Biala, Sarni Stok 93 Street, Poland  
tel.: +48 33 8130402, fax: +48 33 8125038  
E-mail: [sekretariat@ptnss.pl](mailto:sekretariat@ptnss.pl)  
WebSite: <http://www.ptnss.pl>

The Publisher of this magazine does not endorse the products or services advertised herein. The published materials do not necessarily reflect the views and opinions of the Publisher.

© Copyright by  
**Polish Scientific Society of Combustion Engines**  
All rights reserved.  
No part of this publication may be reproduced, stored in a retrieval system or transmitted, photocopied or otherwise without prior consent of the copyright holder.

**Subscriptions**  
Send subscription requests to the Publisher's address.  
Cost of a single issue PLZ30 + VAT.  
**Preparation for print**  
ARS NOVA Publishing House  
60-782 Poznań, ul. Grunwaldzka 17/10A  
**Circulation: 700 copies**  
**Printing and binding**  
Zakład Poligraficzny Moś i Łuczak, sp. j., Poznań, ul. Piwna 1

The journal is registered  
in the Polish technical  
journals content database  
– **BAZTECH** [www.baztech.icm.edu.pl](http://www.baztech.icm.edu.pl)



The journal is listed  
in the international database  
**IC Journal Master List**  
– **Index Copernicus** [www.indexcopernicus.com](http://www.indexcopernicus.com)



Declaration of the original version  
*The original version of the Combustion Engines journal  
is the printed version.*

**Cover**  
I – Mercedes-AMG C 63, 4,0-liter V8-biturbo engine  
(*for media.daimler.com*); background (Drawing modern electronic circuit  
© Marisha – Fotolia.com)  
IV – Cylinder cutoff, 4-cylinder-gasoline engine, A-Class  
(*for media.daimler.com*)



## Diagnostics of common rail components based on pressure curves in the fuel rail

Majority of modern diesel engines is fitted with common-rail (CR) fuel systems. In these systems, the injectors are supplied with fuel under high pressure from the fuel rail (accumulator). Dynamic changes of pressure in the fuel rail are caused by the phenomena occurring during the fuel injection into the cylinders and the fuel supply to the fuel rail through the high-pressure fuel pump. Any change in this process results in a change in the course of pressure in the fuel rail, which, upon mathematical processing of the fuel pressure signal, allows identification of the malfunction of the pump and the injectors. The paper presents a methodology of diagnosing of CR fuel injection system components based on the analysis of dynamic pressure changes in the fuel rail. In the performed investigations, the authors utilized LabView software and a  $\mu$ DAC data acquisition module recording the fuel pressure in the rail, the fuel injector control current and the signal from the camshaft position sensor. For the analysis of the obtained results, 'FFT' and 'STFT' were developed in order to detect inoperative injectors based on the curves of pressure in the fuel rail. The performed validation tests have confirmed the possibility of identification of malfunctions in the CR system based on the pressure curves in the fuel rail. The 'FFT' method provides more information related to the system itself and accurately shows the structure of the signal, while the 'STFT' method presents the signal in such a way as to clearly identify the occurrence of the fuel injection. The advantage of the above methods is the accessibility to diagnostic parameters and their non-invasive nature.

Key words: combustion engine, fuel pressure, FFT signal analysis, common rail

### 1. Introduction

Modern Common Rail diesel engines are widely applied in light-duty vehicles, light-duty trucks and heavy-duty vehicles. The currently applied generation of these systems, whose injector design and control, allows executing several injections per single engine work cycle. The first injection (pilot) warms up the combustion chamber and provides a swirl of the charge. Further injections increase the efficiency of formation of the quasi homogenous mixture and reduced the exhaust emissions. The final injection is executed during the exhaust stroke to reduce the emission of particulate matter. A consequence of the nonoccurrence of any of the injections or changes in the proper rail pressure results in limited engine performance and excess emissions. Therefore, quick identification of malfunctions in the fuel system that prevents engine incorrect operation is extremely important [1].

Every time a fuel dose is injected into the cylinder, it immediately results in a drop of pressure in the rail immediately compensated with the help of a high pressure pump and its regulator.

The paper presents the method of analysis of a high pressure sensor signal that enables an assessment of the course of injection and the operation of the pump. This analysis enables identification of malfunctions in the CR components for different volumes of the pilot (injector opening time 200  $\mu$ s to 400  $\mu$ s) or the main (injection time in excess of 450  $\mu$ s) fuel doses [2, 5].

### 2. Object and methodology of research

The object of the research was a CR system of a G9T-720 engine. The system is composed of a low pressure circuit: fuel tank, fuel pump, fuel cooler, fuel filter, fuel heater and high pressure circuit: high pressure pump, accumulator (fuel rail) and electromagnetic injectors. The control of the fuel pressure in the rail is done through a pressure regulator fitted in the high pressure pump. The fuel is pumped into the rail from which the only outlet are the lines

leading to the injectors. The pressure in the rail is measured by a pressure sensor. The injectors are supplied with fuel under the same pressure as the one in the rail. The value of the pressure and the opening time of the injector are decisive of the dose of injected fuel, which translates into instantaneous pressure variations in the rail.

The fuel rail is fitted with a standard 5 V Bosch pressure sensor. The signal from the sensor is received through wires connected to terminals 2 and 3. In order to measure the instantaneous pressure in the rail, an ADPT-25-S connector of the  $\mu$ DAQ USB-26 data acquisition module (Eagle Technology) was connected to the control unit with the existing wires. The signal was sent via a USB port to the computer running the LabView application. The investigations were carried out in two stages:

- on the test stand, which allowed a validation and optimization of the software for the signal analysis and performance of reconnaissance tests,
- on the G9T engine operating on the engine dynamometer, which enables a validation of the developed methodology.

In the first stage of the investigations, the measurements were carried out on the STPiW-2 test stand (Fig. 1) designed for testing of CR system components. Components of the CR system from the Renault G9T engine were installed on the test table. The measurements aimed at determining the operating characteristics of the fuel systems and configuring the 'VI' (virtual instrument) software developed in LabView whose job was to diagnose the CR system components, [5]. Another precise AVL SL31D2000 sensor was fitted on the fuel rail along with the conditioning equipment to compare the pressure curves and evaluate the accuracy of the pressure reading of the standard pressure sensor.

During the investigations, two measurement strategies were applied and validated differing with the method of analysis of the signal from the pressure sensor and the

method of presentation of the results. For both methods, the programs were developed in the LabView environment [2, 3].

a)



b)



Fig. 1. STPiW-2 testing table: a) general view, b) AVL SL31D2000 pressure sensor fitted in the adapter: 1 – fuel injector tester, 2 – high-pressure pump tester, 3 – testing table control module, 4 – injectors, 5 – fuel dose measurements cylinders, 6 – high-pressure pump, 7 – overflow measurement cylinders

The first method is based on a fast Fourier transform (FFT) and low-pass signal filtering. The block diagram of the 'FFT' has been presented in Fig. 2. The software allows configuring the settings of the data acquisition module (sampling frequency, number of samples, upper and lower measurement range). In this method, one constant component of the rail pressure signal (being its average value) was subtracted from that signal. The modified signal underwent a discrete Fourier transform that enables observing the signal in the amplitude-frequency coordinates [3]. Such a graph shows, from which constant harmonic components the signal is composed and what the value of the amplitude is. In order to catch a clear reading without static, a low-pass filter was applied. The effect has been presented in Fig. 4.

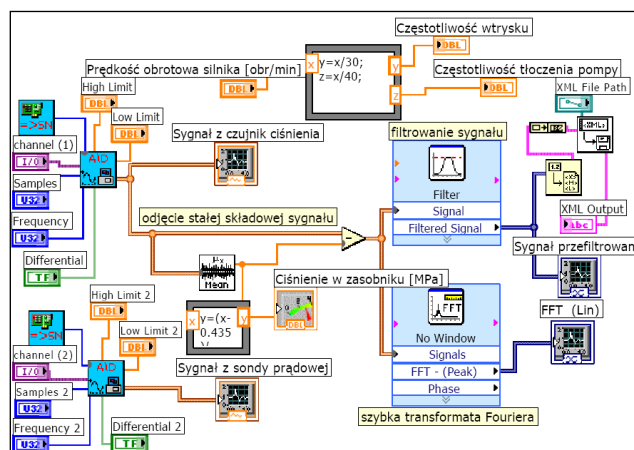


Fig. 2. Block diagram of 'FFT'

The second method is based on a short term Fourier transform (STFT). The block diagram of the 'STFT' has been presented in Fig. 3. The data acquisition module can be configured similarly to 'FFT'. The constant component (average value) of the signal was subtracted from it. Then, the signal underwent a low-pass filtering and a short term Fourier transform. The brightness of individual streaks (Fig. 5) shows the value of the amplitude of the signal components. The program allows setting the parameters for the analysis during the transform, which is impactful on the type of information presented in the graph. Depending on the setting, we may determine the time, in which the signal values are changed or precisely determine the frequency of the harmonic signal components.

In the first stage of the investigations, the validation tests were performed on the testing table (Fig. 1a). It allowed a free control of the following parameters: rotational speed of the high-pressure pump, pressure in the fuel rail, injector opening time and injector opening frequency. The validation of both methods consisted in comparing the parameters set at the system input (settings in the control panel of the testing table) with the results of the analysis of the pressure change in the fuel rail. Both methods were tested for small (pilot) and large (main) fuel doses.

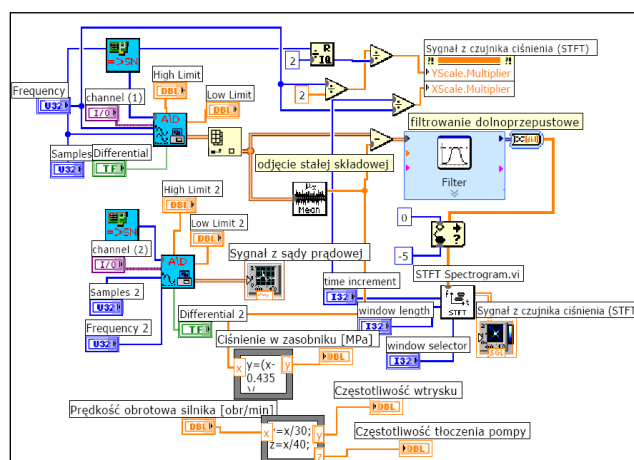


Fig. 3. Block diagram of 'STFT'



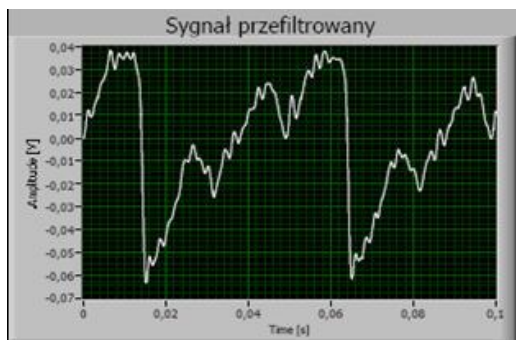
### 3. Results

In the first stage, validation tests were performed for the main fuel doses on the testing table. In order to validate the method, the following parameters were set:

- rotational speed of the high-pressure pump: 1200 rpm;
- injector opening frequency: 20 Hz;
- injector opening time: 1000  $\mu$ s;
- fuel pressure in the rail: 80 MPa.

The sampling parameters of the signal were selected in such a way as to analyze a fragment of the signal of the duration of 0.1 s. During this time, two injections were executed. On the graph of the filtered signal (Fig. 4a), we can clearly see two steep drops in the fuel pressure in the rail that indicate the occurrence of the injections. On the FFT graph (Fig. 4b), the components of the signal frequency have been presented. Aside from the injector opening frequency, there is a component related to the frequency of the fuel pumping in the high-pressure section that allows an evaluation of the correct pump operation. Since the results of the analysis of the obtained signals confirmed the settings of the parameters on the testing table, the authors concluded that the first method is good for detecting of the main doses.

a)



b)

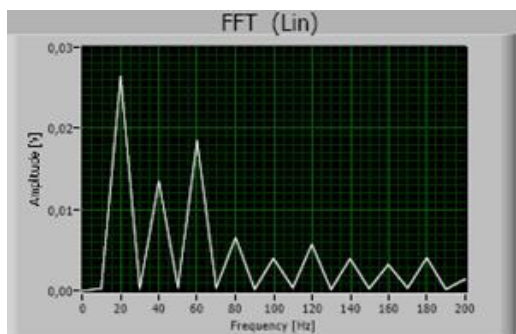


Fig. 4. The 'FFT' method. Signal curve in the domain of: a) time, b) frequency for the main fuel doses

During the validation of the 'TFT' method, the sampling parameters were identical as in the first method. At the moment of occurrence of the fuel injection, streaks of different hues of blue appear on the graph depending on the fuel pressure amplitude in the rail (Fig. 5). On the time scale, we can clearly see that the injections take place at even time intervals, which corresponds to the frequency of 20 Hz. The advantage of this method is that the information

on the occurrence or non-occurrence of the injection was isolated from the signal. This method is also appropriate for detecting the main fuel doses.

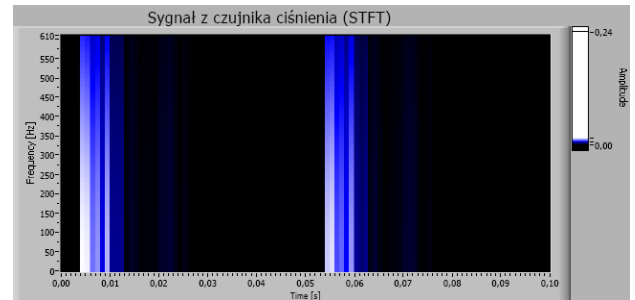


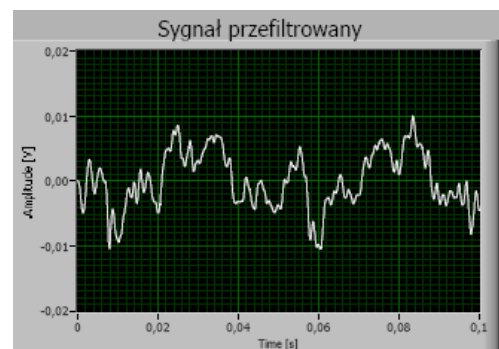
Fig. 5. The 'STFT' method. The STFT graph of the signal from the pressure sensor for the main fuel doses

The next step was the validation of the small doses on the testing table. In order to validate this method, the following parameters were set:

- rotational speed of the high-pressure pump 400 rpm,
- injector opening frequency 20 Hz,
- opening time of the injector 300  $\mu$ s,
- fuel pressure in the rail 40 MPa.

As for small fuel doses, the pressure drops are miniscule, hardly seen on the time curve and the high-pressure pump rapidly compensates them (Fig. 6a). On the FFT graph (Lin) (Fig. 6b) a component frequency is visible that is triggered by the injection, yet, the filtered signal is unclear, which may result in difficulties when identifying faulty injectors.

a)



b)

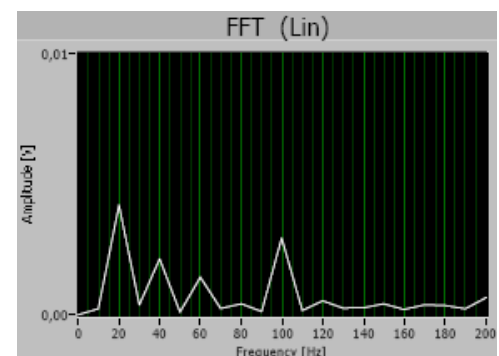


Fig. 6. The 'FFT' method; signal curve of the fuel pressure in the rail for small fuel doses in the domain of: a) time, b) frequency

When the STFT method was applied (Fig. 7), two injections were recorded at a 0.05 second interval. The indications are not as clear as they are for the main fuel doses, but they allow confirming the occurrence of two subsequent injections. This information is sufficient to deem this method as good for detecting small fuel doses.

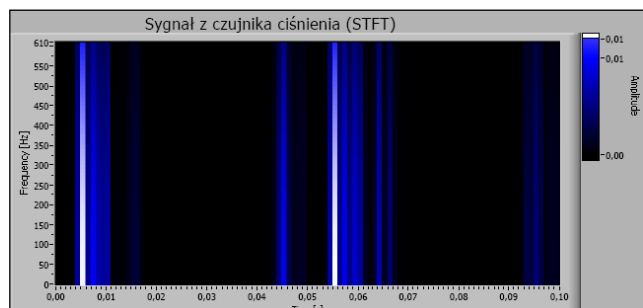
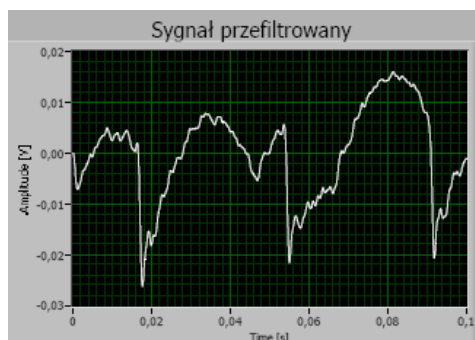


Fig. 7. The 'STFT' method. STFT graph of the signal from the pressure sensor for small fuel doses

Next, the validation of the developed method was carried out on the Renault G9T engine installed on a dynamometer. The investigations were first carried out on an injection system having all injectors operative. The engine started easily and operated at idle with the speed of 800 rpm.

The signal and its spectrum recorded in 'FFT' has been presented in Fig. 8. The signal curve is correct. There are small deviations of the amplitude interrupted with cyclic steep peaks occurring at the moment of injection. The pump and the injectors' operating frequency at the set engine speed should be 20 Hz and 27 Hz respectively.

a)



b)

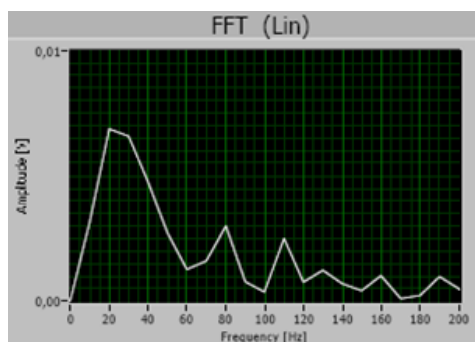


Fig. 8. Measurement of the signal performed with 'FFT' (all injectors operative)

The fuel pressure in the rail was approx. 35 MPa. On the spectrum, we can see that the main signal components are 20 Hz and 26.7 Hz. The signal recorded in 'STFT' has been shown in Fig. 9. The bright streaks on the spectrum clearly show at which moment the injections occurred. The cyclicity of occurrence of the streaks corresponds to the frequency of operation of the injectors. The information on the occurrence of an injection presented in the 'STFT' graph clearly (as in a zero-one method) determines whether the injection was executed or not.

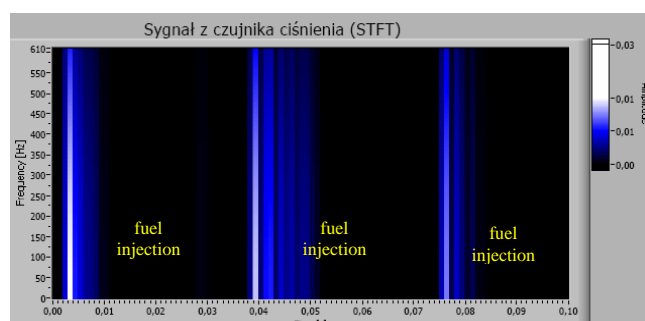


Fig. 9. Measurement of the signal performed with 'STFT' (all injectors operative)

The next step was a simulated fuel injector malfunction in the first cylinder. A control module wiring was disconnected from the engine injector and connected to a separate one. The wire could not have stayed disconnected because the signal from the control module must reach the injector for the engine to start. The simulated malfunction reflects a situation of a faulty injector (seizure). The control module sends a signal to the injector but the injection to the cylinder is not executed.

The engine started properly and operated at idle with the speed of 800 rpm. The engine was louder and a higher vibration of the engine block was observed. The settings of the measurement equipment were the same as for the tests described earlier in the paper.

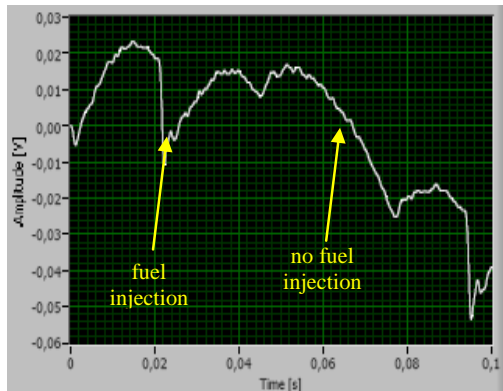
In the first place, the signal from the pressure sensor was analyzed in 'FFT'. On the time tracing of the signal (Fig. 10a) we can see one peak missing caused by the lack of injection. Instead of the downward peak, there is a smooth drop in the amplitude. The signal spectrum clearly differs from the one in Fig. 9. The highest peak occurs for the frequency of 10 Hz, i.e. for the signal frequency caused by the lack of injection (Fig. 10a).

In order to facilitate the injector diagnostics, the signal from the sensor was subjected to an analysis in 'STFT'. In the signal spectrum, the bright streaks indicate when the injection was executed. Fig. 10 shows that only two streaks appeared instead of three. Additionally, between some of the streaks a long interval was visible resulting in uneven streak occurrence. These are evident symptoms of a malfunctioning injector.

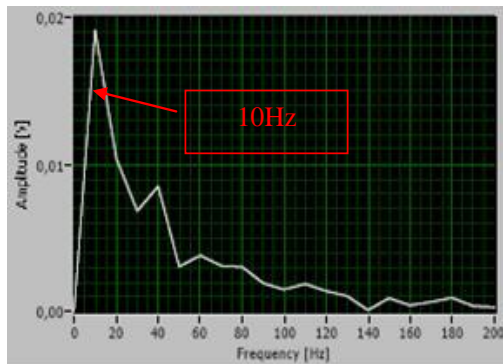
Upon diagnosing of a malfunction of one of the injectors, the faulty injector must be identified without removing all of the injectors from the engine. To this end, an additional diagnostic parameter was measured – the injector supply current. The current probe was connected to channel 2 of the microDAQ module.



a)



b)



c)

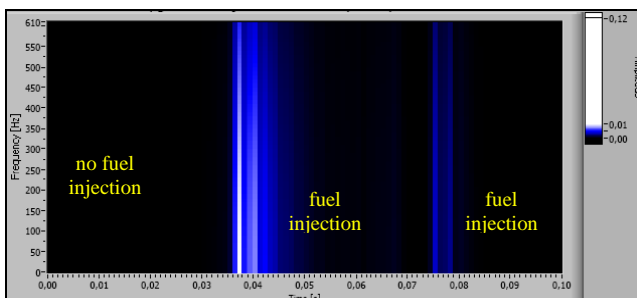


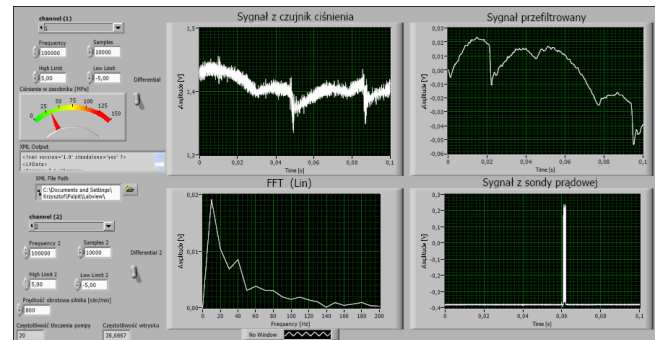
Fig. 10. The 'FFT' method (one injector inoperative): a) pressure curve in the fuel rail, b) signal spectrum, c) STFT curve of the pressure signal for one injector malfunctioning

Both signals were recorded on the graphs with the same time interval, one after another, to easily refer the current reaching the coil to the injection. The injectors are diagnosed one after another and monitored whether the supply current triggers the injection, which is seen as a pressure drop. If there is a supply current and the signal from the pressure sensor on the time line is not reflected as a steep drop of pressure, it means that the injector is faulty. One should note the delay between the supply current and the pressure signal. The inertia of the injector components results in the delay at the moment of activating and deactivating of the injector. A simultaneous recording of the two parameters in 'FFT' has been presented in Fig. 11.

In order to facilitate the method of identifying the faulty injector, 'STFT' was applied, in which we can observe the induction signal in the form of a supply current and the system response in the form of a bright streak resulting

from the injection (Fig. 11). The current probe was fitted on the wiring of the faulty injector. The signal curve of the probe seen in the lower screen indicates that the injector is electrically functional. It is not hydraulically functional though, because at the moment when the supply current is sent, as seen on the upper screen, the bright streak does not appear, which is tantamount to the lack of injection.

a)



b)

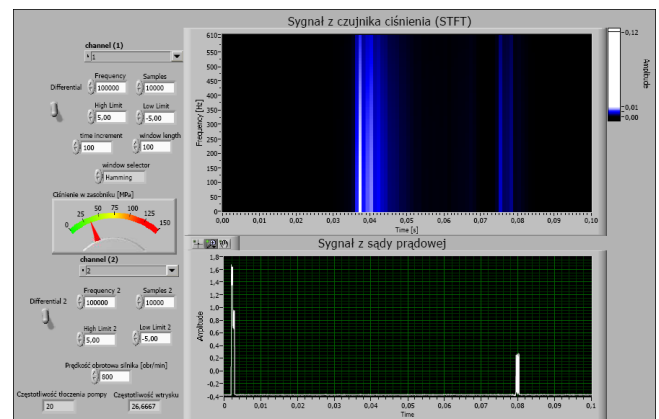


Fig. 11. View of the program windows: a) simultaneous recording of the pressure in the rail and the supply current of the injector, b) detection of the faulty injector with 'STFT'

To confirm the applicability of this method, an additional test was carried out for the engine speed of 1200 rpm, only this time the operative injector was replaced with a seized one. The injector operating frequency for a given engine speed should be 40 Hz, i.e., four injections should take place within 0.1 s. On the screen, only three streaks appear, which indicates that one injector is not injecting fuel.

The faulty injector was identified by the measurement of the supply current of the subsequent injectors. The current probe was connected to the first injector. On both screens we can see a convergence of signals consisting in an almost simultaneous presence of the current signal and the streak indicating the pressure drop. This confirms that the first injector is hydraulically and electrically functional. After excluding the first injector the probe was connected to the second one. As of the moment when the supply current reaches the injector, there is no streak on the upper screen, which indicates a lack of the fuel injection into the cylinder. The injector is hydraulically inoperative. The applied method allowed identifying the faulty injector.

In between two signals, in a properly operating injection system, four injections should take place numbered as in the firing order of the cylinders. The lack of the downward peak (pressure drop) in the 'FFT' method and the lack of the streak in the 'TFT' method may be directly referred to the faulty injector.

#### 4. Conclusions

The analysis of the signal from the high-pressure sensor allows an assessment of the course of the injection and the process of pumping by the supply pump. This analysis allows identification of malfunctions of components of the CR injection system for different volumes of both the pilot and the main fuel doses

The described types of software outrank oscilloscopes with their potential as they can be constantly expanded with new functionalities to improve the diagnostic process. The development of software should aim at the improvement of

potential in the analysis of the acquired data and autonomous reporting of the diagnostic results. This would be more time efficient and would reduce the costs of workshop diagnostic equipment.

Both methods are applicable in injection systems diagnostics. The 'FFT' method provides more information related to the operation of the system itself and accurately presents the structure of the signal. The 'STFT' method presents the signal in such a way as to clearly indicate the execution of an injection. An advantage of the said methods is the accessibility to the diagnostic parameters. For the pressure measurement, both methods utilize a factory made sensor originally fitted in the fuel rail.

It is justified to continue further research aiming at confirmation of the applicability of the developed methods for other types of Common-Rail fuel systems.

#### Bibliography

- [1] GUNTHER, H. Diagnostowanie silników wysokoprężnych. WKiŁ, Warszawa 2014.
- [2] KARCZEWSKI, M., KOLIŃSKI, K. Diagnostyka wtryskiwaczy układu Common Rail na podstawie pomiarów ciśnienia w zasobniku. *Zeszyty Naukowe WSOWL*. 2011, **1**(159).
- [3] PAYRI, F., LUJÁN, J.M., GUARDIOLA, C. et al. Injection diagnosis through common-rail pressure measurement. *Proceedings of the Institution of Mechanical Engineers*. 220 Part D: Journal Automobile Engineering.
- [4] TŁACZAŁA, W. Środowisko LabVIEW w eksperymencie wspomaganym komputerowo. WNT. Warszawa 2002.
- [5] Poradnik Serwisowy. Zasilanie silników HDI, 2004, **4**, Wydawnictwo Instalator Polski.
- [6] Zasobnikowe układy wtryskowe Common Rail. WKiŁ, Warszawa 2005.

Mirosław Karczewski, DEng. – Faculty of Mechanical Engineering at Military Academy of Technology.

e-mail: [Mirosław.Karczewski@wat.edu.pl](mailto:Mirosław.Karczewski@wat.edu.pl)



Krzysztof Koliński, MEng. – Military Aviation Works No. 4, Warsaw, Poland.





## Evaluation of the possibilities of adapting a constant volume combustion chamber for research on ignition of hypergolic propellants under low and high-pressure conditions

*In this study, the adaptation possibilities of a constant volume combustion chamber (CVCC) for research on the ignition of hypergolic propellants are presented. The application of hypergolic bipropellants and crucial parameters regarding their ignition behaviour are discussed. The initial studies on ignition delay measurements presented here does not cover the whole range of conditions present in practical systems where hypergolic ignition occurs. In the study, a need for an evaluation of the influence of pressure on the ignition delay was indicated as the reason to conduct research on hypergolic ignition in low and high-pressure environments. Moreover, the study reviews the state-of-the-art experimental methods of investigating the ignition under atmospheric, low and high-pressure conditions, including those utilizing a constant volume combustion chamber. The drop test was pointed out as the most commonly used method; this makes it advantageous in terms of comparing the results with those obtained by other researchers. Therefore, the drop test was selected as a method to be used in a CVCC. The test rig developed here was designed based on a CVCC initially designed for diesel sprays' visualization in high-pressure conditions. All the required modifications, especially the design of the oxidizer dosing unit, are presented in the study.*

**Key words:** hypergolic ignition, hypergolic propellant, ignition delay, drop test, constant volume combustion chamber

### 1. Introduction

Hypergolic propellants are pairs of liquid fuels and oxidizers in which ignition occurs spontaneously upon contact between the two liquids; thereby eliminating the need for a complex ignition system [16]. The reliable restart capability of engines based on hypergolic propellants makes them ideal for spacecraft manoeuvring. An important criterion to evaluate the performance of hypergolic bipropellants is the ignition delay, which is defined as the time from the physical contact of the liquid fuel and the oxidizer to the onset of ignition. A long ignition delay can cause a 'hard-start' problem in which unburnt fuel and oxidizer in the combustion chamber accumulate, then suddenly ignite to generate damaging pressure peaks [5].

Although the existence of hypergolic propellants has been known since 1937 [11], the mechanisms controlling ignition are not yet well understood. The development of hypergolic propellants is highly empirical and current bipropellant hypergolic technology has been in use for more than fifty years. The conventional hypergolic combinations are hydrazine or its derivatives (monomethylhydrazine–MMH, or unsymmetrical dimethylhydrazine–UDMH) as a fuel and nitric acid or nitrogen tetroxide (NTO) as an oxidizer. Although these dense, storable propellants give a high performance and were or are used in many systems like the Space Shuttle [7] or Falcon 9 rocket [4], they are highly toxic, difficult to handle and furthermore, hydrazine-based fuels are suspected carcinogens. Accordingly, using the toxic propellants increases the development cost and lead time as well as the risk of disaster for manned space missions. For these reasons, there is strong interest in finding and developing non-toxic hypergolic propellants that have an equal or greater performance than the currently used toxic propellants [6]. Many institutes around the world make efforts to enhance their capabilities in the field of so-

called green space propulsion. In numerous cases, a green oxidizer such as high-test peroxide (HTP) was selected and a non-toxic energetic fuel having hypergolicity with this oxidizer was developed [1, 13]. In this study HTP was also used as an oxidizer.

In order to investigate hypergolic properties of bipropellants, some research methods and procedures have been developed: the drop test and the impingement test. They are focused on investigating ignition delay time. The schematic of the drop test stand is presented in Fig. 1 [9]. The procedure for this experiment is simple: a droplet of an oxidizer is released from a syringe or pipette; it falls down into the pool of a propellant stored in a vessel, e.g. in a small Petri dish; and then the hypergolic ignition is observed.

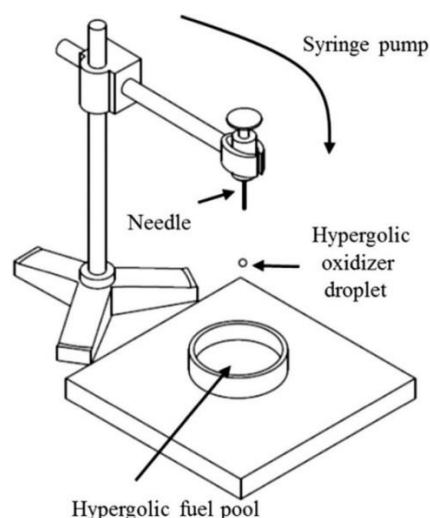


Fig. 1. Schematic drawing of the drop test stand [9]

The drop test allows the exploration of the variations of ignition delay under two extreme operating conditions: extreme fuel-rich combustion (oxidizer released as a droplet, fuel in the pool); or extreme oxidizer-rich combustion (fuel released as a droplet, oxidizer in the pool). The whole process is recorded by a high-speed camera. In order to more accurately capture the instant of contact of a falling drop with the pool and time of ignition, additional equipment can be utilized, e.g. pressure sensors, photodiodes [18].

The second method of investigating the ignition delay is the impingement test. This test is very similar to the drop test. However, in the impingement test the droplet of the propellant is impinged with a speed of up to 3 m/s [8], not dropped as in the drop test. This results in more intensive collision of the fuel and oxidizer; thereby, the ignition delay time is slightly different to that obtained in the drop test.

The drop test stand presented in Fig. 1 enables the conducting of experiments in atmospheric conditions; which is a good starting point to investigate hypergolic properties of bipropellants. Therefore, it can be used as an initial test for the pre-selection of hypergolic propellants, as applies in this study. Here the triglyme with the HTP pair was initially tested in atmospheric conditions in order to evaluate if it is worth further studies.

The drop test in an atmospheric environment is a successful method for initial determination of ignition delay, especially in the early stage of propellant selection. However, it is far away from the conditions in which these propellants are supposed to operate. In combustion chambers of engines used for spacecraft manoeuvring two states of extreme conditions occur—vacuum or very low pressure before the start of the engine and very high pressure after the start of the engine [15]. In terms of the power of the influence of pressure on the ignition delay [2, 14], it is extremely important to measure this parameter under low and high-pressure conditions. In order to do this, substantial modifications have to be applied to the standard drop test stand. The drop test stand needs to be isolated from the ambience; this can be done by using a CVCC. These are usually used to conduct optical diagnostics on fuel sprays [10]. High and low-pressure conditions inside the constant volume combustion chamber are achieved by a gas supply system and a vacuum pump. The first is responsible for high pressure conditions and the second for low pressure conditions. When an experiment is supposed to be conducted under high-pressure conditions, air or inert gas from a pressurized tank is supplied to the CVCC. If low-pressure conditions are demanded, then the tank with the gas is closed and vacuum pump removes gases from the CVCC.

There are already a few drop test rigs which utilize the aforementioned solutions [3, 12, 17]. Each of them has different configurations and enables its users to gain some original data from tests. However, there is still room for improvements and fresh ideas in this area. In this study a connection between proven and novel solutions is presented and the possibilities of further development are discussed.

## 2. Ignition delay study in atmospheric conditions

In order to examine the procedures of drop tests and gain initial input for the design assumptions of the high-

pressure test rig, a number of experiments under atmospheric conditions (0.1 MPa, 22 °C) were conducted. As a fuel, triglyme (triethylene glycol dimethyl ether) was selected; and as an oxidizer, high-test peroxide (HTP) was used. In order to react hypergolically with HTP, triglyme requires an addition of, for example, sodium borohydride.

The ‘open-air’ test rig (Fig. 2) consists of a simple oxidizer dosing system which utilizes a pipette attached to a tripod. Fuel is kept in a watch glass located 200 mm below the tip of the pipette.

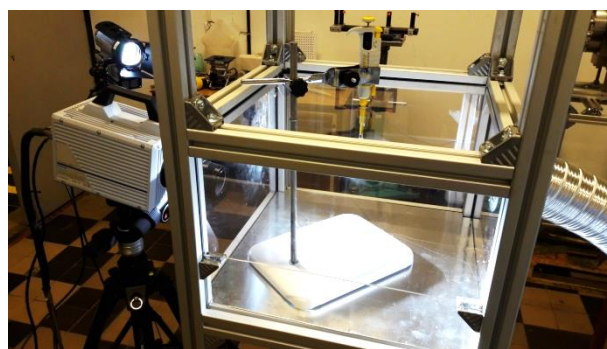


Fig. 2. Drop test rig for measurements in ambient conditions used in the study

As shown in Fig. 2 the operator is separated from the drop test area with polycarbonate sheets. The test volume restricted by polycarbonate walls is continuously scavenged by a ventilation system, which is responsible for removing fumes created during combustion of hypergolic propellants. The falling droplet and ignition are captured using the Photron Fastcam SA-1.1 camera at a frame rate of 10000 fps, which requires an additional light source to visualize the droplet and the instant of collision.

### Results of tests in atmospheric conditions

The results of the measured ignition delay obtained in the study are shown in Fig. 3.

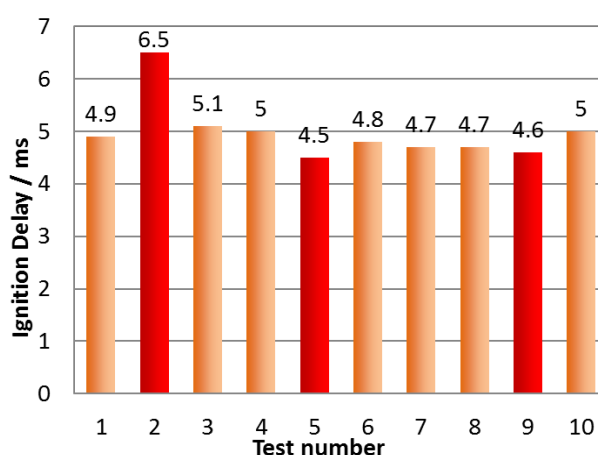


Fig. 3. Measured ignition delay of triglyme-HTP; the cases where the oxidizer droplets did not hit the pool in the centre are marked red

As shown in Fig. 3, the measured ignition delay did not vary between the cases much. The average ignition delay was 4.98 ms and the standard deviation was 0.57 ms. However, if the cases where the droplets did not hit the fuel pool



in the centre are excluded (case numbers 2, 5 and 9), then the standard deviation decreases to 0.16 ms. This indicates the importance of a repeatable place of contact between the oxidizer and the fuel. The other issue which can be observed in Fig. 4 is that after releasing a droplet of an oxidizer from a pipette, an additional group of little droplets tend to follow the main droplet. However, these additional droplets did not disturb the ignition delay measurements, because high distance between them and the main droplet caused that they collided with the fuel after the ignition occurred. Nevertheless, this indicates that a more accurate oxidizer dosing system is necessary.

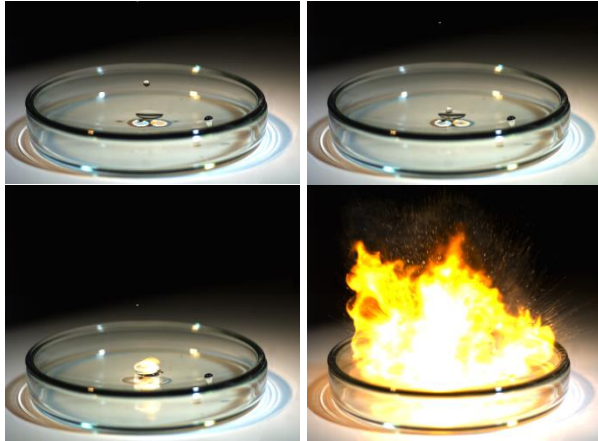


Fig. 4. Drop test of the triglyme-HTP pair; frames obtained at -5, 0, 5 and 10 ms after the contact of the HTP droplet with the triglyme pool

### 3. Drop test stand design

A constant volume combustion chamber frame (Fig. 5) was the basis for the drop test set-up developed in this study. It was primarily utilized to perform research on fuel sprays [10].

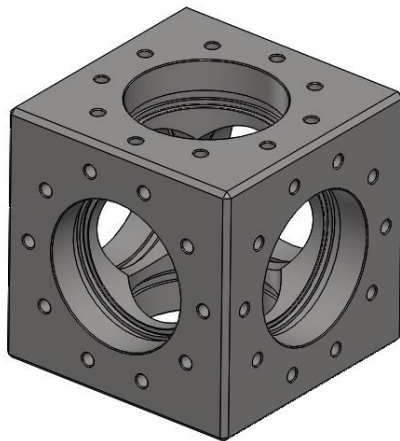


Fig. 5. CVCC frame used as a basis for creating a drop test stand for research in low and high-pressure environments

The major way to adapt the CVCC to drop test experiment was to design the parts attached to the CVCC main frame. Several components attached to the main frame of the vessel were designed:

- Fuel holder

- Oxidizer dosing unit
- Sensors' cover

The fuel holder unit has three main tasks: it closes the CVCC at its bottom; it holds the pillar with a Petri dish filled with fuel; and it is connected to the systems responsible for maintaining low and high pressure inside the CVCC, i.e. the vacuum line and pressurized ambient gas line respectively. Thus, the fuel holder has two ports dedicated to the respective systems. The systems responsible for maintaining low or high-pressure conditions inside the CVCC utilize a vacuum pump and tank with pressurized  $N_2$  respectively. When high-pressure conditions are demanded, a valve at the tank is opened and inert gas is supplied to the CVCC. When low-pressure conditions are demanded, the valve at the tank is closed and the vacuum pump is turned on. The vacuum and  $N_2$  lines' connections are shown in Fig. 6.

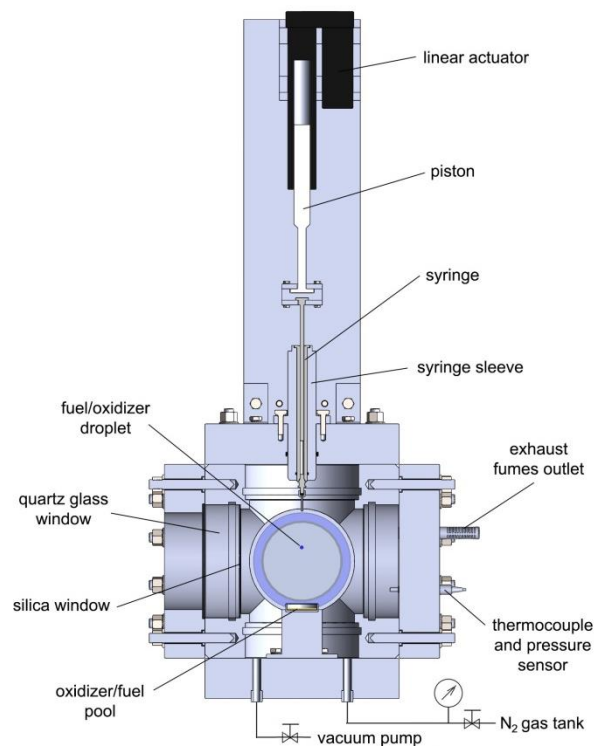


Fig. 6. Schematic diagram of the drop test rig

The oxidizer dosing unit is integrated with an oxidizer supply system which consists of two main elements – a syringe of 2 ml capacity and an electric linear actuator. A droplet of an oxidizer of 2.5–3.0 mm diameter is released from the syringe and then falls down into a pool of fuel. The syringe is perched in a stainless steel sleeve which prevents it from movement. The distance from the end of the syringe's needle and the pool of fuel is 120 mm. It was decreased compared to the set-up for the atmospheric tests described in section II. The process of droplet formation is controlled by the electric linear actuator. A part of the actuator referred to as a piston, which moves along a stainless steel guide, pushes the syringe's piston and thereby releases a portion of liquid from the syringe at the end of the needle. The reason why the electric linear actuator was used in the

study relates to the reliability of the process of droplet formation under high-pressure conditions.

The sensor cover is mounted on the side of the CVCC and it is integrated with three systems:

- pressure measurement system
- temperature measurement system
- exhaust system

The first system includes a pressure transducer and charge amplifier which is connected to a data acquisition unit. The second system consists of a thermocouple, which is connected to the same data acquisition system as the charge amplifier. The third system consists of a gas outlet port connected with a line to release the fumes away from the CVCC after combustion.

In the modified CVCC two quartz windows were designed. The first provides optical access for the camera; while the other allows an externally located light source to illuminate falling droplets. The whole drop test set-up with a high-speed camera is shown in Fig. 7.

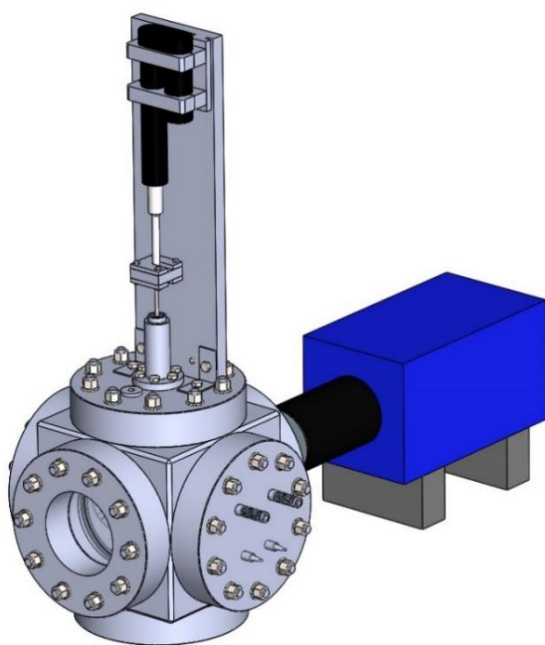


Fig. 7. 3D model of the drop test rig with the camera set-up

#### 4. Conclusions

The obtained ignition delay times of the triglyme-HTP pair at atmospheric conditions show that this fuel-oxidizer combination is very promising. The value of 4.98 ms obtained here is close to the benchmark of hypergolic propellants—monomethylhydrazine-nitrogen tetroxide with an

ignition delay time of 3 ms [16]. However, to fully investigate the potential of this propellant, it is necessary to conduct drop tests not only under atmospheric conditions, but also in a low and high-pressure environment. Therefore, in this study these design solutions intended to adapt a constant volume combustion chamber for research on the ignition of hypergolic propellants under low and high-pressure conditions were proposed.

The initial drop tests in ambient conditions presented in the study revealed also a need for precise droplet dosing, in order to avoid formation of a series of droplets and for an accurate drop test fall into the centre of a fuel pool. These aspects were included in the design process of the high pressure drop test rig.

The test rig development presented here proved that a constant volume vessel initially designed for fuel injection visualization at high-pressure conditions can be utilized to perform drop test studies of hypergolic propellants in low and high-pressure environments.

The number of new systems and modifications were incorporated to the base experimental set-up, e.g. oxidizer dosing system, pressure measurement system, temperature measurement system, exhaust system and systems for creating low and high-pressure conditions in the vessel.

Among these newly designed systems, the most important CVCC upgrade in terms of drop test studies is the oxidizer dosing system. As explained previously, the experiments on the triglyme-HTP propellant conducted in ambient conditions proved that an oxidizer dosing system is of great importance for repeatability of drop tests (formation of droplets and place of contact with the fuel).

All the applied modifications are supposed to ensure high reliability of the experiments; however, further development of the rig is planned, with a number of solutions which are being considered for implementation in the future, e.g. a photodiode which detects the moment of ignition. These, however, will be applied if the first CVCC studies indicate a need for such upgrades.

#### Acknowledgments

The paper was prepared as a part of the Hipergol project which is financially supported by the National Centre for Research and Development (NCBiR) under Grant No. 8/2016.



#### Bibliography

- [1] CONG, Y., ZHANG, T., LI, T. et al. Propulsive performance of a hypergolic  $\text{H}_2\text{O}_2$ /kerosene bipropellant. *Journal of Propulsion and Power*. 2004, **20**(1), 83-86.
- [2] CORBETT, A., SEAMANS, T., DAWSON, B. et al. Hypergolic ignition at reduced pressures. Edwards Air Force Base, CA: AFRPL-TR-64-175, 1964.
- [3] DAMBACH, E., CHO, K., POURPOINT, T. et al. Ignition of advanced hypergolic propellants. *46th AIAA/ASME/SAE/ASEE Joint Propulsion Conference & Exhibit*, 2010.
- [4] Falcon 9 SpaceX. [www.spacex.com/falcon9](http://www.spacex.com/falcon9).
- [5] HOLTZMANN, R. *Chemical rockets*. Marcel Dekker, New York 1969.
- [6] HURLBERT, E., APPLEWHITE, J., NGUYEN, T. et al. Nontoxic orbital maneuvering and reaction control systems for reusable spacecraft. *Journal of Propulsion and Power*. 1998, **14**(5), 676-687.
- [7] HURLBERT, E., SUN, J., ZHANG, B. Instability phenomena in earth storable bipropellant rocket engines. *Progress in Astronautics and Aeronautics*. 1995, **169**, 122.



- [8] Hypergolic Propellants Laboratory – High Velocity Drop Impact Experiment. [engineering.purdue.edu/Hypergol/high\\_velocity\\_impact/index.html](http://engineering.purdue.edu/Hypergol/high_velocity_impact/index.html).
- [9] KANG, H., LEE, E., KWON, S. Suppression of hard start for nontoxic hypergolic thruster using H<sub>2</sub>O<sub>2</sub> oxidizer. *Journal of Propulsion and Power*. 2017, **33**(5), 1111-1117.
- [10] LEWIŃSKA, J., KAPUSTA, Ł.J. Analysis of the micro-structure of the fuel spray atomized by marine injector. *Combustion Engines*. 2017, **169**(2), 120-124.
- [11] LEY, W. *Rockets, missiles, and space travel*. Viking Press, New York 1951.
- [12] NATAN, B., PERTEGHELLA, V., SOLOMON, Y. Hypergolic ignition of oxidizers and fuels by fuel gelation and suspension of reactive or catalyst particles. *46th AIAA/ASME/SAE/ASEE Joint Propulsion Conference & Exhibit* 2010.
- [13] POURPOINT, T., ANDERSON, W. Hypergolic reaction mechanisms of catalytically promoted fuels with rocket grade hydrogen peroxide. *Combustion Science and Technology*. 2007, **179**(10), 2107-2133.
- [14] SEAMANS, T., DAWSON, B. Hypergolic ignition at reduced pressures. Edwards Air Force Base, CA: AFRPL-TR-64-175, 1967.
- [15] SEAMANS, T., VANPEE, M., AGOSTA, V. Development of a fundamental model of hypergolic ignition in space-ambient engines. *American Institute of Aeronautics and Astronautics*. 1967, **5**(9), 1616-1624.
- [16] SUTTON, G. *History of liquid propellant rocket engines*. Alexandria, VA: American Institute of Aeronautics and Astronautics. 2006.
- [17] WANG, S., THYNELL, S. Experimental investigation of pressure effect on ignition delay of monomethylhydrazine, 1,1-dimethylhydrazine, tetramethylethylenediamine and 2-dimethylaminoethylazide with nitric acid. *8th U. S. National Combustion Meeting* 2013.
- [18] ZARBO, N., BELAL, H., POURPOINT, T. Effect of water and humidity on hypergolic propellant ignition and combustion. *51st AIAA/SAE/ASEE Joint Propulsion Conference* 2015.

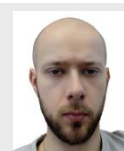
Maciej Krzesicki, MEng. – Faculty of Power and Aeronautical Engineering, Warsaw University of Technology.

e-mail: [Maciej.Krzesicki@ext.itc.pw.edu.pl](mailto:Maciej.Krzesicki@ext.itc.pw.edu.pl)



Łukasz Boruc, MEng. – Faculty of Power and Aeronautical Engineering, Warsaw University of Technology.

e-mail: [Lukasz.Boruc@itc.pw.edu.pl](mailto:Lukasz.Boruc@itc.pw.edu.pl)



Łukasz Jan Kapusta, DEng. – Faculty of Power and Aeronautical Engineering, Warsaw University of Technology.

e-mail: [Lukasz.Kapusta@itc.pw.edu.pl](mailto:Lukasz.Kapusta@itc.pw.edu.pl)



## Analysis of energy management strategies for hybrid electric vehicles in urban driving conditions

The pursuit of fuel consumption reduction by vehicles leads to a sudden increase in the share of hybrid and electric drives in the vehicle market. Replacing hybrid vehicles with electric vehicles requires long-term technological solutions, both for the infrastructure and the vehicles themselves. Therefore, one of the leading types of passenger car drives is currently the hybrid drive. The generated work share of electric drives used to power hybrid vehicles is a determinant of the viability of using electric drives. The article estimates the operating time share of electric and hybrid modes operation in real driving conditions (RDC) based on the latest Toyota hybrid model. The research object was a vehicle from the crossover group equipped with a fourth generation hybrid drive. Analysis of the drive's operation allowed to determine the conditions of energy flow and determine the work share of the electric drive in the total driving time.

Key words: hybrid electric vehicles, energy management, electric range, real driving conditions

### 1. Introduction

For a long time, due to economic and ecological aspects, solutions have been sought that would minimize the use of conventional fuels in transport. Such solutions are used in various branches of transport, including in road, rail and even air transport [7, 11]. One of the proposed solutions is the use of a hybrid drive containing at least two sources of power and energy. The most common system includes a spark-ignition engine and an electric motor. In 2016, road transport accounted for the transport of 84.2% of all cargo [1]. However, the share of passengers transported by this type of transport amounted to 56.2%. Considering this data, it seems justified that the majority of effort in the field of reducing emissions to the environment is carried out towards road transport.

It has been 20 years since the first serial production of full hybrid vehicles by Toyota [4, 8, 9]. During this time the company has been developing the hybrid drive system through several iterations [6, 10, 12, 19].

The current technological trend of reducing emissions from vehicles are technologies that allow the use of alternative fuels or alternative drives themselves. Tests of vehicles powered with alternative fuels (ethanol, CNG, bi-fuel) or with alternative propulsion systems (full and mild hybrid system) are carried out with respect to energy flow [3, 13, 14, 19] and their harmful components emissions in real operating conditions and in RDE (Real Driving Emissions) tests [5, 15–17].



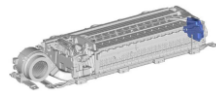

### 2. Aim of research

At present, there is a strong emphasis in the construction of hybrid vehicles on increasing their travel range in electric mode. This means an increased share of electric motor operation in the total operating time of the hybrid system [2]. In order to demonstrate the electric mode work participation, tests were conducted in urban driving conditions. The practical goal of the conducted research was to analyze the energy flow in the latest generation hybrid drive system on the example of Toyota C-HR and indication of the actual shares of electric and hybrid drive time when driving in urban conditions.

### 3. Research object

The Toyota C-HR vehicle, which was used to test the hybrid drive system in urban driving conditions, has a propulsion system construction similar that of the newest 2015 Toyota Prius (IV generation). The basic parameters of the drive system components are presented in Table 1.

Table 1. Test vehicle technical data [18]

Combustion engine 2ZR-FEX		
Engine type		16-valve DOHC with VVT-i
Displacement [cm <sup>3</sup> ]		1798
Bore x stroke [mm]		80.5 x 88.3
Compression ratio [-]		13:1
Fuel injection system		electronic multi-point injection
Max power [kW] at speed [rpm]		72/5200
Max torque [Nm] at speed [rpm]		142/3600
Emission standard		Euro 6
Electric front motor		
Max power [kW]		53
Max torque [Nm]		153
Max speed [rpm]		12400
Battery system		
Type of battery		Nickel-metal hydride (Ni-MH)
Cell quantity [-]		168 cells (6 cells x 28 modules)
Battery capacity [Ah]		6.5
Hybrid drive system		
Total power of the hybrid drive system [kW]		90
Top vehicle speed [km/h]		170
CO <sub>2</sub> emission combined [g/km]		87

The hybrid drivetrain consists mainly of a 1.8 dm<sup>3</sup> Atkinson-cycle petrol engine (assembled at the Toyota plant in Derby), a 1.31 kWh HV battery, and an electric motor all tied together by Toyota's planetary gear transmission. The effect of combining these motors provides 90 kW (120 KM) of power and 142 Nm of torque at 3600 rpm.

The Toyota C-HR is equipped with a fourth-generation hybrid drive. The structure of the drive is a series-parallel system (the scheme and principle of operation are described in [9]), shown in Fig. 1 together with the measuring devices used during the tests. The drive consists of a battery, planetary gear, generator, electric motors and an internal combustion engine.

The hybrid drive is mainly meant for use in urban driving, due to the frequency and intensity of traffic, which is associated with acceleration changes and thus, the ability to recover more energy from braking.

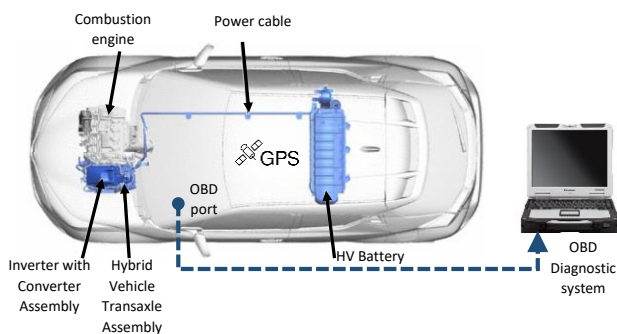


Fig. 1. A schematic of Toyota C-HR hybrid drive system along with the applied measuring devices (based on [18])

Toyota hybrid cars have four drive modes: Normal, EV, ECO and Power. After first starting the car, the system default settings is the 'Normal' drive mode, which automatically manages the most efficient use of both engines. Driver can also select one of the car's on-demand drive modes to achieve better fuel consumption in certain circumstances. Two of these modes, ECO and EV, were analysed in this article.

#### 4. Research methodology

The tests were carried out in Warsaw in real driving conditions on a regular work day. Two drive modes of Toyota C-HR have been compared. The first test was performed with the ECO drive setting, and the other in the ECO setting but with the EV mode active. (further referred to as ECO + EV). Traffic congestion was observed during tests (traffic volume higher than the capacity of a given road). The average route length (Fig. 2) was 11.5 km, and the average test duration was 32.2 minutes.

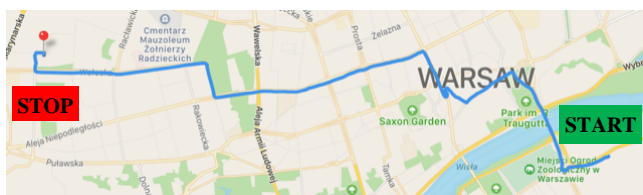


Fig. 2. Map of the road tests route

In order to record the vehicle motion parameters and hybrid drive operating conditions, a diagnostic system was connected that allows reading data directly from the hybrid drive monitor system. The following values were recorded in the tests: vehicle speed ( $S$ ), combustion engine speed ( $n$ ), battery charge status (SOC), electric motor speed and battery current (IB – positive value was defined as charging the battery, and negative indicates battery discharge). In addition, an independent system recorded the geographical position of the vehicle to determine the route. The characteristic drive conditions are shown on Fig. 3 and in Table 2. The conditions in both of the drives are similar and any differences negligible. Therefore, it can be assumed that the tests were repeatable, allowing for further comparative analysis of the drive system parameters depending on the selected driving mode.

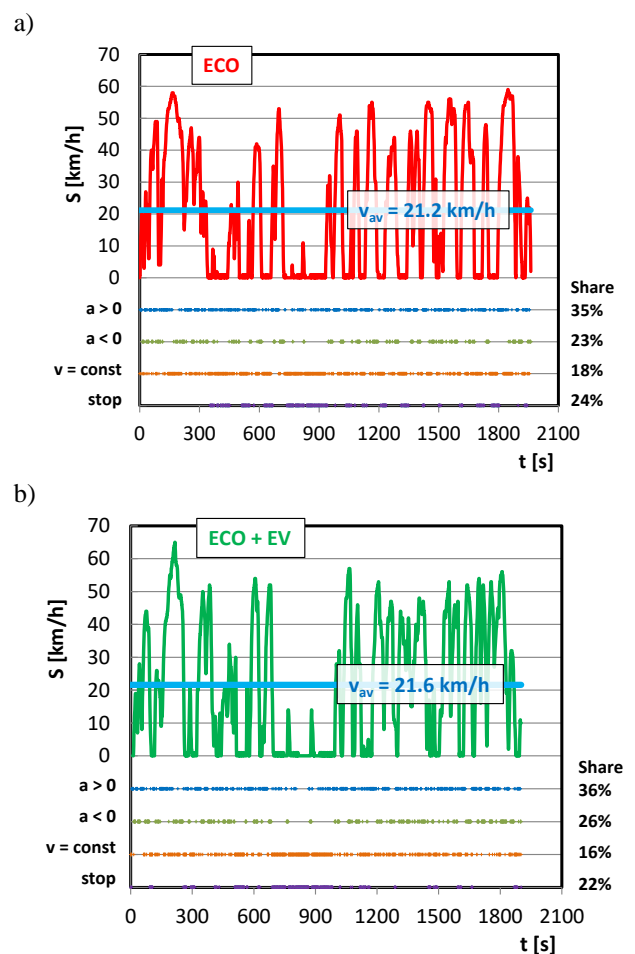


Fig. 3. The route drive characteristics with marked time densities of acceleration, constant speed, braking and stopping of the vehicle in the repeated drives on the same route: a) ECO mode, b) ECO + EV mode

Table 2. Test conditions for hybrid drive in two driving modes

Parameter	Mode	ECO	ECO + EV
Test duration [s]		1962	1902
Test route length [m]		11,554	11,437
SOC (initial/final)		60.4/47.5	47.5/60.4



To determine the share of the electric mode driving, sections of the route characterized by certain specific parameters were determined. Thus, the modes of operation of the hybrid drive system were determined: driving, acceleration and braking during the operation of the hybrid drive (HV), as well as vehicle standstill, driving, acceleration and braking with the internal combustion engine not active, i.e. drive system operation in electric mode (EV). The adopted criteria are listed and presented in Table 3.

The energy flow in the drive system during battery discharging, charging and recuperative braking was also calculated:

energy flow:

$$\Delta E = U * I * \Delta t \quad (1)$$

discharging:

$$\Delta E_{\text{dis}} = U * I * \Delta t \text{ (if } \Delta E < 0 \text{)} \quad (2)$$

charging:

$$\Delta E_{\text{ch}} = U * I * \Delta t \text{ (if } \Delta E > 0 \text{ and } M_{\text{reg}} \geq 0 \text{)} \quad (3)$$

recuperative braking:

$$\Delta E_{\text{reg}} = U * I * \Delta t \text{ (if } \Delta E > 0 \text{ and } M_{\text{reg}} < 0 \text{)} \quad (4)$$

where:

$U$  – voltage [V],  $I$  – current [A],  $\Delta t$  – time [h],  $M_{\text{reg}}$  – braking torque [Nm].

Table 3. Criteria for determining individual modes during the test

Mode	Parameters
HV drive	$a = 0, n > 600, v > 0$
EV drive	$a = 0, n < 600, v > 0$
HV acceleration	$a > 0, n > 600, v > 0$
EV acceleration	$a > 0, n < 600, v > 0$
standstill	$v = 0$
braking	$a < 0, v > 0, n > 600$
EV braking	$a < 0, v > 0, IB > 0, n < 600$

## 5. Results analysis

The energy flow rates were calculated with the formulas (1)–(4) and Table 3. The charging of the battery, its discharging and the regenerative braking conditions have been taken into account. The results are shown in Fig. 3 and 4. The energy flow rate is influenced also by the state of charge of the battery, both the initial and the final values (Fig. 4).

Driving in ECO mode results in increased energy flow values (up to 0.23 kWh) compared to the ECO + EV mode (up to 0.03 kWh). This is due to the lower initial charge status of the battery (SOC = 47%). Using the ECO + EV mode means that the battery discharge time density is much greater than during the ECO mode (by 37%). In spite of the varied changes in the discharge energy, the battery charging and energy recovery modes have similar energy flow shares. The differences do not exceed 11% (for charging) and 8% for regenerative braking.

Analysis of the energy flow change (Fig. 4) indicates significant similarities to the battery charge level. There are noticeable changes in the energy flow proportional to the battery charge level. However, it is not possible to specify the proportionality value. During the battery discharge (ECO + EV mode) changes in both these quantities are proportional in varying degrees.

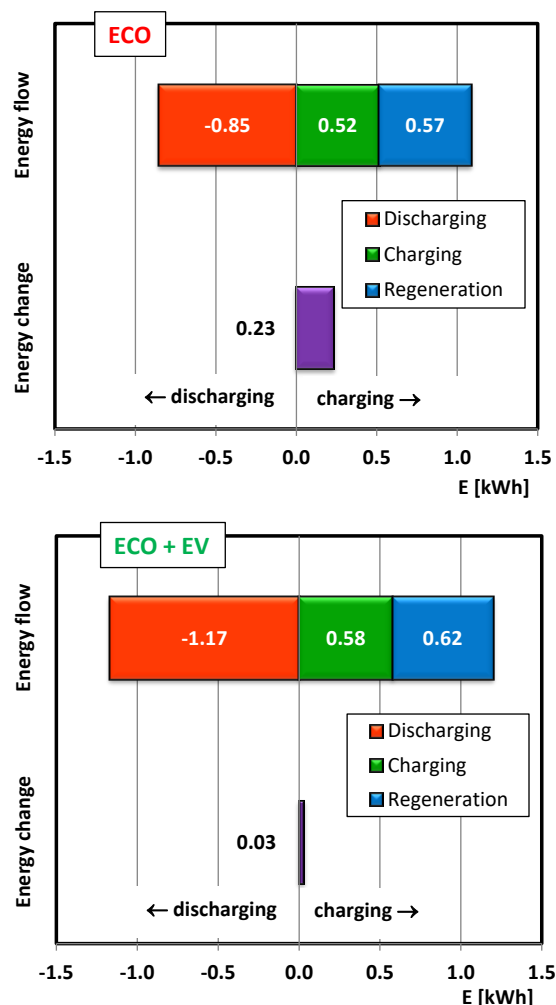


Fig. 3. Energy flow to/from the battery in a hybrid drive in urban conditions (negative values indicate discharging the battery)

From the data in Table 3 the operating time density of individual vehicle driving modes have been calculated. The results were presented in terms of both the time and the distance traveled (the differences in the result are from the vehicle's standstill).

The data comparison is included in Fig. 5, where the distance and time are shown in relative terms. Despite the different driving modes, there are significant similarities in the time densities of individual driving modes. Driving in electric mode at a constant speed ( $a_0$  EV) and braking in this driving mode ( $a-$  EV) represent high total drive time contributions. Their shares are large both in relation to the test route distance and the total travel time.

Using these analyzes, the percentage share of electric mode operation time was determined, this was done by summing the values of the EV system operation modes, i.e.

driving without the active combustion engine, acceleration and braking with energy recovery without the internal combustion engine being on. The obtained results are compared in Fig. 6.

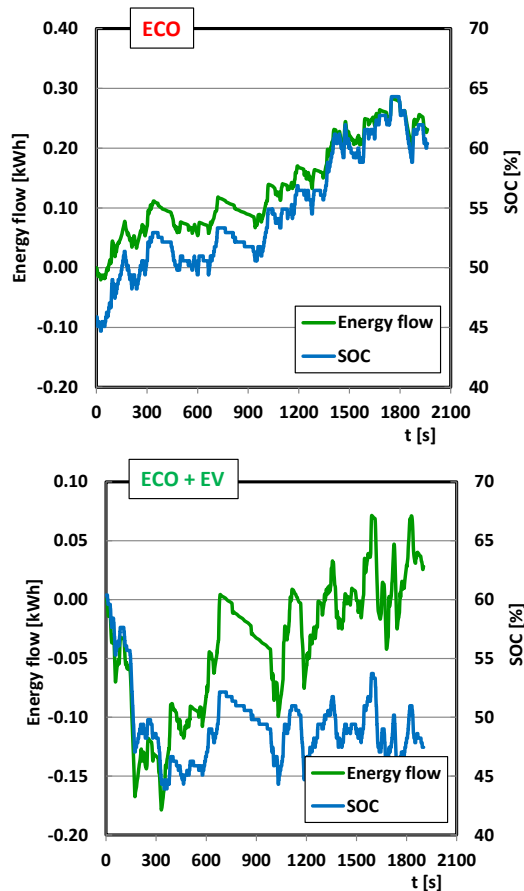


Fig. 4. Comparison of energy flow and changes in battery charge

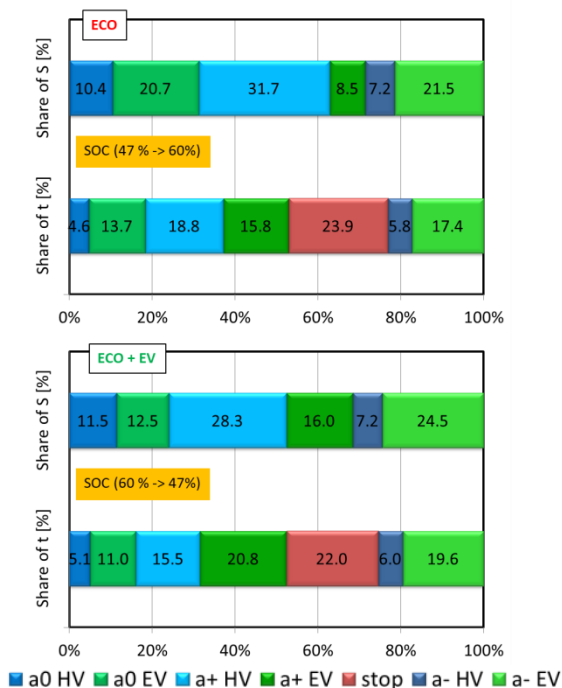


Fig. 5. The percentage share of individual driving modes in relation to time and distance traveled during the test

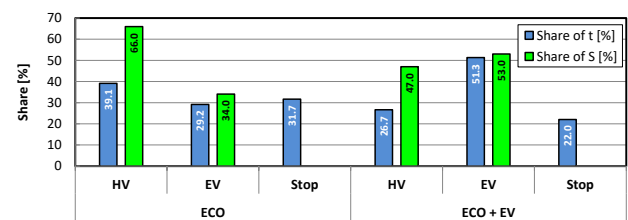


Fig. 6. The share of hybrid and electric mode in urban traffic conditions in relation to the road and time of the vehicle test drive

After summing up individual vehicle energy flow types in electric mode, the EV mode participation in the overall drive was determined (Fig. 6).

## 6. Conclusions

Based on the obtained results, it can be stated that the latest hybrid vehicles are characterized by a larger share of the system's operation in electric mode than in the hybrid mode. The percentage share of the electric mode operation was in the range 51%–53% of the distance traveled and about 46–51% of the test duration (depending on the test). The final percentage result is influenced by many factors, including the current traffic volume, vehicle load, initial high-voltage battery charge (SOC), standstill time at the intersection with traffic lights, and the driving style of the driver.

The performed tests in urban conditions indicate, the share of energy recovery from regenerative braking is over 50% of all energy supplied to the battery while driving (from both charging from the generator and regenerative braking). This indicates the efficiency of energy recovery from braking and indicates the desired energy flow (battery charge) in the hybrid drive system. Braking energy recovery, a significant share of electric drive operation, operating costs reduction, lower emission of harmful and toxic compounds into the environment without significant financial costs are undoubtedly arguments in favor of using hybrid drives.

The obtained results apply to currently used vehicles with hybrid drive systems using Ni-MH batteries. The share of hybrid vehicles in electric mode with Li-Ion batteries in use (vehicles that can also be charged from a plug-in electrical socket) should be much larger. This is influenced by the much larger electric capacity of the batteries and the higher discharge values relative to the nickel-metal hydride batteries. However, this solution is also associated with much greater battery pack mass and dimensions. When choosing a vehicle, its place of exploitation should be taken into account. In the hybrid systems of current vehicles with Ni-MH batteries, the usefulness of a vehicle in urban traffic means a reduction of the classic internal combustion engine use by more than 50%. However, this trend will not be reflected in vehicles used on non-urban routes, where an increased operating time share of the internal combustion engine is necessary to achieve higher vehicle speeds.

*The research presented in this paper was performed within the statutory work, project no. 05/52/DSMK/0265.*

## Acknowledgement

The authors would like to thank Mr Andrzej Szalek – representatives at Toyota and Lexus Academy in Toyota Motor Poland Company Ltd. in Warsaw, Poland for their provision of an vehicle for testing.

## Nomenclature

a	acceleration	$M_{reg}$	braking torque
CNG	compressed natural gas	n	engine speed
CO <sub>2</sub>	carbon dioxide	NiMH	nickel hydride battery
E	energy	RDC	real driving conditions
ECO	eco mode	RDE	real driving emission
EV	electric vehicle	SOC	state of charge
HEV	hybrid electric vehicle	S	vehicle speed
I	current	t	time
IB	battery current	U	voltage
Li-Ion	lithium-ion battery	v	velocity

## Bibliography

- [1] Central Statistical Office. Transport – results of operations in 2016, [www.stat.gov.pl](http://www.stat.gov.pl) (accessed 26.11.2017).
- [2] CIEŚLIK, W., PIELECHA, I. SZALEK, A., Indexes of performance of combustion engines in hybrid vehicles during the UDC test. *Combustion Engines*. 2015, **160**(1), 14-27.
- [3] HUTCHINSON, T., BURGESS, S., HERRMANN, G. Current hybrid-electric powertrain architectures: Applying empirical design data to life cycle assessment and whole-life cost analysis. *Applied Energy*. 2014, **119**, 314-329, DOI: 10.1016/j.apenergy.2014.01.009.
- [4] IWATA, K., MATSUMOTO, S. Use of hybrid vehicles in Japan: An analysis of used car market data. *Transportation Research Part D: Transport and Environment*. 2016, **46**, 200-206. DOI: 10.1016/j.trd.2016.03.010.
- [5] KAPUSTIN, A., RAKOV, V. Methodology to evaluate the impact of hybrid cars engine type on their economic efficiency and environmental safety. *Transportation Research Procedia*. 2017, **20**, 247-253. DOI: 10.1016/j.trpro.2017.01.057.
- [6] KISHI, H.T. Towards Sustainability – Toyota's way to develop the next generation vehicles. 38. *Internationales Wiener Motorensymposium*. 2017.
- [7] KORTAS, P., KROPIWNICKI, J. Analysis of accumulation possibility of energy dissipated in the braking process of train driven by hybrid locomotive. *Combustion Engines*. 2015, **162**(3), 631-638.
- [8] MATSUBARA, T., YAGUCHI, H., TAKAOKA, T. et al. Development of new hybrid system for compact class vehicles. *SAE Technical Paper* 2009-01-1332, 2009. DOI: 10.4271/2009-01-1332.
- [9] MATSUMURA, M., SHIOZAKI, K., MORI, N. Development of new hybrid transaxle for mid-size vehicle. *SAE Technical Paper* 2018-01-0429, 2018. DOI: 10.4271/2018-01-0429.
- [10] MERKISZ, J., PIELECHA, I. Mechanical systems for hybrid vehicles. 2015, *Publishing House Poznan University of Technology*.
- [11] MERKISZ, J., PIELECHA, J. Nanoparticle emissions from combustion engines. Springer Tracts on Transportation and Traffic. 2015, **8**, Springer International Publishing Switzerland.
- [12] OSHIMA, K., KATO, S. New multi stage hybrid system for the LC500h with innovative drivability of the THSII. 39. *Internationales Wiener Motorensymposium*. 2018.
- [13] PIELECHA, I., CIEŚLIK, W., SZALEK, A. Operation of electric hybrid drive systems in varied driving conditions. *Eksploatacja i Niezawodność – Maintenance and Reliability*. 2018, **20**(1), 16-23. DOI: 10.17531/ein.2018.1.3.
- [14] PIELECHA, I., CIEŚLIK, W., SZALEK, A. Operation of hybrid propulsion systems in conditions of increased supply voltage. *International Journal of Precision Engineering and Manufacturing*. 2017, **18**, 1633-1639. DOI: 10.1007/s12541-017-0192-3.
- [15] PIELECHA, J., MERKISZ, J., MARKOWSKI, J. et al. Analysis of passenger car emission factors in RDE tests. *International Conference on the Sustainable Energy and Environment Development*, SEED, 2016. DOI: 10.1051/e3sconf/20161000073
- [16] SAXENA, S., PHADKE, A., GOPAL, A. Understanding the fuel savings potential from deploying hybrid cars in China. *Applied Energy*. 2014, **113**, 1127-1133. DOI: 10.1016/j.apenergy.2013.08.057.
- [17] STELMASIAK, Z., LARISCH, J., PIELECHA, J. et al. Particulate matter emission from dual fuel diesel engine fuelled with natural gas. *Polish Maritime Research*. 2017, **24**(2), 96-104. DOI: 10.1515/pomr-2017-0055.
- [18] [toyota-tech.eu](http://toyota-tech.eu) (accessed 10.01.2018)
- [19] WILBERFORCE, T., EL-HASSAN, Z., KHATIB, F.N. et al. Developments of electric cars and fuel cell hydrogen electric cars. *International Journal of Hydrogen Energy*. 2017, **42**(40), 25695-25734. DOI: 10.1016/j.ijhydene.2017.07.054.

Prof. Ireneusz Pielecha, DSc., DEng. – Faculty of Machines and Transport, Poznan University of Technology.

e-mail: [Ireneusz.Pielecha@put.poznan.pl](mailto:Ireneusz.Pielecha@put.poznan.pl)



Wojciech Cieślík, DEng. – Faculty of Machines and Transport, Poznan University of Technology.

e-mail: [Wojciech.Cieslik@put.poznan.pl](mailto:Wojciech.Cieslik@put.poznan.pl)



Kinga Fluder, MEng. – Faculty of Machines and Transport, Poznan University of Technology.

e-mail: [Kinga.Fluder@student.put.poznan.pl](mailto:Kinga.Fluder@student.put.poznan.pl)





## The injector location impact on the fuel combustion process in a direct gasoline injection system

The article contains an analysis of the fuel dose combustion phenomena and exhaust emissions in a direct injection system of an SI engine for variable injector location in the combustion chamber. The research performed is a continuation of the research presented in the article CE-2018-104. The tests were performed using the AVL Fire 2017 simulation environment. 27 injector placement combinations in three planes were analyzed: axial distance from the cylinder axis, injector depth relative to the head and angular position relative to the cylinder axis. An optimal solution was chosen, taking into account the significance of individual indicators. It was shown that the greatest impact in terms of the most advantageous combustion process indicators is the injector setting depth in the combustion chamber cavity, while the distance from the cylinder axis is of secondary importance. The smallest changes in the combustion and emission factors values are seen with the change of the injector placement angle (in the value range used in this study).

Key words: gasoline direct injection, fuel combustion, exhaust emission, simulation software

### 1. Introduction

Combustion process tests carried out on real combustion engines require high financial and material investment relative to the same type of research conducted using the CFD (computational fluid dynamics) technique. The initial stage of combustion system design relies on data from simulation projects [1, 13, 16, 22]. Despite this fact, the final verification of such results are tests performed on real test objects and prototypes [2, 7, 15, 20].

Numerous research works conducted by scientists around the world confirm the usefulness of research on the hydrocarbon fuel mixtures combustion process. Huang et al. [9] found that direct injection of a dose of ethanol into a homogeneous gasoline-air mixture has a positive effect on the combustion knock prevention, but it also has a negative impact on the exhaust emission values. The compromise can, however, be achieved by a more careful choice of the ethanol injection angle. The earlier it is, the smaller is the negative impact on exhaust emissions, but then the ethanol cooling properties are not fully exploited to prevent knock.

Research on fuel mixing is also one of the subjects in the development of CI engines. Lee et al. [14] have demonstrated the high potential of using additional gasoline injection for the SI engine at low loads to significantly reduce nitrogen oxides emissions.

The results presented below are a continuation of research on the fuel injection process shaping by modifying the injector placement in the combustion chamber. The results of these tests can be found in [18]. These previous tests allowed to determine the most advantageous position of the injector in the aspect of injection and fuel atomization. The same variants of injector placement settings were used in this article to analyze the combustion process and exhaust emissions.

The presented considerations are aimed overall at analyzing a dual-fuel system in which both injectors are placed in the combustion chamber. Similar studies of the dual-fuel system in the PFI-DI configuration have already been carried out earlier [4, 5, 8, 16, 19]. These studies, however, do not encompass the same methods and measurement parameters as intended for this article, and subsequent tests

are aimed at determining the fuel mixing indicators in the combustion chamber immediately before ignition.

### 2. Research aim and goals

The proposed tests constitute the injection and combustion process study stage for a direct injection system of liquid hydrocarbon fuels [17]. This stage focuses on determining the engine processes indicators using one direct gasoline injection injector while changing its location in the engine combustion chamber.

The goal of the research is to determine the optimal spatial position of the injector relative to the spark plug and the angular position of its axis relative to the cylinder axis. The optimal location will be defined as such a position, at which the sum of thermodynamic combustion and emission indicators will be the highest, while remaining within the set limits and considering the weight of each indicator.

### 3. Research methodology

#### 3.1. Combustion chamber geometry

The combustion process tests were done using the AVL Fire 2017.1 simulation software. The shape of the combustion chamber was modeled (Fig. 1a) and imported into the simulation software (Fig. 1b). The displaceable mesh with a square side of 1 mm was automatically condensed in the vicinity of the spark plug to a value of 0.1 mm. The engine specifications are shown in Table 1.

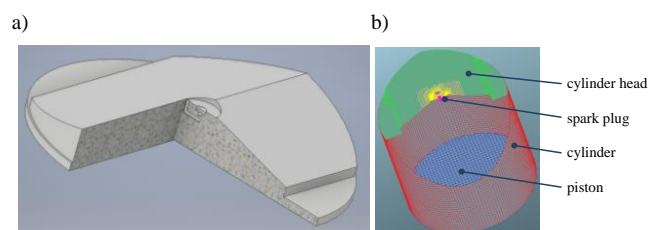


Fig. 1. The combustion chamber including the spark plug: a) 3D drawing, b) the mesh in AVL Fire program

Each injector position is described by a code describing the position change with respect to the y-axis, with respect to the z-axis and a change of angle with respect to the axis of the cylinder:

$$y(i)z(j)\alpha(k) \quad (1)$$

where:  $i = 7 \text{ mm}, 8 \text{ mm}$  and  $9 \text{ mm}$ ,  $j = 9 \text{ mm}, 10 \text{ mm}$  and  $11 \text{ mm}$ , and  $k = 15, 17.5$  and  $20 \text{ deg}$ .

Table 1. Modeled engine technical data

Parameter	Unit	Value
Type	—	Piston engine, 4-stroke, spark ignition
Cylinder number	—	1
Displacement	$\text{cm}^3$	385
Compression ratio	—	10.2
Bore	mm	83
Stroke	mm	71.2
SOI	deg	670
Injection duration	ms	0.6
Injected fuel dose	mg	13.1
$\lambda$ -value	—	1
Ignition CA	deg	690

Test conditions include 27 injector placement configurations. These configurations are shown in Fig. 2, and the matrix of test settings in Fig. 3.

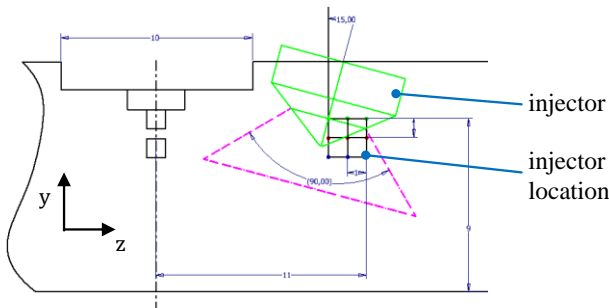


Fig. 2. The combustion process tests configuration considering the change of the linear and angular position of the injector

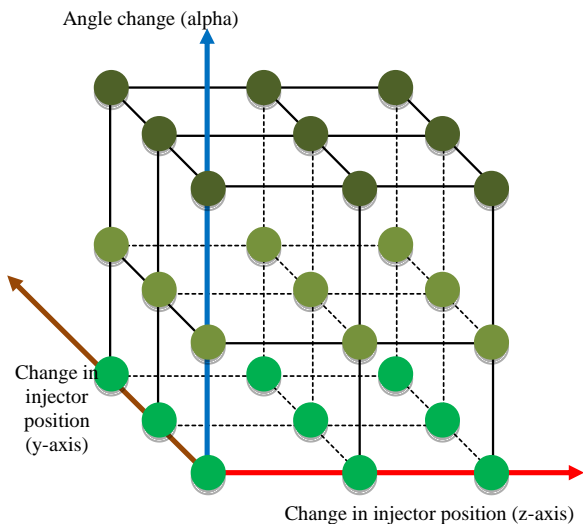


Fig. 3. The combustion process test with injector placement variants matrix

### 3.2. Initial conditions

The initial conditions of the compression process and the combustion process were adopted in accordance with the values listed in Table 2. Such conditions correspond to a spark-ignition engine with direct petrol injection operating at the speed of 2000 rpm.

Table 2. Initial conditions accepted for simulation calculations

Parameter	Unit	Value
Pressure	bar	0.6
Temperature	K	300
Turbulence kinetic energy (specific)	$\text{m}^2/\text{s}^2$	10
Turbulence integral length scale	mm	3
Turbulence dissipation rate	$\text{m}^2/\text{s}^3$	1732.05
Tumble rotational speed	rpm	3000
Engine speed	rpm	2000
Crank angle	deg CA	570–800

### 3.3. Combustion process and exhaust emission modeling

#### 3.3.1. Combustion modeling

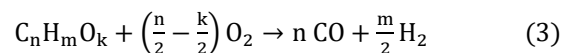
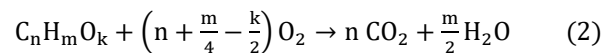
The conditions inside the combustion chamber before combustion were determined according to the process described in [18]. The Extended Coherent Flame Model (ECFM) with the spherical shape of the initial flame nucleus was adopted for combustion simulation calculations [3].

Coherent Flame Model (CFM) is built on the basis of a laminar flamelet concept, whose velocity  $S_l$  and thickness  $\delta_l$  are mean values, integrated along the flame front, only dependent on the pressure, the temperature and the fresh gases content.

ECFM is often used to model combustion in spark-ignition engines. Ji et al. [10] compared the combustion process of gasoline and gasoline mixtures with hydrogen modeled using ECFM with a simulated combustion process. The error was deemed to be less than 6%. This model is also used to analyze the combustion process in hydrogen-only engines. Knop et al. [11] used this model to simulate combustion in an engine with indirect and direct hydrogen injection. Colin et al. [6] showed a good correlation between the ECFM model and the combustion process in the first 1.8 GDI engine used in a passenger car.

#### 3.3.2. Modeling the exhaust emission

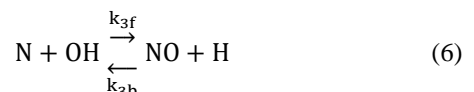
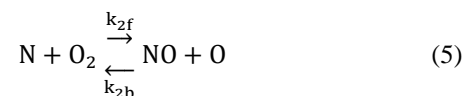
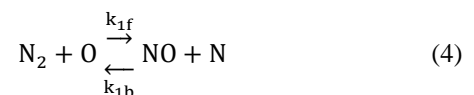
The use of the Extended Coherent Flame Model results in a two-step fuel combustion reaction according to reactions (2) and (3).



In the above formulas  $n$ ,  $m$  and  $k$  represent the number of carbon, hydrogen and oxygen atoms of the considered fuel.

The mean laminar fuel consumption rate is the sum of the reaction rates of the above reactions, whereas their respective values are dependent on the local equivalence ratio and the number of carbon and hydrogen atoms.

The Extended Zeldovich Model, which utilizes the reaction formulas (4)–(6), was used to describe the NO formation.

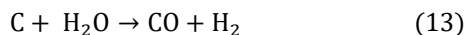
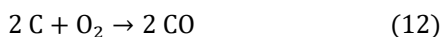
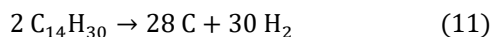
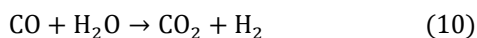
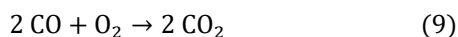
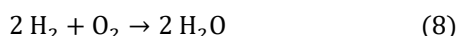
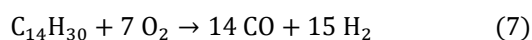


The thermal NO reactions are highly dependent on the temperature, process duration and atomic oxygen concentration. The first reaction (4) has a very high activation energy due to the strong N<sub>2</sub> triple bond. The rate of formation of NO is significant only at high temperatures (greater than 1800 K).

All the required radicals for this NO formation model are calculated based on the equilibrium approach, known and used in the ECFM combustion model (mentioned above) [3].

According to Kosmadakis et al. [12], the Zeldovich extended model is the most commonly used for the nitrogen compounds formation analysis. Analyzing four different calculation models, the authors also found that for the stoichiometric mixture 90% of the produced NO corresponds to the equations of this model.

To describe the soot formation, the Kinetic Soot Model was used. The model can describe the behavior of soot formation and oxidation for different fuel classes. Exact reactions have been implemented for methane, propane, ethanol, n-heptane and tetradecane. If the fuel, which has been specified by the user, does not exactly match one of these species, FIRE decides automatically the best parameter set to be used. The reactions (7)–(13) describe the chemical behavior for tetradecane.



The soot is oxidized due to the presence of oxygen and water. The reaction parameters for the main soot formation are dependent on the local equivalence ratio [3].

Tan et al. [21] collected and described the conclusions of using the kinetic soot model in the analysis of exhaust emissions from direct injection spark-ignition engines. They acknowledged in their paper that multi-step semi-empirical models provide a relatively complete characterization of soot processes at affordable computational cost and effort, considering the trade-off between accuracy and applicability.

## 4. Impact of the injectors placement on the combustion conditions

### 4.1. Thermodynamic indicators of the combustion process

For the quantitative analysis of the combustion process, the mean combustion temperature, the mean combustion pressure, the heat release rate and the total heat released in the combustion process were selected as its thermodynamic indicators. The impact of the injector location on these indicators values is presented in Figs. 4–6.

Figure 4 shows the impact that the injector position change along the y axis (according to Fig. 2) has on the

combustion process thermodynamic indicators. From the graphs and values of these indicators, it can be concluded that the most desirable position of the injector is the one in which the injector is the furthest out (the smallest value of the y coordinate). In this position (value y = 7 mm), the mean combustion temperature, the mean combustion pressure, the maximum heat release rate and the total heat released obtain their highest respective values. This is due to the best mixture preparation (as shown in [18]) and the fuel atomization and flame propagation that are best coordinated in time and space. The extreme positions of the injector along the variable y (position changes in relation to the cylinder axis) relative to the solution adopted (y = 7 mm) result (relative to maximum values) in:

- increasing the mean temperature by 4.2%;
- increasing the mean pressure by 5.6%;
- increasing the heat release rate by 24.3%;
- increasing the total heat release by 3.9%.

Changes in the position of the injector relative to the z axis (distance from the spark plug) do not cause such large changes in the analyzed indicators (Fig. 5). The best solution for the selected values of other parameters (y = 7 mm, alpha = 15 deg) is the value (z = 10 mm), which does not confirm the spray analysis described in article [18]. Three out of four indicators have the highest value for this position. Comparing this choice of the z axis position (z = 10 mm) with the position which give the least favourable indicator values (z = 11 mm) result in:

- increasing the mean temperature by 1.6%;
- increasing the mean pressure by 4.1%;
- increasing the heat release rate by 1.2%;
- increasing the total heat release by 0.9%.

The indicator values do not clearly reveal the most favourable injector position in terms of z axis position. The z = 10 mm position gives the maximum values for mean temperature, mean pressure (ex aequo at z = 9 mm) and for total heat released, the z = 9 mm position gives the highest values for maximum pressure (mentioned previously) and the heat release rate, whereas position z = 11 mm gives the total heat released value higher by 2.0% than position z = 9 mm.

This example also shows that it is reasonable to perform parallel research on the spray and combustion processes.

Following the conclusion on the injector position selection in the combustion chamber during the atomization analysis described in the [18], the remaining geometric parameters of the injector axis relative to the cylinder axis: y = 7 mm and z = 9 mm were selected for determining the injector angle position.

Analyzing the impact of the injector position angle in the combustion chamber, it can be stated that it has a much more significant impact on changes in the researched combustion indicators than on changes in the injection indicators. This is due to the introduction of the initial turbulence before ignition, which affects the flame development. The most favorable results in this analysis were obtained at an angle of 20 deg. Three of the four analyzed indicators reach their highest values: mean temperature, mean pressure and total heat released. Comparing the most extreme angular positions of the injector with respect to the angle alpha = 15 deg, resulted in:



- increasing the mean temperature by 3.5%;
- increasing the mean pressure by 11.9%;
- decreasing the heat release rate by 10.9%;
- increasing the total heat release by 3.3%.

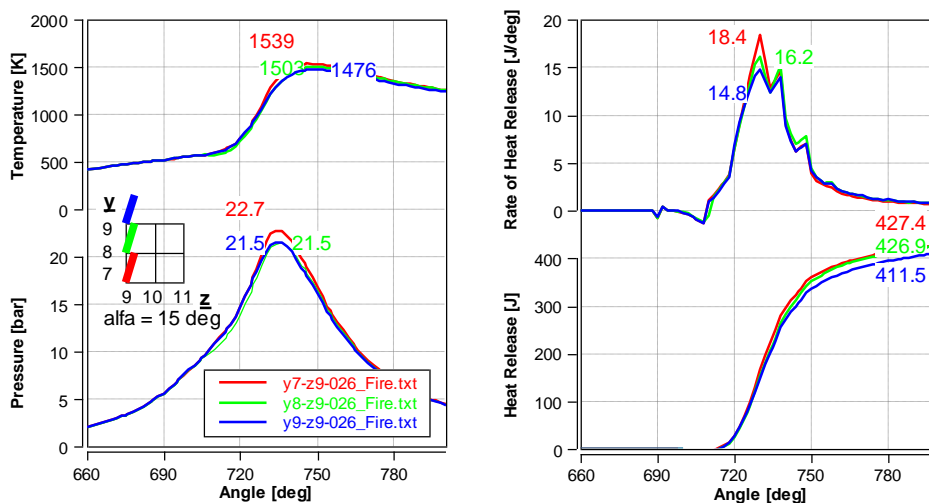


Fig. 4. Effect of the injector position change on the combustion process indicators – y coordinate (change of the injector placement height in the combustion chamber)

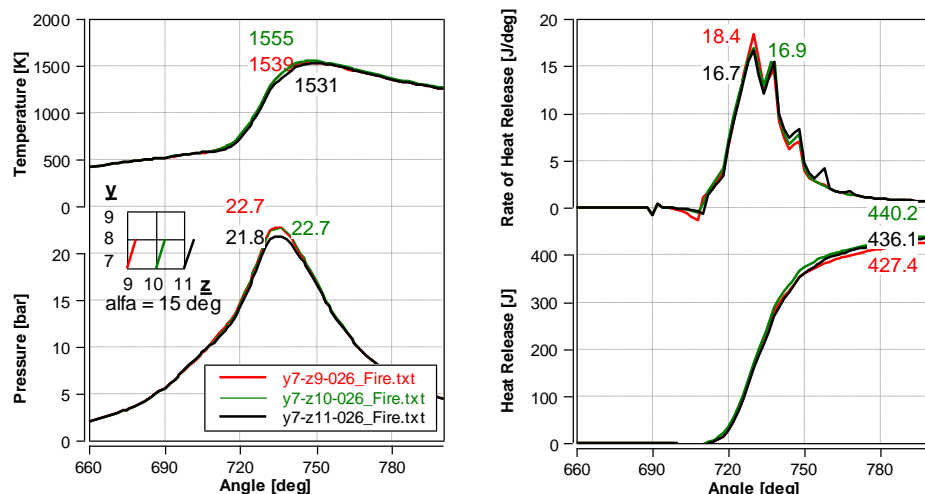


Fig. 5. Effect of the injector's position change on the combustion process indicators – coordinate z (changes of the injector distance from the spark plug in the combustion chamber)

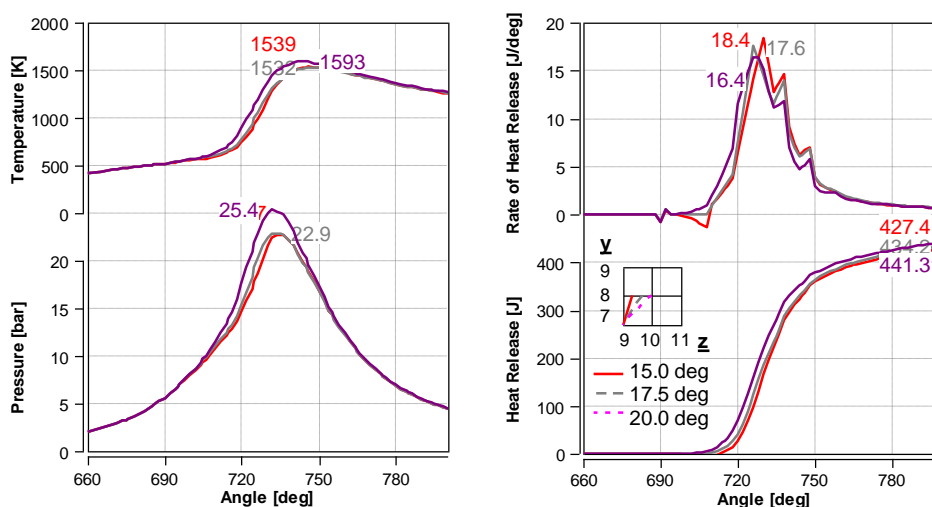


Fig. 6. The effect of the injector position change in the combustion chamber on combustion process indicators – alpha angle

#### 4.2. Process combustion indicators

Complementing the combustion process analysis in relation to the injector location geometric parameters in the combustion chamber, the emission of exhaust gases was tested (concentration was used because the results refer to a single engine operating point). Four indicators were used: nitrogen oxide emission, soot emission, carbon dioxide emission and carbon monoxide emission. Minimum CO and soot emission values as well as maximum values of NO and CO<sub>2</sub> emissions were assumed as the most desirable.

An increase of the NO concentration was assumed to indicate a more favorable combustion process, despite the fact that high NO concentration itself is undesirable. The reduction of NO emissions, however, was not the subject of this research.

As shown in Fig. 7, change in the geometric coordinate  $y$  affects the concentration of soot and carbon monoxide the

most. This is due to the preparation of the mixture in the initial combustion phase, during which the proportion of oxygen per hydrocarbon molecules in the fuel around the spark plug is insufficient for full and complete combustion to occur.

The largest injector insertion in the combustion chamber ( $y = 7$  mm) results in the formation of an area around the spark plug, where the concentration of soot is the lowest, while the highest NO concentration in this configuration indicates a high combustion process efficiency.

Comparing the extreme positions of the injector in the  $y$  axis (7 and 9 mm) relative to the selected position ( $y = 7$  mm), the following results were obtained:

- increasing the NO concentration by 7.8%;
- decreasing the soot concentration by 55.0%;
- increasing the CO<sub>2</sub> concentration by 2.0%;
- increasing the CO concentration by 12.6%.

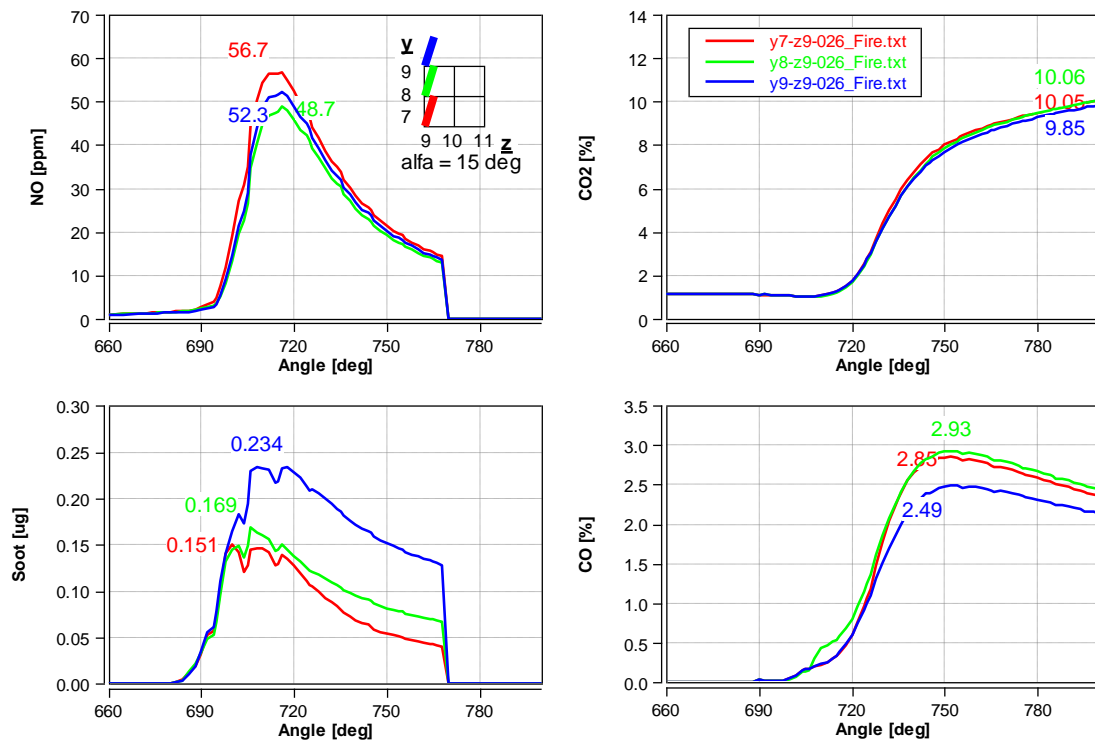


Fig. 7. The effect of the injector position change on emission indicators –  $y$  coordinate (change of the injector placement height in the combustion chamber)

According to the adopted criteria for the exhaust emissions quality assessment and the adopted fixed geometric parameters,  $y = 7$  mm and the angle  $\alpha = 15$  deg, the analysis of the effect of changing the  $z$ -coordinate on the concentration of selected exhaust components was performed. It has been shown in Fig. 8 that the most effective combustion process takes place at the injector position with  $z = 11$  mm. For this injector position relative to the other extreme position along the  $z$  axis ( $z = 9$  mm) the results were:

- increasing the NO concentration by 26.3%;
- increasing the soot emission by 3.3%;
- increasing the CO<sub>2</sub> concentration by 0.7%;

- decreasing the CO concentration by 3.2%.

Analysis of the injector angular position relative to the cylinder axis with respect to the exhaust emissions (with a fixed linear position of the injector tip at  $y = 7$  mm and  $z = 9$  mm) does not indicate clear results for optimal injector placement inside the combustion chamber. Comparison of the angular position 20 deg with respect to the  $\alpha = 15$  deg position results in the following changes:

- increasing the NO concentration by 33.7%;
- increasing the soot concentration by 160.3%;
- increasing the CO<sub>2</sub> concentration by 3.5%;
- decreasing the CO concentration by 5.3%.

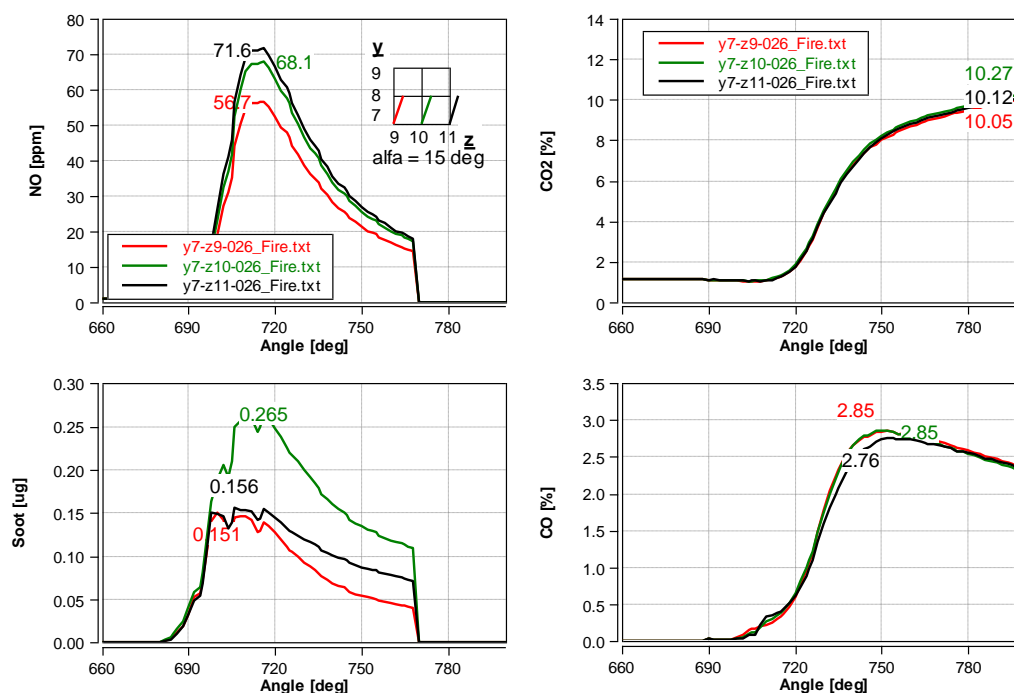


Fig. 8. Effect of the injector position change on emission indicators (concentration) – z coordinate (change of the injector distance from the spark plug in the combustion chamber)

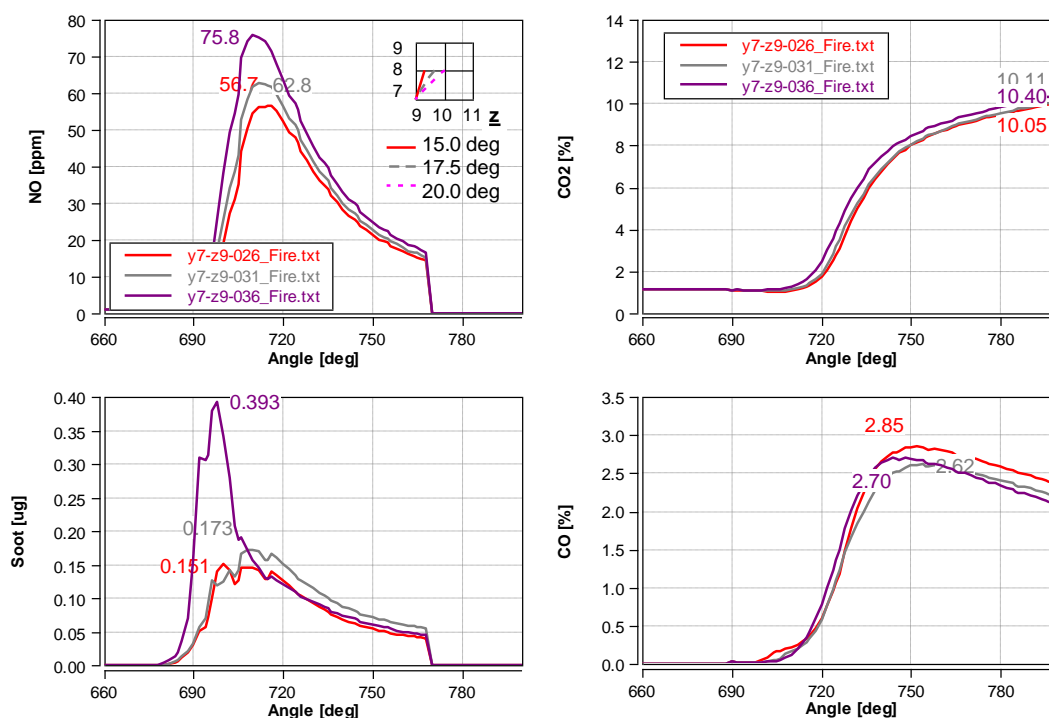


Fig. 9. The effect of the injector position change in the combustion chamber on exhaust emission indicators – alpha angle (injector position)

The next research stage was the spatial analysis of selected thermodynamic indicators. The temperature distribution in the combustion chamber as well as the distributions of NO and soot concentration are presented below.

The analysis of Fig. 10 shows the most rapid combustion process for the injector angular position  $\alpha = 20^\circ$ . The most rapid temperature increase was obtained in this case, as seen in the figure when the whole chamber is covered with high temperature values at a fairly late stage.

Analysis of the 3D exhaust compounds formation results indicates that the angular position of the injector has a large impact on the intermediate states of nitric oxide and soot formation (Fig. 11–12). This means that the average values presented in Fig. 8 do not allow a full compounds formation assessment during combustion. Detailed analysis can be used to further optimize the injector placement with regard to shaping the combustion products.



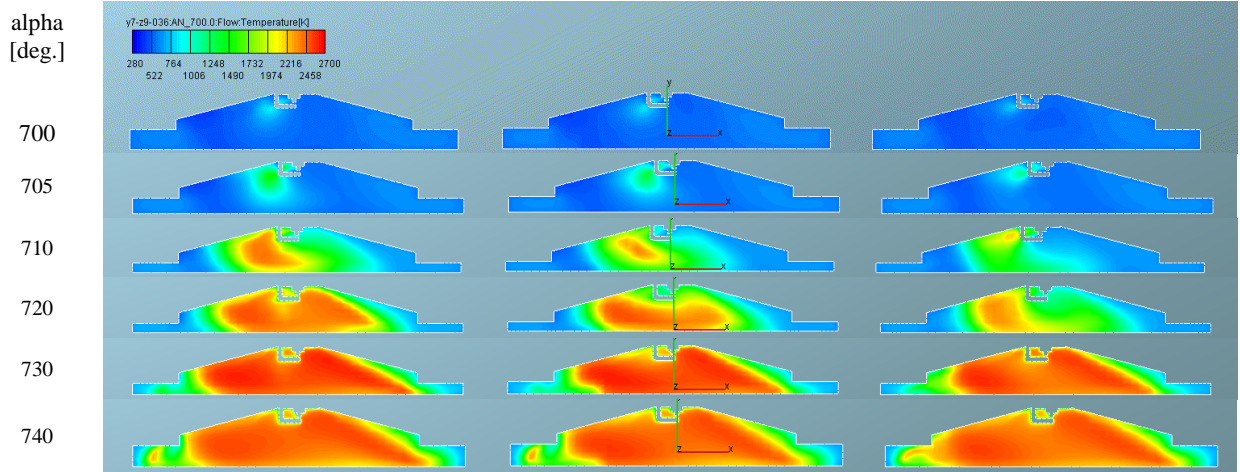


Fig. 10. Temperature distribution during combustion at the injector position  $y = 7$  mm,  $z = 9$  mm and angle value being respectively:  $\alpha = 15$  deg,  $\alpha = 17.5$  deg and  $\alpha = 20$  deg

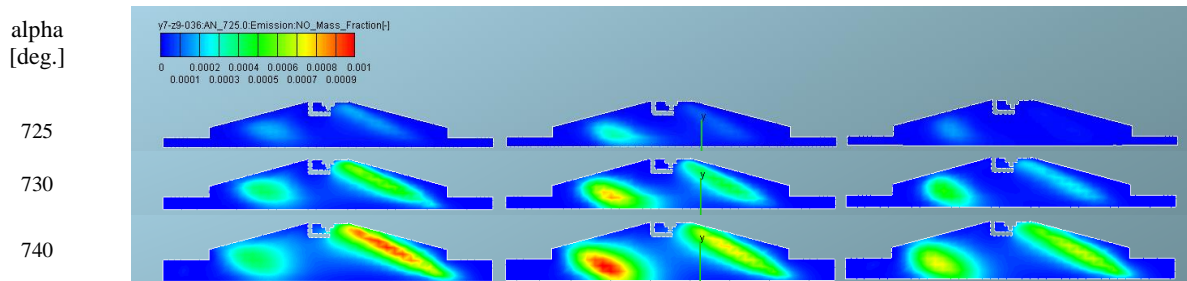


Fig. 11. The NO concentration distribution during combustion at the injector position  $y = 7$  mm,  $z = 9$  mm and angle value being respectively:  $\alpha = 15$  deg,  $\alpha = 17.5$  deg and  $\alpha = 20$  deg

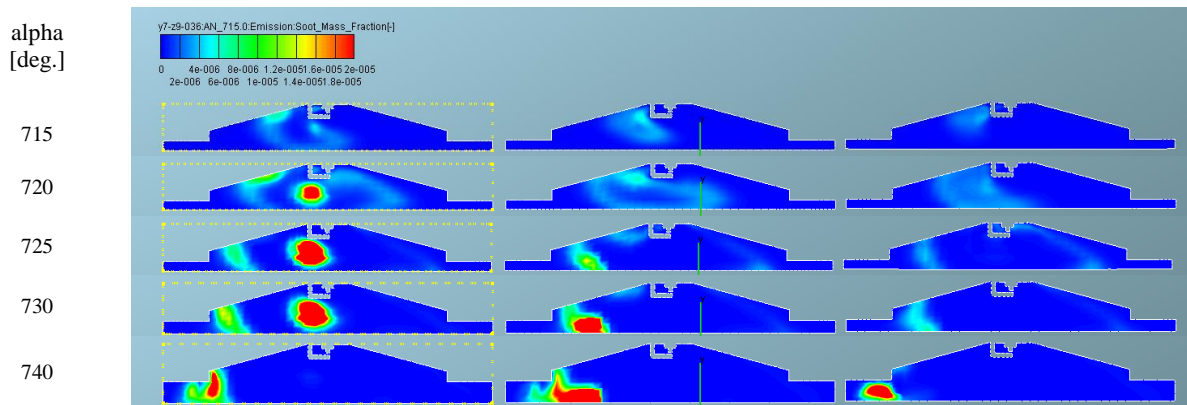


Fig. 12. The spatial soot formation distribution during the combustion process at the injector position  $y = 7$  mm,  $z = 9$  mm angle value being respectively:  $\alpha = 15$  deg,  $\alpha = 17.5$  deg and  $\alpha = 20$  deg

## 5. Combustion process evaluation using combustion indicators – determining the best configuration

First, the maximum pressure was determined for all injector positions relative to the angle of its location (Fig. 13a). The comparison indicates that the highest maximum cylinder pressure value does not occur at the same injector position at each one of its placement angles. The highest maximum pressure values were obtained at the injector coordinates of  $y(7)z(9)\alpha(15)$  and  $y(7)z(9)\alpha(20)$  – which means  $y = 7$  mm and  $z = 9$  mm at the angles of 15 and 20 deg. However, at an angle of 17.5 deg, the best option was to place the injector at the coordinates  $y = 9$  and  $z = 9$  (code  $y(9)z(9)\alpha(17.5)$ ).

Analysis of the total heat released in the combustion chamber shows tendencies similar (Fig. 13b) to previous considerations. The largest values of the total heat released were obtained for the different sequences.

These considerations prompted the authors to determine the best injector position through pseudo-optimization. With the obtained values of maximum cylinder pressure, maximum cylinder temperature, total heat released, CO, CO<sub>2</sub> and NO emission, and soot formation, the data was scaled.

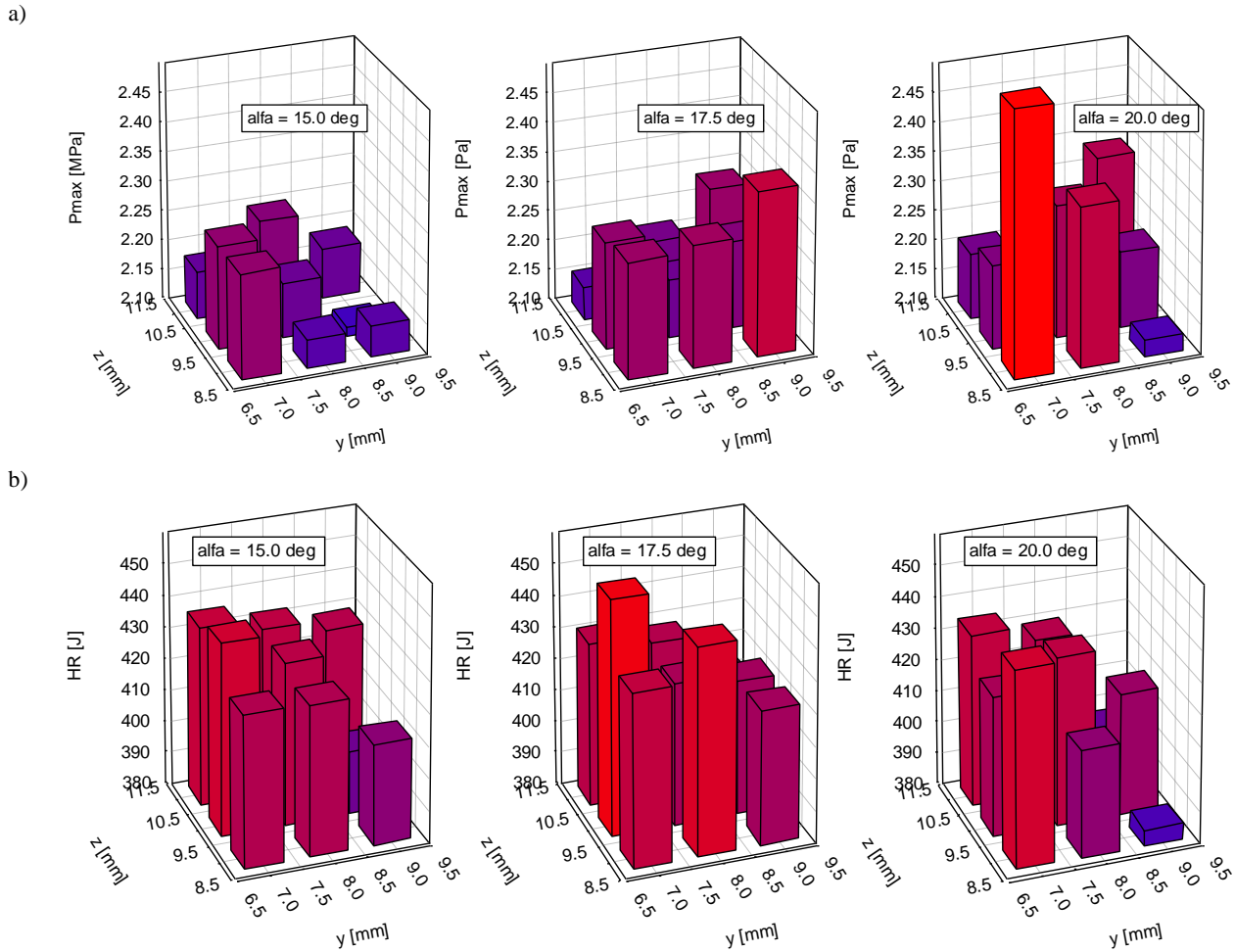


Fig. 13. Rate of combustion changes: a) maximum pressure in the cylinder, b) maximum amount of heat produced at various injector positions in the combustion chamber

Thus the following values have been used:

- the best value for a given indicator to take (the highest cylinder temperature, the highest cylinder pressure, the largest amount of heat released, the largest CO<sub>2</sub> and NO concentration, the smallest CO fraction and the smallest formed soot factor) that can be obtained is equal to 1;
- the worst possible indicator value is 0.

The scaling was performed on this basis, and the results are presented in Table 3. The values of specific indicators have been assigned to each of the injector's positions. Changes in these values occur in the range of  $<0;1>$ . The table also contains a pictogram analysis, which shows that the most positive results occur when placing the injector at the coordinates  $y = 7$  mm and  $z = 9$  mm or  $z = 10$  mm. The worst position of the injector is the one with the  $y$  coordinate of  $y = 9$  mm.

Due to the fact that it was still impossible to determine the best injector position, the normalized values of process indicators were summed for each injector position (Fig. 14). Using such a summation method, the maximum possible value became 7 (when all normalized indicator values obtained were equal to 1). The highest value of 5.57 normalized indicators was obtained for the injector position with the coordinates  $y = 7$ ,  $z = 9$  and the angle  $\alpha = 20$  deg (code:  $y(7)z(9)\alpha(20)$ ), as shown in the column titled

"Index" in Table 3. It should be noted, however, that the values do not show any tendency of the injector positioning based upon the indicators used, as it took place in spray analysis [18].

Additionally, in Fig. 14, the sums of normalized combustion indicators are summarized (sum of the "Index" column for individual injector positions). They were calculated as follows:

$$y(7 \text{ mm}) = \sum y(7)z(j)\alpha(k) \quad (14)$$

$$y(8 \text{ mm}) = \sum y(8)z(j)\alpha(k) \quad (15)$$

$$y(9 \text{ mm}) = \sum y(9)z(j)\alpha(k) \quad (16)$$

$$z(9 \text{ mm}) = \sum y(i)z(9)\alpha(k) \quad (17)$$

$$z(10 \text{ mm}) = \sum y(i)z(10)\alpha(k) \quad (18)$$

$$z(11 \text{ mm}) = \sum y(i)z(11)\alpha(k) \quad (19)$$

$$\alpha(15 \text{ deg}) = \sum y(i)z(j)\alpha(15) \quad (20)$$

$$\alpha(17,5 \text{ deg}) = \sum y(i)z(j)\alpha(17,5) \quad (21)$$

$$\alpha(20 \text{ deg}) = \sum y(i)z(j)\alpha(20) \quad (22)$$

where:  $i = 7, 8$  and  $9$  mm,  $j = 9, 10$  and  $11$  mm, while  $k = 15, 17,5$  and  $20$  deg.

Table 3. Relative values of fuel combustion rate and concentration of exhaust components at specified injector positions

y	z	alpha	Pmax	Tmax	HRmax	CO2-max	NO-max	CO-min	Soot-min	Index
mm	mm	deg	Pa	K	J	-	-	-		[-]
7	9	15	0.42	0.71	0.62	0.63	0.18	0.07	1.00	3.63
		17.5	0.46	0.67	0.72	0.68	0.32	0.29	0.84	3.98
		20	1.00	1.00	0.82	0.93	0.61	0.21	0.99	5.57
	10	15	0.41	0.80	0.81	0.82	0.44	0.07	0.98	4.32
		17.5	0.42	0.93	1.00	1.00	0.32	0.26	0.86	4.79
		20	0.34	0.52	0.57	0.71	0.55	0.23	0.93	3.85
	11	15	0.21	0.67	0.75	0.69	0.52	0.16	0.89	3.88
		17.5	0.15	0.59	0.67	0.72	0.31	0.03	0.92	3.40
		20	0.28	0.61	0.72	0.71	0.18	0.49	0.83	3.81
8	9	15	0.14	0.52	0.61	0.64	0.00	0.00	0.97	2.88
		17.5	0.48	0.81	0.87	0.90	0.30	0.32	0.97	4.65
		20	0.62	0.51	0.41	0.51	1.00	0.67	0.97	4.70
	10	15	0.24	0.66	0.67	0.88	0.79	0.20	0.98	4.43
		17.5	0.25	0.61	0.58	0.75	0.22	0.54	0.95	3.88
		20	0.52	0.71	0.70	0.75	0.72	0.41	0.85	4.66
	11	15	0.36	0.72	0.69	0.75	0.12	0.09	0.86	3.59
		17.5	0.29	0.58	0.63	0.73	0.62	0.18	0.91	3.94
		20	0.32	0.56	0.65	0.68	0.40	0.52	0.59	3.72
9	9	15	0.15	0.38	0.39	0.46	0.08	0.41	0.67	2.53
		17.5	0.64	0.57	0.54	0.60	0.82	0.65	0.79	4.61
		20	0.10	0.00	0.00	0.00	0.53	1.00	0.91	2.54
	10	15	0.00	0.33	0.22	0.49	0.72	0.50	0.79	3.03
		17.5	0.36	0.54	0.54	0.60	0.53	0.61	0.81	4.00
		20	0.31	0.44	0.48	0.50	0.60	0.52	0.87	3.73
	11	15	0.22	0.71	0.64	0.91	0.49	0.03	0.81	3.82
		17.5	0.45	0.60	0.42	0.70	0.78	0.37	0.70	4.03
		20	0.56	0.39	0.18	0.28	0.48	0.79	0.00	2.68

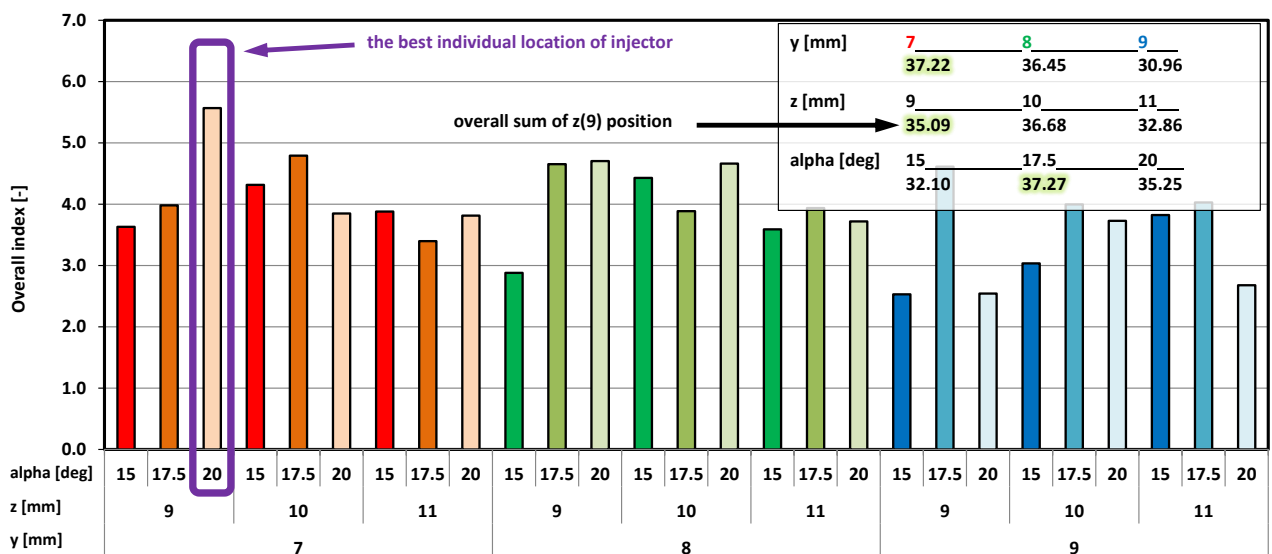


Fig. 14. Indicators of the best injector position selection based on the obtained parameters regarding fuel combustion conditions (based on Table 4)

The performed comparison leads to the conclusion that the highest point value was obtained for the injector position  $y = 7$  mm. This means that combustion indicators take the highest values at this injector position, regardless of the other position variables. This position, selected for the variable  $z$ , is  $z = 9$  mm. Although the best individual angular position turned out to be 20 deg (code  $y(7)z(9)\alpha(20)$  – at  $y = 7$  and  $z = 9$  mm), the best overall results were obtained at an angle of 17.5 deg without taking into account the  $y$  and  $z$  coordinates.

The injector position change sensitivity range was determined to be:

$$\Delta y = 0.5 \{ \max(y(i)z(j)\alpha(k)) - \min(y(i)z(j)\alpha(k)) \} \quad (23)$$

where the values  $\max()$  and  $\min()$  can be found in Table 3 ( $i, j, k$  are the same as in eq. (14)–(22)).

The results of these calculations are presented in Fig. 15. It follows that the results are most sensitive to the  $y$  coordinate injector position change – the injector position height. Another variable determining the total index sum



value (expressed in numerical form in Fig. 14) is the change in distance from the axis of the spark plug. The least sensitive parameter for changes in fuel atomization indicators is the injector position angle within the limits adopted for the performed simulation tests.

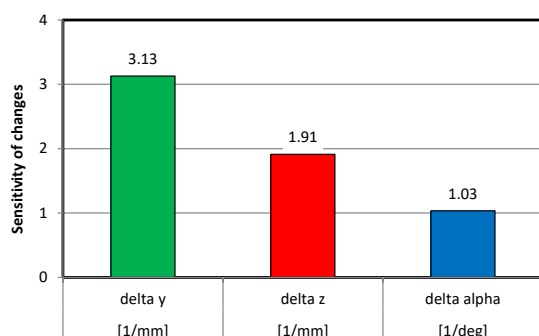


Fig. 15. The weighed impact of changes in y and z coordinates and the injector angle on the combustion process

## 6. Conclusions

Injector location tests were conducted using computer simulations, which were used to analyze the combustion indicators. The best solution was defined as one which, as a result of normalizing the indicators, it was possible to obtain the largest sum value of all these indicator values.

The pseudo-optimal location (within the adopted model boundaries), was characterized by:

- the largest inset in the combustion chamber  $y = 7$  mm,
- the shortest distance from the spark plug  $z = 9$  mm,
- the highest angle in relation to the axis of the cylinder  $\alpha = 20$  deg.

The differences in the indicator values between the maximum changes in the injector inset in the combustion chamber were:

- 4.2% mean value of maximum temperature;
- 5.6% mean value of maximum pressure;
- 3.9% total heat release;
- 7.8% NO concentration;
- 55.0% soot concentration;
- 2.0% CO<sub>2</sub> concentration;
- 12.6% CO concentration.

The differences between indicator values in most and least favourable position in terms of the injector distance from the spark plug were:

- 1.6% mean value of maximum temperature;
- 4.1% mean value of maximum pressure;
- 0.9% total heat release;
- 26.3% NO concentration;
- 3.3% soot concentration;
- 0.7% CO<sub>2</sub> concentration;
- 3.2% CO concentration.

The differences in the indicator values between the maximum changes in the injector angle relative to the cylinder axis were:

- 3.5% mean value of maximum temperature;
- 11.9% mean value of maximum pressure;
- 3.3% total heat release;
- 33.7% NO concentration;
- 160.3% soot concentration;
- 3.5% CO<sub>2</sub> concentration;
- 5.3% CO concentration.

Sensitivity of injector position changes was determined on the basis of the total indicator sum of changes in a given coordinate or angle (Fig. 15). This sensitivity analysis resulted in the following conclusions:

- the longitudinal injector position change is the most important parameter affecting combustion indicators changes;
- this change is about 1.6 times more significant than the change in the position of the injector's distance from the axis of the spark plug and about 3 times more significant than the angle of the injector's position.

The authors' previous study, focused on the fuel atomization in the described system [18] results in the same conclusion on the selection of the most favourable injector position ( $y = 7$  mm,  $z = 9$  mm,  $\alpha = 20$  deg). However, the analysis of both phenomena cannot be conducted separately, as the intermediate results vary upon different tendencies.

The conclusions obtained after the simulation analysis of the phenomenon will be taken into account in comparison of fuel atomization rates in the two injectors system and during combustion analysis in such a system.

## Acknowledgements

The study presented in this article was performed within the statutory research (contract No. 05/52/DSMK/0265).

## Bibliography

- [1] AHMADI, R., HOSSEINI, S.M. Numerical investigation on adding/substituting hydrogen in the CDC and RCCI combustion in a heavy duty engine. *Applied Energy*. 2018, **213**, 450-468. DOI: 10.1016/j.apenergy.2018.01.048.
- [2] AKANSU, S.O., TANGÖZ, S., KAHRAMAN, N. et al. Experimental study of gasoline-ethanol-hydrogen blends combustion in an SI engine. *International Journal of Hydrogen Energy*. 2017, **42**(40), 25781-25790. DOI: 10.1016/j.ijhydene.2017.07.014.
- [3] AVL Fire 2017, AVL Documentation.
- [4] CATAPANO, F., DI IORIO, S., SEMENTA, P. et al. Experimental analysis of a gasoline PFI-methane DI dual fuel and an air assisted combustion of a transparent small displacement SI engine. *SAE Technical Paper* 2015-24-2459, 2015. DOI: 10.4271/2015-24-2459.
- [5] CATAPANO, F., DI IORIO, S., SEMENTA, P. et al. Investigation of ethanol-gasoline dual fuel combustion on the performance and exhaust emissions of a small SI engine. *SAE Technical Paper* 2014-01-2620, 2014. DOI: 10.4271/2014-01-2620.
- [6] COLIN, O., BENKENIDA, A., ANGELBERGER, C. 3D modeling of mixing, ignition and combustion phenomena in highly stratified gasoline engines. *Oil & Gas Science and Technology*. 2003, **58**, 47-62.
- [7] GARCÍA-MORALES, J., CERVANTES-BOBADILLA, M., ESCOBAR-JIMENEZ, R.F. et al. Experimental implementation of a control scheme to feed a hydrogen-enriched E10 blend to an internal combustion engine. *International*

- Journal of Hydrogen Energy*. 2017, **42**(39), 25026-25036. DOI: 10.1016/j.ijhydene.2017.08.110.
- [8] GOLZARI, R., LI, Y., ZHAO, H. Impact of port fuel injection and in-cylinder fuel injection strategies on gasoline engine emissions and fuel economy. *SAE Technical Paper* 2016-01-2174, 2016. DOI: 10.4271/2016-01-2174.
- [9] HUANG, Y., HONG, G., HUANG, R. Effect of injection timing on mixture formation and combustion in an ethanol direct injection plus gasoline port injection (EDI+GPI) engine. *Energy*, 2016, **111**, 92-103. DOI: 10.1016/j.energy.2016.05.109.
- [10] JI, C., LIU, X., GAO, B. et al. Numerical investigation on the combustion process in a spark-ignited engine fueled with hydrogen-gasoline blends. *International Journal of Hydrogen Energy*, 2013, **38**(25), 11149-11155. DOI: 10.1016/j.ijhydene.2013.03.028.
- [11] KNOP, V., BENKENIDA, A., JAY, S. et al. Modelling of combustion and nitrogen oxide formation in hydrogen-fuelled internal combustion engines within a 3D CFD code. *International Journal of Hydrogen Energy*, 2008, **33**(19), 5083-5097. DOI: 10.1016/j.ijhydene.2008.06.027.
- [12] KOSMADAKIS, G.M., RAKOPOULOS, D.C., RAKOPOULOS, C.D. Investigation of nitric oxide emission mechanisms in a SI engine fueled with methane/hydrogen blends using a research CFD code. *International Journal of Hydrogen Energy*, 2015, **40**(43), 15088-15104. DOI: 10.1016/j.ijhydene.2015.09.025.
- [13] KRISHNARAJ, J., VASANTHAKUMAR, P., HARIHARAN, J. et al. Combustion simulation and emission prediction of different combustion chamber geometries using finite element method. *Materials Today: Proceedings*. 2017, **4**(8), 7903-7910. DOI: 10.1016/j.matpr.2017.07.126.
- [14] LEE, J., CHU, S., MIN, K. et al. Classification of diesel and gasoline dual-fuel combustion modes by the analysis of heat release rate shapes in a compression ignition engine. *Fuel*. 2017, **209**, 587-597. DOI: 10.1016/j.fuel.2017.07.067.
- [15] LIU, K., LI, Y., YANG, J. et al. Comprehensive study of key operating parameters on combustion characteristics of butanol-gasoline blends in a high speed SI engine. *Applied Energy*. 2018, **212**, 13-32. DOI: 10.1016/j.apenergy.2017.12.011.
- [16] RANGA, A., SURNILLA, G., THOMAS, J. et al. Adaptive algorithm for engine air – fuel ratio control with dual fuel injection systems. *SAE Technical Paper* 2017-01-0588, 2017. DOI: 10.4271/2017-01-0588.
- [17] SIDOROWICZ M., PIELECHA I. Simulation study of the injector location impact on the combustion process thermodynamic indicators of a spark ignition combustion engine. *Journal of Mechanical and Transport Engineering*. 2018, **71**(1), 63-69. DOI: 10.21008/j.2449-920X.2017.69.3.06.
- [18] SIDOROWICZ, M., PIELECHA, I. The impact of injector placement on the dose preparation conditions in a gasoline direct injection system. *Combustion Engines*. 2018, **172**(1), 35-44. DOI: 10.19206/CE-2018-104.
- [19] SONG, K., XIE, H., JIANG, W. et al. On-line optimization of direct-injection-timing for SI-CAI hybrid combustion in a PFI-DI gasoline engine. *SAE Technical Paper* 2016-01-0757, 2016. DOI: 10.4271/2016-01-0757.
- [20] SU, T., JI, C., WANG, S. et al. Improving the combustion performance of a gasoline rotary engine by hydrogen enrichment at various conditions. *International Journal of Hydrogen Energy*. 2018, **43**(3), 1902-1908. DOI: 10.1016/j.ijhydene.2017.11.175.
- [21] TAN, J.Y., BONATESTA, F., NG, H.K. et al. Developments in computational fluid dynamics modelling of gasoline direct injection engine combustion and soot emission with chemical kinetic modelling. *Applied Thermal Engineering*. 2016, **107**, 936-959. DOI: 10.1016/j.applthermaleng.2016.07.024.
- [22] WIEMANN, S., HEGNER, R., ATAKAN, B. et al. Combined production of power and syngas in an internal combustion engine – Experiments and simulations in SI and HCCI mode. *Fuel*. 2018, **215**, 40-45. DOI: 10.1016/j.fuel.2017.11.002.

Maciej Sidorowicz, MEng. – Faculty of Machines and Transport, Poznan University of Technology.

e-mail: [Maciej.Sidorowicz@doctorate.put.poznan.pl](mailto:Maciej.Sidorowicz@doctorate.put.poznan.pl)



Prof. Ireneusz Pielecha, DSc., DEng. – Faculty of Machines and Transport, Poznan University of Technology.

e-mail: [Ireneusz.Pielecha@put.poznan.pl](mailto:Ireneusz.Pielecha@put.poznan.pl)



## Comparison of the results of mathematical modeling of a GTM 120 miniature turbine jet engine with the research results

*The paper presents gas-dynamic calculations of a GTM 120 miniature turbine jet engine. The engine performance parameters have been determined and then validated with theory contained in literature as well as the results of research carried out on a laboratory test stand.*

Key words: miniature jet engine, jet engine

### 1. Introduction

Airplane model jet engines are becoming increasingly popular and recognized in the community of model makers as their primary objective is to make their models possibly close to the original and they are reluctant to apply conventional propellers in jet plane models. Unfortunately, high velocities of flying models fitted with jet engines lead to their relatively frequent crashes and that, in turn, renders airplane model engine manufacturers less eager in their attempts to extend the engine life. Despite the above, one can observe a continuous advancement in this type of drivetrains and its increasingly wider application. One of the examples of miniature turbine jet engines is a GTM 120 engine of Polish design.

The aim of the study was the performance of gas-dynamic calculations of a GTM 120 miniature turbine jet engine, the determination of its parameters and then their comparison with theory contained in literature and the results of investigations carried out in a laboratory.

### 2. GTM 120 design

GTM 120 is a turbojet engine designed for subsonic airplane models. It is fitted with an non-adjustable intake and a single stage radial compressor (Fig. 1).

It has an axial combustor and a single stage axial turbine. The engine outlet nozzle is non-adjustable. The engine shaft is supported on two ceramic bearings. The engine start is carried out with an electric motor fitted before the intake. The engine is mainly designed for use in flying models but it can also be used as a didactic tool.

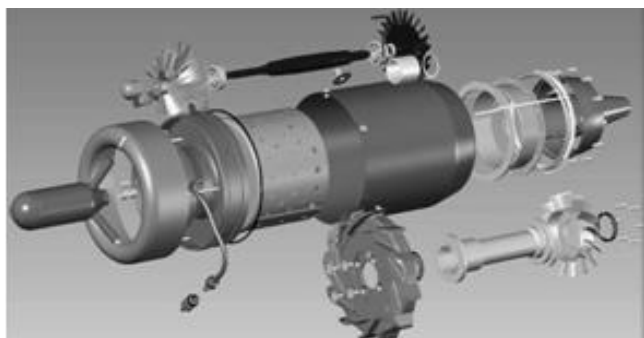


Fig. 1. GTM-120 engine [8]

The main priority when designing this engine was its simplicity of design and unification of components. This is confirmed by the centrifugal compressor and the turbine rotor (ready made subassemblies available at other manufacturers) as well as the non-adjustable intake and the outlet system.

### 3. Reproduction of the GTM 120 turbine engine cycle parameters with the analytical method

The gas-dynamic calculations can be divided into two stages [3].

The first, also referred to as preliminary gas-dynamic calculations includes the calculation or selection of the basic parameters of the cycle (compression rate of the compressor and temperature of the gas upstream of the turbine), determination of the engine mass flow rate that ensures an obtainment of the preset thrust as well as a preliminary selection of the flow channel dimensions.

The second, referred to as, as detailed gas-dynamic calculations trims the results of the preliminary calculations. At this stage the parameters are finally set in individual characteristic flow channel cross-sections (Fig. 2) as well as its final shape and size.

Because the task of the authors was to reproduce the parameters of the cycle of an existing engine, the first stage was modified. In order to accurately reproduce the GTM engine cycle parameters, these quantities were measured during the tests and then adopted as output ones for the preliminary gas-dynamic calculations in individual cross-sections of the engine. As the calculation engine operating point, the authors chose the engine speed at which the engine produced the greatest specific thrust.

The outstanding parameters were assumed based on the data contained in the literature [1, 3].

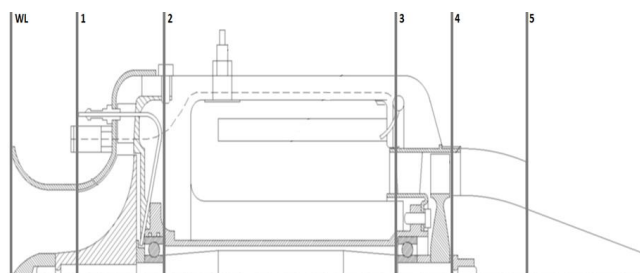


Fig. 2. Diagram of the jet engine with marked stations [5]



The results of the calculations have been shown in the form of a curve of parameters changes in individual cross-sections of the engine (Fig. 3). The curve made based on the performed investigations has the same character as the reference one, shown e.g. in [2], which confirms that the calculations are correct. Validation and discussion of the results has been presented in the further part of this paper.

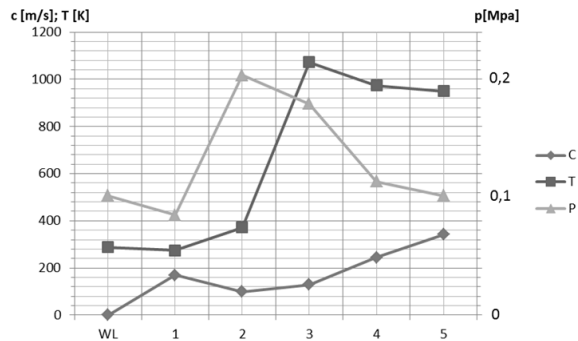


Fig. 3. Aerothermodynamic parameters in characteristic stations

#### 4. Reproduction of the GTM 120 turbine jet engine cycle parameters with the GasTurb software

GasTurb provides a possibility of a quick and simple creation of models of different engines and determining their operating parameters. The obtained engine model can be freely modified, checking which setting would optimize the engine operation. With the use of the said software, it is possible to generate engine thermodynamic cycles as well as many characteristics describing the changes of selected parameters during the simulated engine operation. Using the obtained data, one can evaluate the differences among individual engine types, examine the impact of the surroundings on the engine operation etc.

Because of the fact that the analytical calculations were made for stationary conditions on the ground, according to ISA, also in the GasTurb software, a model reproducing the same conditions was developed.

During in-depth analyses within the software, a specially prepared compressor characteristics was implemented.

The eventually generated engine model produces a usable torque of  $K = 0.08$  kN and has a specific fuel consumption on the level of  $C_j = 60.32$  g/(kN·s). The second-by-second fuel consumption is  $C_s = 0.00454$  kg/s. The area of the outlet cross-section is  $A_8 = 0.0019$  m<sup>2</sup>.

The changes of selected parameters of the working medium alongside the working channel have been shown in Fig. 4.

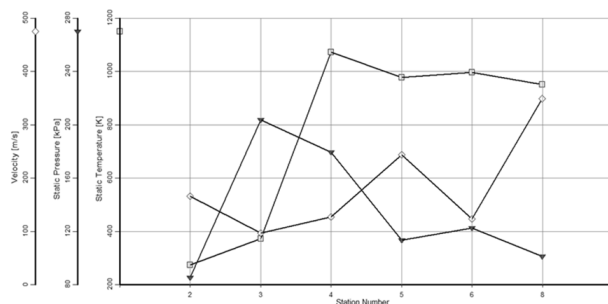


Fig. 4. Aerothermodynamic parameters in the characteristic stations

In the analytical calculations there are 5 characteristic cross-sections, while the GasTurb assumes 8 of them. Fig. 5 presents a diagram of the engine with the GasTurb software cross-sections marked.

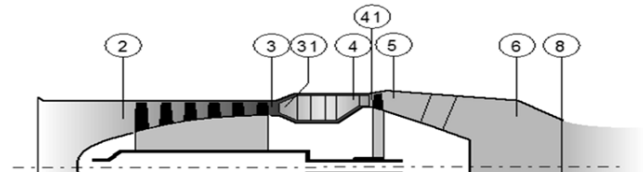


Fig. 5. Characteristic stations in the GasTurb software [7]

#### 5. Research of the GTM 120 turbine jet engine

The investigations that the authors relied on, were carried out during the test of the GTM 120 engine throughout several measurement sessions. The GTM 120 engine parameters were recorded at different rotational speeds. During the tests, the following parameters were recorded: temperature, pressure, thrust, fuel consumption and engine speed.

During the tests, mass flow in the intake was determined using the Venturi tube.

The measured value also allowed calculating the engine specific parameters (specific thrust and specific fuel consumption). In order to compare the results of the investigations, they were converged to reduced parameters with the help of appropriate formulas. Then, they were put in tables and, on this basis, curves of the measured changes and calculated parameters were created depending on the engine rotational speed (test stand characteristics (Fig. 6 and 7). On their basis, the selection of the operating point was made for the aerothermodynamic calculations.

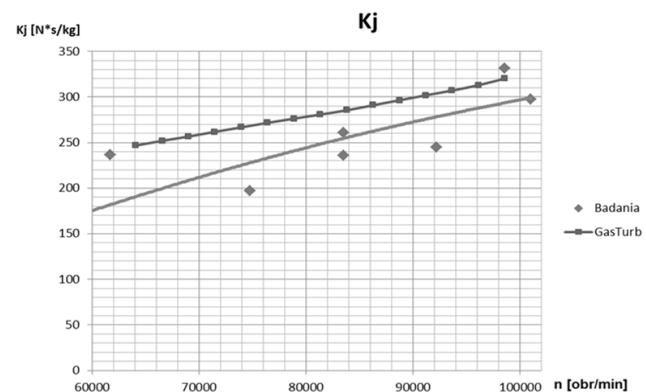


Fig. 6. Specific thrust as a function of engine rotational speed

Figure 6 presents a comparison of the curves of the specific thrust in relation to the engine rotational speed. In both cases, the curves are similar. It is noteworthy that there was a significant spread of the laboratory tests results, which may have been caused by the measurement method. The specific thrust in the laboratory tests is measured indirectly. Its values are determined based on the thrust and the mass airflow. The results of the mass airflow were characterized by a significant spread, which had impact on the  $k_j$  curve.

When analyzing the curves of the changes of the specific fuel consumption (Fig. 7), one can observe that the curve generated by GasTurb decreases much faster than the actual one. The curves cross at the point corresponding to the

engine speed of 94 000 rpm and above that value they are highly convergent. At lower engine rotational speeds, the specific fuel consumption is much more divergent. This results from the fact that the gas-dynamic calculations were carried out for the engine speed of 98 000 [rpm], while the quantities impacting the fuel consumption in the miniature model may vary along with the engine speed a bit differently compared to the full size counterpart bearing in mind that the adopted measurement methods were developed based on the full size versions.

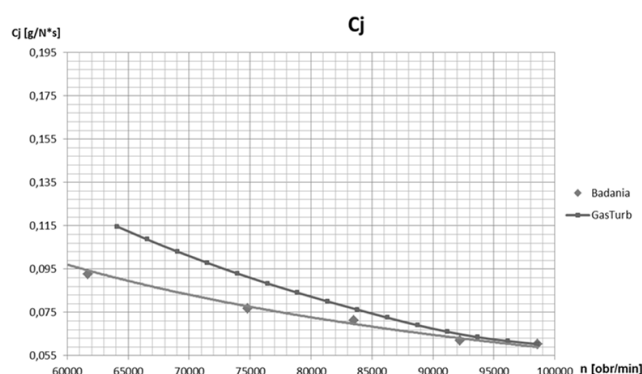


Fig. 7. Specific fuel consumption as a function of engine rotational speed

## 6. Comparison of the research results with the calculations

Figure 8 presents the comparison of the results of the GasTurb and the analytical calculations with the results for selected engine operating points. When analyzing the bar graph, one may observe that the greatest divergence between the calculations and the experiment is for the thrust. In this case, a smaller error occurs for the analytical calculations (Table 1) and amounts to 2.6%, while for the GasTurb it is 3.46%. The thrust calculated analytically is greater than that measured on the laboratory test stand and the thrust generated by the software is lower. This is caused by the fact that the results of the measured and calculated values of thrust were different as well. The thrust calculated analytically at a given operating point is greater than the actual one by 3.95 N, while the GasTurb result is lower by 2.8 N. This gives a relative error of 5.06% and 3.59% respectively. These differences may be caused by the fact that in both cases such quantities as the efficiency of individual subcomponents is not precisely known. The coefficients were selected based on the subsequent iterations so that the calculations were coherent and logical and any deviations from the real engine as little as possible. The lower value of the thrust generated by GasTurb may result from the fact that when the software is in the computing mode, it allows for more factors influencing the engine thermal cycle.

Another calculated value that rather significantly deviates from the results of the experiment is the temperature  $T_2$  downstream of the compressor. In this case, however, the results of both the software and the analytical calculations are very similar. The difference of the order of 3.4% from the actual value may be caused by the unknown flow losses in the flow channel. Both these factors were not allowed for in the calculations on this level of detail.

The smallest deviation from the actual value occurred when calculating the total pressure  $P_2^*$  downstream of the compressor. For the calculations, the compression rate of the compressor and its efficiency were selected through iteration, each time comparing the outcome with the test results. Such a small divergence may confirm that the said parameters (compression rate and efficiency) were properly selected.

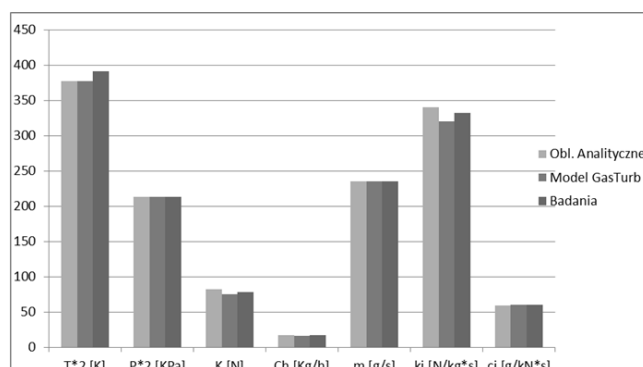


Fig. 8 Comparison of the calculations with the test results

The smallest deviation from the actual value occurred when calculating the total pressure  $P_2^*$  downstream of the compressor. For the calculations, the compression rate of the compressor and its efficiency were selected through iteration, each time comparing the outcome with the test results. Such a small divergence may confirm that the said parameters (compression rate and efficiency) were properly selected.

Table 1 Error values for individual parameters for selected operating point

Parameter	$\Delta$ Analytical calculations	X% Analytical calculations	$\Delta$ GasTurb	X% GasTurb
$T_2^*$ [K]	13.18	3.37	13.24	3.39
$P_2^*$ [KPa]	0.19	0.09	0.20	0.09
K [N]	3.95	5.06	2.80	3.59
$C_h$ [Kg/h]	0.41	2.44	0.58	3.45
m [g/s]	0.19	0.08	0.19	0.08
$k_1$ [N/kg*s]	8.78	2.65	11.47	3.46
$c_1$ [g/kN*s]	1.51	2.50	0.06	0.10

## 7. Conclusions

The above analysis allowed a comparison of the calculations of the created engine model and its characteristics with the data obtained in the tests on a real engine. The task was rather difficult because the related literature is scarce [4].

During the works, the authors generated a computer model close to a real engine and performed proper gas-dynamic calculations. As we can see in the above comparison, the results obtained in the analytical method are very similar to those obtained in the computer calculations and the deviations from the real model are on a similar level for both methods. The deviations may be caused by the model engine (GTM 120) imperfections or inadequacy of the selected calculation methods for this type of engine.

The performance parameters of the GTM 12 engine are comparable to other engines in this class. Analyses of the performance parameters of other engines have been presented in [6]. The performed works also confirmed the

compliance of the engine cycle with the theoretical assumptions related to aviation engines. For a more in-depth analysis, additional investigations must be carried out along with detailed calculations including the geometry of the object, which would validate the above assumptions. Lack of detailed validation, despite a rather high convergence of the calculations with the results of the experiment hints treating

the presented characteristics and results rather illustratively. Nevertheless, the aim of the work was fulfilled and this area in aviation propulsion should be treated as interesting and worthy of notice. It would be interesting to perform investigations of several different engines of similar design to validate the applicability of the presented theories, thus creating a trustworthy source of scientific information.

## Bibliography

- [1] CICHOSZ, E., KORDZIŃSKI, W., ŁYŻWIŃSKI, M. et al. Napędy lotnicze. Charakterystyka i zastosowanie. Warszawa: WKiŁ 1980.
- [2] DZIERŻANOWSKI, P., KORDZIŃSKI, W., ŁYŻWIŃSKI, M. et al. Turbinowe silniki odrzutowe. Warszawa, WKiŁ 1983.
- [3] DZIERŻANOWSKI, P., OTYŚ, J., SZCZECIŃSKI, S. et al. Konstrukcja silników lotniczych. Projektowanie przejściowe i dyplomowe. Warszawa, Wydział Wydawniczy WAT 1972.
- [4] GIERAS, M. Miniaturowe silniki turbodrzutowe. Warszawa, Oficyna Wydawnicza Politechniki Warszawskiej 2016.
- [5] KAU, H-K. Optimization of a model jet engine. Institute of Flight Propulsion, Technische Universität München 2009.
- [6] TRZECIAK, A. Odtworzenie parametrów obiegu i wyznaczenie osiągnięć i charakterystyk turbinowego silnika odrzutowego GTM 120. Praca dyplomowa. WAT Warszawa 2012.
- [7] [www.gasturb.de](http://www.gasturb.de); accessed 01.2012.
- [8] [www.jetpol.tech](http://www.jetpol.tech); accessed 01.2012.

Ryszard Chachurski, DSc., DEng. – Faculty of Mechatronics and Aeronautics, Military University of Technology, Warsaw.

e-mail: [Ryszard.Chachurski@wat.edu.pl](mailto:Ryszard.Chachurski@wat.edu.pl)



Bartosz Jędrówiak, MEng. – Faculty of Mechanical Engineering, Łódź University of Technology.

e-mail: [BartoszJedrowiak@gmail.com](mailto:BartoszJedrowiak@gmail.com)



Adrian Trzeciak, MEng. – Faculty of Power and Aeronautical Engineering, Warsaw University of Technology.

e-mail: [Adrian.Trzeciak@itc.pw.edu.pl](mailto:Adrian.Trzeciak@itc.pw.edu.pl)





## Changes of properties of engine oils diluted with diesel oil under real operating conditions

*The aim of the article was to analyze changes in the trends of selected physical, chemical and functional properties of lubricating engine oil operating in a diesel-engine vehicle equipped with DPF. The vehicle was operated mainly in urban driving conditions (app. 70%), which impeded the DPF regeneration cycle and caused dilution of oil with unburned fuel. Changes in the following physical and chemical properties were assessed: the DF level in engine oil, viscosity (kinematic, dynamic HTHS and structural CCS), total base number, acid number as well as the degree of oxidation, nitration and sulphonation. The tests have shown that the amount of unburned fuel that goes to the engine crankcase due to the unfinished DPF regeneration cycle is as high as 26.0–34.6%. Dilution of the lubricating oil with fuel leads to a significant reduction of its viscosity – about 30% of the fuel content causes a decrease in the kinematic viscosity measured at 100°C to the level of 7.7 mm<sup>2</sup>/s. There was also a significant decrease in total base number (TBN) < 2 mg KOH/g, and an increase in the total acid number (TAN). Moreover, the results obtained were analyzed for potential effects that could have been caused during prolonged engine operation by assessing the content of trace elements in the samples taken.*

**Key words:** oil condition monitoring, lubricant properties, DPF, degradation, reliability, dilution of the lubricating oil

### 1. Introduction

Increasingly stricter standards in the field of environmental protection have led, as far as compression ignition engines (CI) are concerned, to the widespread distribution of diesel particulate filters (DPFs), which require at least periodic regeneration processes to function properly. In the case of an LD (Light Duty) engine it is common practice to actively regenerate plus apply an additional fuel dose injected by the high pressure fuel injection system at the end of the combustion stroke so that, as a result of combustion in the exhaust system, the exhaust gas temperature increases before it reaches DPF [18]. The high temperature corrosion effect is also expected during the demanding regeneration phases, when temperature peak values on some DPFs substrates eventually exceed 1200°C [7]. Unfinished cycles of filter regeneration lead to the penetration of excess unburned fuel into the engine oil, which results in a significant deterioration of its physical, chemical and functional properties. The viscosity of the lubricating oil is systematically lowered as a result of diluting it with fuel and the leaching of elements included in the additives package follows. This contributes to an accelerated reduction of the base number, with the simultaneous increase in the acid number of the lubricating oil. Sejkorova et al. [16] singled out two factors influencing the durability of engine oils and loss of the functional properties of lubricating systems. The first is degradation – thermal and oxidative, as a result of a decrease in anti-oxidant, anti-abrasive and detergent additives efficiency owing to the destruction of polymer viscosity modifiers. The other is contamination with combustion products, due to solid particles such as dust, outer contaminants, abrasive metals, water and cooling liquid as well as to diluting the oil with unburned fuel.

The aim of this article is to analyze change trends in selected physical, chemical and functional properties of lubricating engine oil as a result of app. 70% urban operation (driving and stoppages in traffic jams, driving on relatively short distances without heating the engine, repeated heating

and cooling as well as multiple cycles of a cold engine, which are very harmful for both the oil and diesel particulate filter) in a diesel-engine vehicle equipped with DPF after the dilution of oil (about 30% Diesel Fuel – DF, measured after the operation phase) with unburned fuel. Changes in the following physical and chemical properties occur: DF level in engine oil, viscosity (kinematic, dynamic HTHS and structural CCS), total base number, acid number as well as the degree of oxidation, nitration and sulphonation. The results obtained were analyzed for potential effects that could have been caused during prolonged engine operation by assessing the content of trace elements in the samples taken. In the literature on the subject many scientists have investigated the changes in the properties of engine oils under real operating conditions. Sejkorova and Glos [14] conducted an analysis of the degradation of engine oils used in Zetor tractors which showed that the lubrication and friction processes in their engines were affected negatively which resulted in increased wear. Bulsara et al. [5] predicted about the residual life of lubricant oil in a four stroke engine. Severa et al. [17] dealt with the evaluation of changes in the flow of oil in motorcycle engines during their life cycle. Wolak and Zajac [22] developed a statistical model enabling to calculate average predictive values of kinematic viscosity for a given mileage under similar operating conditions. Naikan et al. [12] proposed a procedure (statistical models ‘fitted’ to experimental data) for reliability analysis of oil used for engine lubrication in wheeled vehicles. Sejkorova et al. [15] presented the results of tests on two types of used engine oils from two different suppliers. The evaluation of selected parameters did not prove that after the exceeding of 40,000 km oil change interval the more expensive engine oil would ensure all the required functions as it had been declared by the supplier’s sales representative. Kral et al. [9] tested long-life engine oils (the engine oil change intervals for those cars are somewhere between 30,000 and 50,000 km) used in unfavourable or difficult conditions. However, the results they ob-

tained did not correspond to onboard computer readings. Many scientists have proposed the use of various sensors to control the quality of engine oil during the engine operation [1, 4, 8, 21]. However, the problem with using engine operating parameters is that they do not monitor the physical properties of the lubricant directly, therefore critical problems such as fuel contamination, can be overlooked. Diluting engine oil with fuel can cause very dangerous effects to the engine, including occurrence of boundary lubrication, accelerated wear of cylinder liners, piston rings, bearings and crank pins, reduction of lubricating oil pressure, reduction of engine performance or, ultimately, reduction of engine's life time [19].

## 2. Characteristics of the research material

The experimental materials were engine oils in the viscosity class SAE 0W-40 and 5W-30 and the quality ACEA 2016 – C3 (coded as CE and PE). The level of changes was assessed in the properties of oil used in the BMW model 520 vehicle, equipped with self-ignition engine, driven by the same manufacturer's fuel.

Table 1 contains the general specification of the selected model. Before starting the operation, the output parameters for the sample of unused (fresh) engine oil were determined, and then the same test cycle was carried out five times every 15,000 km (details in Table 2). During the experiment, three samples of CE oil and two samples of PE oil were obtained. No refills were used. To the contrary, oil surplus in the lubrication system under the inflow of DF was a real problem.

Table 1. The general specification of the BMW 520 D

Production year	2006
Engine displacement	1995 cm <sup>3</sup>
Engine type	diesel
Engine power	120 kW at 4000 rpm
Maximum torque	340 Nm at 2000 rpm
Forced induction	by turbocharger (gas compressor)
Number of cylinders	4
Cylinder arrangement	straight (inline)
Number of valves	16
Injection type	Common Rail
Lubrication system capacity	5.5 dm <sup>3</sup>
Manual gearbox	6-gear
Transmission type	rear axle

Table 2 lists the oils selected for testing in the viscosity class SAE 0W-40 and 5W-30 together with the API, ACEA requirements specified by the manufacturer as well as the requirements of the engine makers.

When analyzing the obtained results of engine oil properties it should be taken into account that the vehicle was operated in 70% in the urban cycle and in 30% in the non-urban cycle. The actual operating conditions of the vehicle in the urban cycle involved:

- operation of the car requiring a large, variable load on the engine (alternating, rapid acceleration and deceleration, driving with heavy load),
- prolonged engine idling (driving and stoppages of the car in traffic jams),
- driving the car on short distances using an unheated engine,

- frequent starts at low engine temperatures.

Table 3 presents the details related to the operation of the test facility containing engine oil.

Table 2. Quality and viscosity classification of engine oils selected for testing

Oil Code	SAE	ACEA	API	Classification according to engine manufacturers
CE	0W-40	C3	SN	BMW Longlife-04, dexos2®, Meets Fiat 9.55535-S2, MB-Approval 229.31/ 229.51, Porsche A40, Renault RN 0700 / RN 0710, VW 502 00 / 505 00
PE	5W-30	C3	-	VW Standard 504 00/ VW Standard 507 00, Mercedes-Benz 229.51, BMW Longlife-04, Porsche C30, Audi, Skoda, Seat

Table 3. Operational characteristics of the test facility

Sample code	Initial car mileage [km]	Car mileage / sampling [km] / (date)	Number of kilometers driven [km]
CE 1; Sample One	130 600	147 000 / (21.07.2013)	16 400
CE 2; Sample Two	147 000	164 085 / (30.04.2014)	17 085
CE 3; Sample Three	164 085	180 400 / (15.06.2015)	16 315
PE 1; Sample One	180 400	196 300 / (23.05.2016)	15 900
PE 2; Sample Two	196 300	206 900 / (02.03.2017)	10 600

## 3. Methods of research

In order to ensure the required physical, chemical and functional properties of lubricating oil during operation, in recent years procedures for their monitoring have been developed and widely applied. Detailed verification of oil change intervals is carried out depending on the operating conditions, which are closely related to both the quantitative and qualitative lubricating oil degradation processes.

Considering the above-presented issues, the focus was on assessing the changes in physical, chemical and functional properties affecting the operational usefulness of motor oils, i.e. viscosity (kinematic, dynamic HTHS and structural CCS), total base number, acid number, DF content and oxidation, nitration and sulfonation. The kinematic viscosity was calculated on the basis of the flow time, specific volume of liquid by the calibrated capillary (Ubbelohde capillary viscometer), under strictly defined measurement conditions (flow time, capillary constant etc.) and at the strictly determined temperature, according to the EN ISO 3104 standard. Dynamic viscosity HTHS (high temperature high shear) was determined at 150°C at the shear rate of  $10^6 \text{ s}^{-1}$ , using the Ravenfield viscometer with coaxial cones, in accordance with the ASTM D4741 standard. The determination of structural viscosity at low temperatures was carried out according to the PN-C-04150:2004 standard by means of a cold cranking simulator, by measuring the rotational speed of the impeller immersed in oil cooled down to -35°C (CE) and -30°C (PE). The content of acidic substances (ASTM D664) and weak bases in the paraffin products was measured by the potentiometric titration method. The measure unit of their content is the so-called total base number, also referred to as the alkaline reserve

(ASTM D2896). The determination of diesel oil content in engine oil was performed by capillary gas chromatography with FID flame-ionization detection. The capillary column used, with an average film thickness of the dimethylpolysiloxane stationary phase, enabled the separation of the diesel oil and engine oil fractions. Using the infrared spectroscopy method (ASTM E2413 A.2), the oil aging process was monitored, which occurs under operating conditions due to three processes: oxidation (binding of oxygen to hydrocarbons contained in oil), sulfonation (binding of sulfur oxides) and nitration (binding of nitrogen oxides). On the basis of the nature of the operated oil spectrum, the signal measurement was analyzed in a specific area of infrared radiation absorption. The levels of the previously discussed carbonyl, nitro and sulphonic groups for used oils were determined not directly from their spectra, but from the difference spectra, i.e. the spectra resulting from the mathematical operation: the spectrum of used oil minus the spectrum of fresh oil. The contents of elements derived from the additives and of metals which polluted the oil due to the wear of engine components, were determined by the ICP-OES technique in an environment of organic solvents using the internal standard method, according to the ASTM D 5185 method.

#### 4. Presentation and analysis of test results

Figure 1 shows the diesel oil content in the analyzed engine oil lubricating samples. Definitely more fuel was found in oils from the CE group (on average 34.6% (m/m)) than from the PE group (on average 26% (m/m)). The most DF was found in the CE1 sample and it was a very dangerous level of 37.1% (m/m).

Booser [3] indicates possible condemning limits for fuel contamination: minor (1.5–4.5%), significant (5–7.5%) and excessive (> 7.5%). Excessive lubricant contamination may lead to dramatic changes in lubricant properties, preventing the lubricant from performing its required functions [6]. The low level of DF in the lubricating oil in PE2 sample can be explained by the lowest mileage of the vehicle (10,600 km).

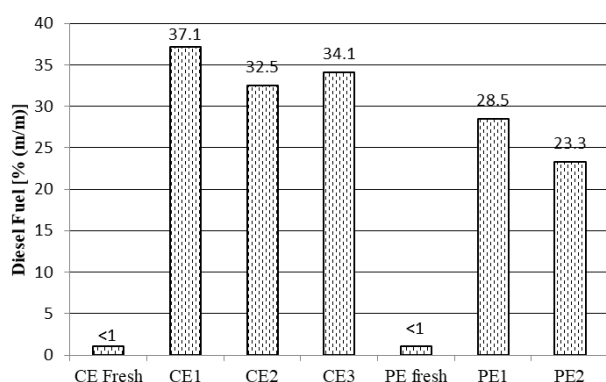


Fig. 1. Change of diesel fuel content in engine oil during operation

Increased dilution of engine oil with diesel fuel is attributed to the use in common rail injection systems of the software supporting the regeneration of diesel particulate filters by means of additional fuel injection after completing the combustion process [19]. If the process is not com-

pleted, due to random occurrences during the DPF regeneration cycle, there is an increased penetration of fuel into the engine oil. This is most often the case during the urban driving cycle.

The high diesel fuel content in the tested samples is confirmed by a significant decrease in the kinematic viscosity determined at 40°C and 100°C. The changes in kinematic viscosity occurring at both temperatures are presented in Fig. 2.

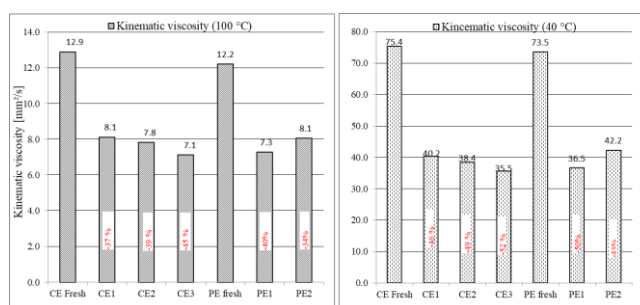


Fig. 2. Changing the kinematic viscosity in the tested lubricating oil samples

On the basis of the obtained test results it was observed that as a result of DF transfer to the engine oil there is a dangerous (about 50%) decrease in the kinematic viscosity at 40°C (after the average mileage of 16,600 km), the largest for CE3 samples (decrease by 52% in relation to the initial value 52%) and PE1 (decrease by 50%), while the lowest for: PE2 (decrease by 34% in relation to the initial value) and CE1 (decrease by 46%). The situation is similar for the changes in the kinematic viscosity of engine oil determined at 100°C. The viscosity value at this temperature, after the same mileage, dropped by about 40% in relation to the initial value (for the CE1 sample: by 37%, CE2: by 39.3%, CE3: by 44.8%, PE1: by 40%, PE2: by 34%). According to the classification SAE J300 from 2015, the kinematic viscosity at 100°C for oils of class 40 should be in the range of 12.5–16.3 mm²/s. The obtained results provide the basis for stating that the kinematic viscosity of the analyzed oil, after the average mileage of approximately 16,600 km, drops to the levels corresponding to viscosity class 20.

Thus, the oil is not kept in the viscosity class declared by the manufacturer (40). On the one hand, it can be considered that reducing the viscosity will bring benefits such as faster circulation in the engine and reduced energy consumption. Nevertheless, the use of viscosity class 40 oil suggests the need to better protect the engine from wear, and not reduce energy consumption, and you can have doubts whether the gap between the piston and the cylinder wall will be effectively sealed. Such a large amount of fuel in oil did not allow for the compensation of the oil viscosity decrease by the increase in viscosity resulting from the oil densification by degradation products. Attention should be drawn to the fact that both CE2 and PE1 oils underwent very similar viscosity drops at 40°C and 100°C, in spite of the fact that they differed significantly in the fuel content (32.5 and 28.5) – this resulted from the fact that the CE oil should have a lower viscosity with a higher fuel content, which was not the case. The reason could be the use of

a different set of antioxidant additives and the emergence of larger amounts of degradation products increasing viscosity. That is also confirmed by the observation of oxidation change presented in Fig. 4. The HTHS dynamic viscosity (Fig. 3) of the tested engine oil samples was not maintained at levels guaranteeing the provision of a suitable lubricating film at high temperatures and at high shear rates.

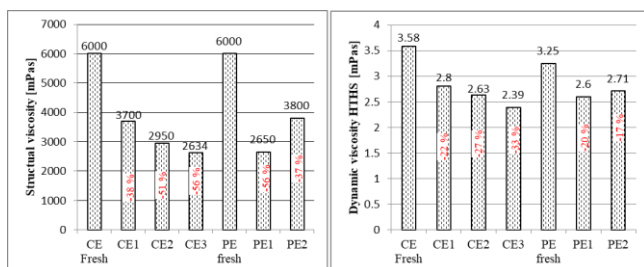


Fig. 3. Changes in dynamic viscosity - structural viscosity CCS (-35°C: CE, -30°C: PE) and HTHS

According to the SAE J300 classification, the HTHS dynamic viscosity should not be lower than 2.9 mPa.s. The highest decrease in HTHS viscosity occurs in relation to the CE3 sample: 33% (mileage 16,315 km), while the lowest for the PE2 sample: 17% (mileage 15,900 km). From the changes in the structural viscosity of the tested engine oils presented in Fig. 3 at -35°C (CE) and -30°C (PE), by the cold start simulator (CCS), it is obvious how significantly the structural viscosity of the oil gets affected under the described operating conditions. The largest decrease in structural viscosity in relation to the initial value was observed for the CE3 and PE1 samples: 56%. For the other samples, the decrease is slightly lower, nevertheless it still remains at a significantly high level (over 37%).

As to the indirect assessment of the oxidation stability loss of oils in a large volume, i.e. changes in the acid number (Fig. 5) and assessment of IR spectrum changes (Fig. 4), it was observed that in each case (for all the tested samples) the changes occurring during operation showed similar levels of engine oil degradation. CE oils were characterized by a lower resistance to oxidation (oil degradation caused by undesirable chemical reactions with oxygen) than PE oils. The value of all the tested oil samples in all the cases after an average mileage of 16,600 km, exceeded level 1 (Abs/0.1 mm). There has been a significant increase in the degree of oxidation. It is assumed that the limit value for oxidation degree is 0.4 (Abs/0.1 mm) [19].

When assessing the reactions occurring during the contact of hydrocarbons with nitrogen oxides, resulting from the engine operation leading to the formation of organic nitrates, it was found out that after the examined mileage there was an increase in the binding of nitrogen compounds exceeding the permissible level (0.4 Abs/0.1 mm) for two samples (CE1 - 0.46 (Abs/0.1 mm) and CE3 - 0.48 (Abs/0.1 mm)). The values of sulphonation of lubricating engine oils under the analyzed conditions stayed at an average level of about 0.16 (Abs/0.1 mm). It can be observed that the binding of sulfur compounds stayed at the highest level, 0.28 (Abs/0.1 mm), for the sample CE2, characterized by the lowest oxidation and nitration (in the group of oils CE).

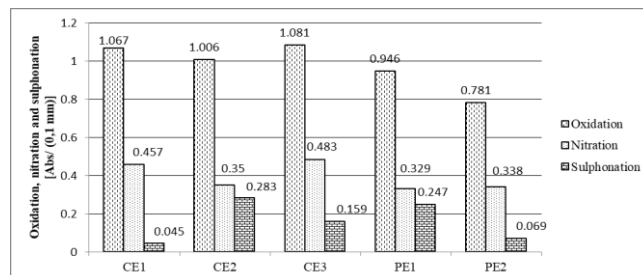


Fig. 4. Oxidation, nitration and sulphonation changes

The mixture of compounds with different physical and chemical properties as well as the group composition of engine oil affect the width of the spectrum of compounds that may be formed under operating condition. The heat generated during the engine operation, contact with fuel and its combustion products, combined with the common presence of oxygen from the air, cause the degradation of the basic engine oil component: hydrocarbons. The accompanying chemical and mechanical-chemical transformations cause a decrease in the content of additives introduced into the engine oil to give it the required quality characteristics. The acid value (Fig. 5), which for fresh oil was 2.21 (CE) and 1.95 (PE) mg KOH/g, significantly increased after the operation period (the largest increase for CE3 samples - 285% and for PE1 - 178%).

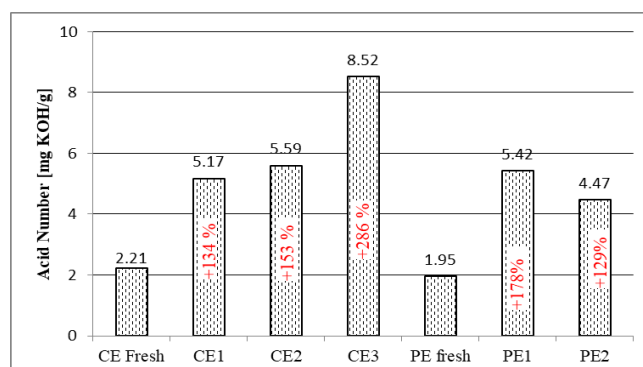


Fig. 5. Changes in the acid number of the tested engine oil samples

The changes in the total base number were equally large as the above-analyzed acid number changes.

The greatest changes were observed for the CE oil samples (over 70%). Such a high drop can be linked to, among others, a high content of fuel, as for PE samples with lower fuel content these changes were not so high. However, it should be taken into account that differences in the drop may also result from the additive package used by the producers. Such a large decrease in the total base number is a warning signal for the owner of the vehicle, because the loss of alkaline reserve is a decrease in the lubricating oil's ability to neutralize acidic combustion products (engine oil should neutralize acidic products from fuel combustion and prevent corrosion processes). These changes will also affect the oil washing and dispersing potential, i.e. the ability of the oil to maintain any deposits in its volume and prevent their deposition on the engine's structural elements.



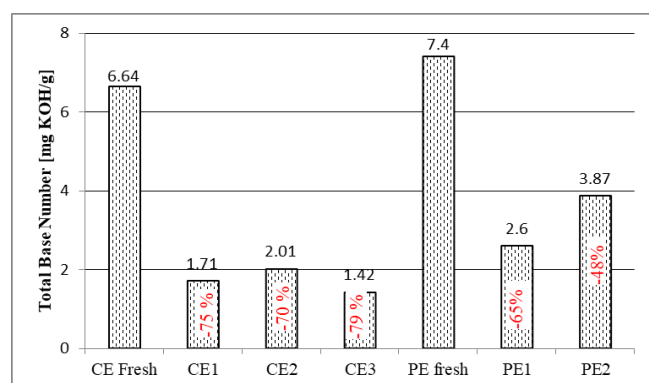


Fig. 6. Changes in the total base number in the tested engine oil samples

The next stage of the research was the assessment of trace elements content in the samples taken. Table 4 summarizes the content of metals originating from the wear processes, impurities, additives package or other aforementioned sources. The ranges of elements and wavelengths are also given.

The analysis of the content of individual chemical elements was carried out for each metal separately:

- Aluminum – wear product – piston damages, aluminum bearings, cylinder block surfaces [20]. Excessive presence can cause damage to the filter and a drop in oil pressure. In the CE2 sample a concentration of 11 mg/kg was recorded, in the other samples the level is below the lower limit of detection.
- Iron – a significant product of wear. The sources of origin include: cylinder liners, piston rings, camshaft and crankshaft, gear teeth, water [20]. Excessive presence of iron can cause oil degradation, insufficient lubrication, corrosion, oil film breakage, abnormal operating temperature and a drop in oil pressure [11]. The highest concentration was recorded in the CE2 sample: > 140 (259) mg/kg.
- Lead, nickel, manganese – products of wear the amount of which increases with the use of oil [20]. In the ana-

lyzed samples, the presence of these elements is below the lower limit of detection.

- Potassium, sodium – classified as the pollutants [24]. The presence of these elements is below the lower limit of detection.
- Chromium – a high level of chromium may indicate excessive wear of chromed components such as rings and sleeves [13, 20]. The highest concentration was recorded in the CE2 sample – 6.1 mg/kg.
- Copper – product of wear (wear of bearings and radiator tubes), or additive [23]. The highest concentration occurs for the CE2 sample: 14 mg/kg, while the average concentration for the remaining samples is 8.6 mg/kg.
- Magnesium – it appears in detergent but also as a product of wear (used in the construction of bearings), its visible significant increase for the CE3 sample: 314 mg/kg. The average for the remaining samples is 7 mg/kg. In the study carried out by Zięba-Palus et al. [25] engine oils generally differed from each other in terms of magnesium content, although these differences were relatively small (in this study, however, the diversity is very high (the coefficient of variation has reached 179%).
- Zinc – a component of an additive. It has anti-corrosive properties. The highest content was recorded in the CE3 sample: 1016 mg/kg. The average for the remaining samples is 608 mg/kg.
- Molybdenum – a component of an additive for engine oil. The highest content occurs in CE1 and CE3 samples (88 mg/kg on average). The average for the remaining samples is 16 mg/kg.
- Boron – a component of an additive [10]. The lowest content remained in the CE2 oil – 6.3 mg/kg.
- Calcium – it may occur as an impurity or an additive [2]. The highest content is found in the CE3 sample (2056 mg/kg). The average for the remaining samples is 1114 mg/kg.

Table 4. Content of trace elements in the collected samples

			C ±U [mg/kg]						
Element	Range [mg/kg]	Wave length [nm]	Fresh CE	Fresh PE	Sample CE 1	Sample CE 2	Sample CE 3	Sample PE 1	Sample PE 2
Metals from wear processes									
Al	6.0–40	167.078	< 6.0	< 6.0	< 6.0 (5.7)	11 ±5	< 6.0 (3.1)	< 6.0 (5)	< 6.0 (4.8)
Fe	2.0–140	259.941	< 2.0	< 2.0	128 ±18	>140 (259)	16 ±3	95 ±14	50 ±8
Pb	10–160	220.353	< 10	< 10)	< 10	< 10	< 10	< 10	< 10
Mn	5.0–700	257.611	< 1.0	< 1.0)	< 5.0	< 5.0	< 5.0	< 5.0	< 5.0
Ni	5.0–40	231.604	< 5.0	< 5.0	< 5.0	< 5.0	< 5.0	< 5.0	< 5.0)
Metals from the contamination of oil									
K	40–1200	766.491	< 10.0	< 10.0	< 10	< 10	< 10	< 10	< 10
Na	7.0–70	589.592	< 7.0	< 7.0	< 7.0	< 7.0	< 7.0	< 7.0	< 7.0
Metals from wear processes and additives package									
Cr	1.0–40	267.716	< 1.0 (0.1)	< 1.0 (0.1)	3.1 ±1.2	6.1 ±1.7	< 1.0 (0.85)	2.9 ±1.1	2.1 ±0.9
Cu	2.0–160	324.754	< 2.0 (0)	< 2.0 (0)	9.6 ±1.6	14 ±2	8.4 ±1.4	8.8 ±1.5	7.4 ±1.3
Mg	5.0–1700	279.553	5.10 ±1.8	6.26 ±2.1	6.6 ±2.2	8.9 ±2.8	314 ±43	6.5 ±2.2	6.21 ±2.1
Zn	60–1600	213.856	800 ±93	833 ±97	537 ±60	632 ±71	1016 ±120	599 ±67	665 ±76
Mo	5.0–200	202.095	163 ±16	153 ±16	93 ±11	14 ±3	83 ±11	12 ±±3	23 ±4
Metals from additives package and from the contamination of oil									
B	4.0–30	249.773	171	171	29 ±10	6.3 ±9.5	54	32	45
Ca	40–9000	317.933	1812 ±184	1797 ±182	961 ±81	1018 ±87	2056 ±217	1148 ±102	1329 ±123
Si	8.0–50	251.612	< 8.0 (4.7	< 8.0 (4.7)	8.6±/4.8	8.4 ±4.7	< 8.0 (4.6)	< 8.9 (4.9)	< 8.0 (6.6)
P	10–1000	177.495	671 ±80	517 ±70	403 ±62	472 ±67	802 ±87	456 ±66	517 ±70

- Silicon – it comes from an anti-foaming oil additive or is part of dust particles intruding into the oil from the outside (higher concentration signals a need for maintenance with the probability of air filter failure [15]. Silicon values above 8 mg/kg have been determined for CE1 and CE2 samples.
- Phosphorus – a component of an additive that provides anti-rust properties [11]. In the three samples, there was a decrease in the level of this element, which indicates its depletion during operation. On the other hand, in the case of the CE3 sample, there was an increase in relation to fresh oil (802 mg/kg), while for PE2 oil the level remained at the fresh oil level.

The analysis of trace elements content in engine oils that were diluted with fuel during operation has not given a definite answer as to the effect of fuel on their content. The observed changes in the concentration of elements did not form a clear trend. Considering that each oil sample is undergoing a different degradation process, changes can occur at various time intervals.

For the CE oil, in the second period an increase was recorded of typical wear elements: Al, Fe, Cr, Cu. In the third measurement period for this oil, the maximum values of Mg, Zn, B, Ca, P were observed with the simultaneous maximum decrease in kinematic, structural and dynamic viscosity, maximum increase in acid number and maximum decrease in base number. At the same time it could be observed that for the PE2 sample with the lowest fuel content (and mileage) the content of wear elements was at the lowest level. It should also be taken into account that the content of trace elements is connected with the dilution intensity. During the research for each of the samples this process looked different, which was due to the nature of driving and ambient temperatures during operation.

## 5. Conclusion

The tests have shown that the amount of unburned fuel that goes to the engine crankcase due to the unfinished DPF regeneration cycle is as high as 26–34.6%. Such a large amount of fuel in oil causes its dilution. Dilution of the lubricating oil with fuel leads to a significant reduction of its viscosity – about 30% of the fuel content causes a decrease in the kinematic viscosity measured at 100°C to the level of 7.7 mm<sup>2</sup>/s. The kinematic viscosity measured at 40°C showed a decrease of approximately 50% (after an average mileage of 16,600 km) – the largest for samples:

CE3 (decrease by 52% in relation to the initial value) and PE1 (decrease by 50%), and the lowest for: PE2 (decrease by 34% in relation to the initial value) and CE1 (decrease by 46%). The dilution of oil also contributed to about a 48% decrease in structural viscosity and a 25% decrease of HTHS. Such large changes in viscosity make the oil film less able to handle large loads that can occur at certain points, such as the main bearings and those of the crankshaft. These changes are also visible in the concentration of trace elements in oil, especially in the CE2 sample (aluminum: 1 mg/kg, Iron: 259 mg/kg). Their potential sources are: wear of the main and crank bearing shell sliding layer, wear of plugs in the shells, seizure of pistons in cylinders, etc. However, there are differences in concentration changes in the analyzed periods of operation.

The gradual dilution of oil with fuel caused premature degradation of engine oils, due, inter alia, to the antagonistic effect of the components (not always compatible) of fuel and oil. It also caused the acceleration of the oxidation process, leading to levels significantly exceeding the limit values (CE over 1 Abs/0.1 mm, PE about 0.8 Abs/0.1 mm). There was also a significant decrease in the ability of lubricating oil to neutralize acidic combustion products: TBN < 2 mg KOH/g, and an increase in the acid number.

The dilution of engine oil with fuel is normal, provided that the amount of fuel does not exceed several percent [3]. The test results have shown that the dilution of engine oil with fuel from unfinished cycles of regeneration of DPF filters is a serious operational problem, especially for vehicles used in typically urban conditions. Changes in the parameters described are really significant and may involve potential accelerated engine wear. Therefore, continuous development and introduction of new methods of testing the changes in lubricating oil properties under operation, adjusted to the quality changes of products placed on the market and the conditions of their use, are indispensable.

## Acknowledgements

The publication was funded by appropriations of the Faculty of Commodity Science, Cracow University of Economics, and Faculty of Production Engineering University of Life Sciences in Lublin within the framework of grants to maintain the research potential.

## Bibliography

- [1] AGOSTON, A., ÖTSCH, C., JAKOBY, B. Viscosity sensors for engine oil condition monitoring—Application and interpretation of results. *Sensors and Actuators A: Physical*. 2005, **121**(2).
- [2] BESSER, C., SCHNEIDHOFER, C., DÖRR, N. et al. Investigation of long-term engine oil performance using lab-based artificial ageing illustrated by the impact of ethanol as fuel component. *Tribology International*. 2012, **46**(1).
- [3] BOOSER, R.E. Handbook of lubrication. Boca Raton. Florida, 1983.
- [4] BROUWER, M.D., GUPTA, L.A., SADEGHI, F. et al. High temperature dynamic viscosity sensor for engine oil applications. *Sensors and Actuators A: Physical*. 2012, **173**(1).
- [5] BULSARA, M.A., HINGUZ, A.D., PATEL, K. Prediction of residual life of lubricant oil in four stroke engine. *Proceedings of International Conference on Advances in Materials and Product Design (AMPD 2015)*. 2015.
- [6] CLARC, R.J. On board monitoring of engine oil. Faculty of The Graduate College in partial fulfillment of the requirements for the Degree of Master of Science of Engineering Department of Aeronautical and Mechanical Engineering Advisor: Claudia Fajardo, Ph.D., 2011.
- [7] GILI, F., IGARTUA, A., LUTHER, R. et al. The impact of biofuels on engine oil performance. *Lubrication Science*. 2011, **23**.

- [8] JAKOBY, B., EISENSCHMID, H., SCHATZ, O. et al. A multi-functional sensor for oil condition evaluation. *Technisches Messen*. 2001, **68**(5).
- [9] KRAL, J., KONECNY, B., MADAC, K. et al. Degradation and chemical change of longlife oils following intensive use in automobile engines. *Measurement*. 2014, **50**.
- [10] KUMBÁR, V., GLOS, J., VOTAVA, J. Monitoring of chemical elements during lifetime of engine oil. *Acta Universitatis Agriculturae et Silviculturae Mendelianae Brunensis*. 2014, **62**(1).
- [11] MALINOWSKA, M. Analiza zanieczyszczeń oleju silnikowego stosowanego w silniku Cegielski-Sulzer 3AL25/30. *Zeszyty Naukowe Akademii Morskiej w Gdyni*. 2014, **83**.
- [12] NAIKAN, V.N.A., KAPUR, S. Reliability modelling and analysis of automobile engine oil. *Proceedings of the Institution of Mechanical Engineers, Part D: Journal of Automobile Engineering*. 2006, **220**(2).
- [13] PALKENDO, J.A., KOVACH, J., BETTS, T.A. Determination of wear metals in used motor oil by flame atomic absorption spectroscopy. *Journal of Chemical Education*. 2014, **91**(4).
- [14] SEJKOROVÁ, M., GLOS, J. Analysis of degradation of motor oils used in Zetor tractors. *Acta Universitatis Agriculturae Et Silviculturae Mendelianae Brunensis*. 2017, **65**(1).
- [15] SEJKOROVÁ, M., HURTOVA, I., GLOS, J. et al. Definition of a motor oil change interval for high - volume diesel engines based on its current characteristics assessment. *Acta Universitatis Agriculturae Et Silviculturae Mendelianae Brunensis*. 2017, **65**(2).
- [16] SEJKOROVÁ, M., POKORNY, J., JILEK, P. The usage of modern instrumental methods in diagnostics of quality of operated engine oils. In: *Proceedings Deterioration, Dependability, Diagnostics*. Brno: University of Defence. 2014.
- [17] SEVERA, L., HAVLICEK, M., CUPERA, J. Changes of engine oil flow properties during its life cycle. *Acta Univ. Agric. Silvic. Mendelianae Brun.* 2010, **58**(4).
- [18] URZĘDOWSKA, W., STĘPIEŃ, Z. Olej silnikowy a biopaliwa – współdziałanie w eksploatacji. *Nafta-Gaz*. 2010, **10**.
- [19] URZĘDOWSKA, W., STĘPIEŃ, Z. Wybrane zagadnienia dotyczące zmian właściwości silnikowego oleju smarowego w eksploatacji. *Nafta-Gaz*. 2012, **12**.
- [20] VASANTHAN, B., DEVARADJANE, G., SHANMUGAM, V. Online condition monitoring of lubricating oil on test bench diesel engine & vehicle. *Journal of Chemical and Pharmaceutical Sciences*. 2015, **9**.
- [21] WANG, S. Engine oil condition sensor: method for establishing correlation with total acid number. *Sensors and Actuators B: Chemical*. 2002, **86**(2–3).
- [22] WOLAK, A., ZAJĄC, G. The kinetics of changes in kinematic viscosity of engine oils under similar operating conditions. *Eksploatacja i Niezawodność – Maintenance and Reliability*. 2017, **19**(2).
- [23] YUNUS, S., RASHID, A.A., LATIP, S.A. et al. Comparative study of used and unused engine oil (perodua genuine and castrol magnatec oil) based on property analysis basis. *Procedia Engineering*. 2013, **68**.
- [24] ZAJĄC, G., SZYSZLAK-BARGŁOWICZ, J., SŁOWIK, T. et al. Designation of chosen heavy metals in used engine oils using the XRF method. *Polish Journal of Environmental Studies*. 2015, **24**.
- [25] ZIĘBA-PALUS, J., KOSCIELNIAK, P. An analysis of the similarity of motor oils on the basis of their elemental composition. *Forensic Science International*. 2000, **112**.

Artur Wolak, DEng. – Faculty of Commodity Science and Product Management, Cracow University of Economics.

e-mail: [Artur.Wolak@uek.krakow.pl](mailto:Artur.Wolak@uek.krakow.pl)



Grzegorz Zajac, DSc., DEng. – Faculty of Production Engineering, University of Life Sciences in Lublin.

e-mail: [Grzegorz.Zajac@up.lublin.pl](mailto:Grzegorz.Zajac@up.lublin.pl)



Magdalena Żółty, DEng. – Oil and Gas Institute – National Research Institute, Cracow, Poland.

e-mail: [Magdalena.Zolty@inig.pl](mailto:Magdalena.Zolty@inig.pl)



Natalia SZYMLET  
 Lukasz RYMANIAK  
 Piotr LIJEWSKI  
 Barbara SOKOLNICKA  
 Maciej SIEDLECKI

CE-2018-207

## Research and analysis of harmful road emissions from a two-wheel vehicle engine in laboratory conditions

The subject of this article is the identification of engine exhaust emissions of two-wheel vehicles under laboratory conditions. For this purpose, analysis of road and time emission of gaseous compounds: HC, CO, CO<sub>2</sub>, NO<sub>x</sub> from a motorcycle equipped with an engine with a displacement volume of 0.7 dm<sup>3</sup> and a maximum power of 55 kW was made. The tests were performed on a dynamometer station designed for testing two-wheel vehicles. The speed characteristic was taken from the European type approval test WMTC, consisting of three parts. Each of these parts lasted 600 seconds and was characterized by a different maximum vehicle speed value. The mobile AXION R/S apparatus part of the PEMS device group was used in the research. What is more, the exhaust emissions results were referred to the values listed by the exhaust emission standard met by the tested vehicle (Euro 4 standard). Laboratory tests presented in the article are only intended as a basis for further research, which includes exhaust emission tests from two-wheel vehicles in real operating conditions.

Key words: two-wheeler, motorcycle exhaust emissions, WMTC test

### 1. Introduction

One of the most important sources of greenhouse gas emission is combustion engines used in transport, heavy machinery, and other equipment. Another aspect tightly related to the operation of combustion engines is exhaust emissions. Today, we know that exhaust components such as CO, HC, NO<sub>x</sub>, and PM (as a mass and particle number – PN) are hazardous to human health. Therefore very important are action lead to reduction exhaust emission from all type of vehicles also two-wheels.

Economic development, and hence the increase in the wealth of the population of all world agglomerations, leads to an increasing share of road transport, in which, apart from cars and trucks, including the two-wheelers vehicle group. This group makes it possible for people to meet everyday transport needs, especially in Africa and Asia, where the share of motorcycles and scooters accounts for 70% of the entire fleet of road vehicles [8]. Asia has the highest number of motorcycles, especially mopeds which are very important transportation tool. The motorcycles sale in Asia is still significant in comparing to the other areas of the world (Fig. 1). In India alone, in one year (2017) the number of sold two-wheeled vehicles amounted to almost 18 million units, which gives a result of 48 thousand vehicles a day. In Europe, the number of newly registered motorcycles and mopeds is dominated by Germany, France and Italy (as of 2016) [11]. Motorcycles emit significant air pollutants. For example, motorcycles with about 54% of the total vehicle population in Jakarta, Indonesia, emit in 1998 to more than 20% of PM<sub>10</sub>, and CO and 40% of HC. A similar is in Hanoi, Vietnam, where motorcycles contributed about 54% of CO and HC and 43% dust [12]. The effect of that, according to the WHO (World Health Organization), each year there are around 600,000 premature deaths from diseases directly related to air pollution in India [3]. The same problem of

motorcycle emissions are taking place in many Asian cities. Therefore it is clear that priority must be given to reduce pollutions from motorcycles.



Fig. 1. Projected motorcycles sales worldwide (in thousand units) in 2018 by region [15]

The advantages resulting from the use of two-wheelers (avoiding road congestion, no problem finding a parking space and the ease of obtaining a license) cause a continuous increase in the share of this vehicle category, in particular in Asian countries. This fact lead to many research and development centers performing intensive research work on the assessment of exhaust emission from this type of vehicles. This is confirmed by numerous publications, in particular by scientists from Indonesia and India, where due to the lack of a developed public transport network two-wheeled vehicles accounts for 80% of private transport sector [9].

The issue of emissivity is connected with increased expenditures of legislators and authorities of all highly developed countries to improve air quality in urban centers. Therefore, increasingly restrictive emission standards for motorcycles are being introduced. Figure 2 presents the development of emission standards in Europe, while Fig.



3 presents the development of exhaust emissions limits, which are more restrictive in next steps. The proposal of Euro 5 limits which will introduce in 2020 most likely will be more restrict than Euro 5. Moreover it is likely that in Euro 5 standards the new methods of measurement will be apply (cycles or real driving emissions measurement). However, many scientific papers [4–7] have shown that adopted type approval tests, such as WMTC (World Motorcycles Test Cycle) do not fully reproduce the real operating conditions of these engines, and thus also their emissions. Therefore, laboratory tests using the current WMTC test presented in this article are only the basis for further work of au-thors, which are exhaust emission tests from two-wheelers in real operating conditions. They were necessary to get to know the parameters of the combustion engine operation.

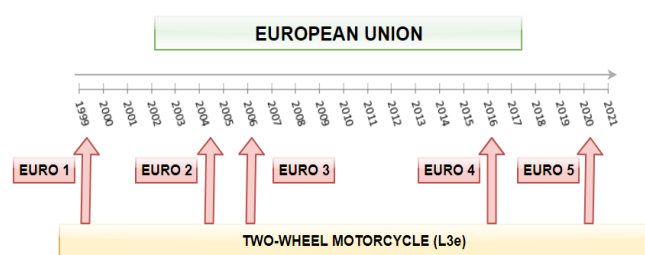


Fig. 2. History of exhaust emission standards for two-wheeled vehicles in Europe [10]

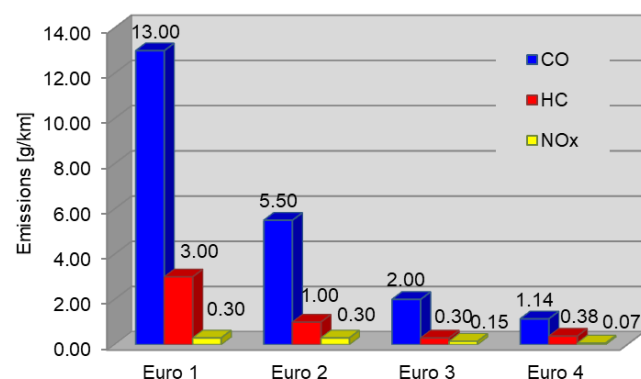


Fig. 3. The exhaust emission limits for motorcycles (category L3e)

The amending regulation „Commission Regulation of European Union 2016/646 on type-approval of motor vehicle include test procedures for RDE (Real Driving Emissions) for Euro 6d homologation LDV (Light Duty Vehicles) vehicles. As of today's date there are not similar regulation for motorcycles. Therefore, it is to be expected that in the coming years the methodology of testing powered two-wheeler-applications will remain unchanged.

## 2. Research methodology

### 2.1. Research object

The test object was a motorcycle type approved in accordance with the Euro 4 standard. The vehicle was equipped with a four-stroke engine with a displacement volume of 0.7 dm<sup>3</sup> and a maximum power of 55 kW. The

motorcycle was produced in 2017. Before the start of the test, its mileage was 740 km. Table 1 presents the technical parameters of the motorcycle. The test vehicle was equipped with a three-way catalytic reactor.

Table 1. Test motorcycle operating parameters

Engine type	2 cylinders, liquid-cooled 4-stroke, DOHC, 4-valve
Displacement	0.7 dm <sup>3</sup>
Maximum power	55 kW/9000 rpm
Maximum torque	68 Nm/6500 rpm
Cylinder diameter/piston stroke	80.0 mm × 68.6 mm
Compression ratio	11.5:1
Lubrication system	wet oil sump

### 2.2. Chassis dynamometer

The tests were performed on a single-cylinder chassis dynamometer designed for testing two-wheeled vehicles. The INTERNAL 70 motorcycle test bench was manufactured by SOFT-ENGINE, and its specification is presented in Table 2. The stand enables the reading of the vehicle's load parameters (instantaneous power, torque, speed, acceleration) as well as the distance traveled.

Table 2. Technical specifications of the dynamometer station [14]

Dynamometr	Inertial
Maximum received power	59 kW (80 HP)
Maximum received velocity	180 km/h
Dimensions: length / width / height	1900/800/4200 mm
Own weight	450 kg
Software	INERTIAL 3.0

### 2.3. Measurement equipment

Measurement of harmful compounds in laboratory conditions was possible thanks to the AxionR/S+ mobile apparatus belonging to the PEMS (Portable Emissions Measurement System) group (Fig. 4). The device allows to measure emissions of harmful and toxic compounds, both gaseous: hydrocarbons (HC), carbon monoxide (CO), carbon dioxide (CO<sub>2</sub>), nitrous oxide (NO) as well as solid particles. Technical data of the apparatus is presented in Table 3, while the test object with the measuring setup on the dynamometer stand is shown in Fig. 5. Electrochemical analyzers are used to determine NO and O<sub>2</sub>. The concentration of the first three of these compounds is measured by an NDIR (Nondispersive Infrared Sensor) non-dispersive analyzer. The PM measurement method uses a Laser Scatter based method.

In addition, the manufacturer equipped the device with a meteorological station, a GPS and a module enabling registration of data from the on-board vehicle diagnostic system (OBD). Measurement and data acquisition was done at a

frequency of 1 Hz. Corrections are made to the obtained results from the recorded data, and then the road/unit emissions of the tested exhaust gases are calculated. Moreover the AxionR/S allows measurement and recording of vehicle and engine data: vehicle speed, acceleration, engine speed, intake air temperature, manifold air pressure.



Fig. 4. The view of AxionR/S+

Table 3. AxionR/S+ device technical data [13]

Gas	Mesaurement range	Accuracy	Resolution	Type of mesaurement
HC	0–4000 ppm	$\pm 8$ ppm abs. or $\pm 3\%$ rel.	1 ppm	NDIR
CO	0–10%	$\pm 0.02\%$ abs. or $\pm 3\%$ rel.	0.001 vol. %	NDIR
CO <sub>2</sub>	0–16%	$\pm 0.3\%$ abs. or $\pm 4\%$ rel.	0.01 vol. %	NDIR
NO	0–4000 ppm	$\pm 25$ ppm abs. or $\pm 3\%$ rel.	1 ppm	E-chem
O <sub>2</sub>	0–25%	$\pm 0.1\%$ ppm abs. or $\pm 3\%$ rel.	0.01 vol. %	E-chem
PM	0 mg/m <sup>3</sup> to 300 mg/m <sup>3</sup>	$\pm 2\%$	0.01 mg/m <sup>3</sup>	Laser scatter



Fig. 5. Picture of the tested motorcycle along with the measuring apparatus on the designated dynamometer

The device is one of the most modern measuring instruments, housing analyzers for measuring both gaseous and solid compounds in a housing with a total weight of

only 18 kg. The main advantages of the device: its low weight and small size dimensions make it possible to use to test the emissions of all legally limited toxic compounds from two-wheeled vehicles in real operating conditions.

What's more, the device also measures the mass emission of solid particles, which legislators are planning to limit through legislation with the Euro 5 standard in 2020. The review of available literature showed the lack of such tests, and the only item [2] describing exhaust emission tests of two-wheeled vehicles in real conditions of operation was based on the measurements made with the use of a dedicated passenger car, whose dimensions and weight made tests possible only on a larger motorcycle unit.

## 2.4. WMTC test

The amount of two-wheeler vehicles in urban regions grow very fast, especially in Asia region. This underlines the need for improving pollution control strategies for motorcycles and mopeds. Therefore, numerous test cycles for chassis dynamometer are available. Test cycles have been developed by real conditions data that shall not be based on fixed legislative driving standards, but reflect local real driving conditions. A driving cycles usually are a speed-time profile, sometimes with the gear information, for a definite length of time for a specific type of vehicle. Cycles represent different driving patterns and modes such as acceleration, deceleration, cruising and idling modes.

The World Motorcycle Test Cycle (WMTC) is a driving cycles used to measure fuel consumption and emissions in motorcycles. The methods of WMTC cycle are set up as part of the Global Technical Regulation established under the United Nations' World Forum for Harmonisation of Vehicle Regulations.

The speed curve was a reflection of the speed characteristic of the harmonized WMTC type approval test, consisting of three phases (Fig. 6). Each of them lasted 600 seconds and was characterized by a different maximum value of the speed. The maximum speeds of the individual test phases are respectively: 50, 94 and 125 km/h, while the average: 24.4, 54.7, 94.4 km/h. The total distance in the test is 28,912 m, and the individual phases: 4065, 9111 and 15,736 m.

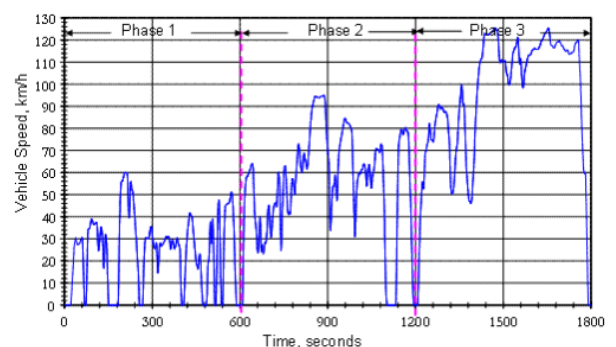


Fig. 6. WMTC test cycle speed curve [11]

## 3. Analysis and results

### 3.1. Engine operating parameters analysis

The data obtained during the WMTC test on the chassis dynamometer allowed to obtain the engine operation time

share characteristics. This is a graphical representation of the share of operating time (in relation to the duration of the entire test) for individual engine speed ranges and its fuel consumption. Fuel consumption depends on carbon dioxide emissions and load, hence these terms will be used interchangeably. Based on the obtained results, it was found that the motorcycle engine worked most often in rotational speed range of 2000–4000 rpm and fuel consumption in the range of 0–0.75 g/s (Fig. 7). The share of operating time in this range amounted to almost 62%. This is also confirmed by the average speed and average fuel consumption values, which amounted to 3220 rpm and 0.54 g/s, respectively. A significant share of operating time was also found for the speed range of 1000–1500 rpm and for fuel consumption in the range of 0–0.25 g/s, which accounts for 12% of its operation.

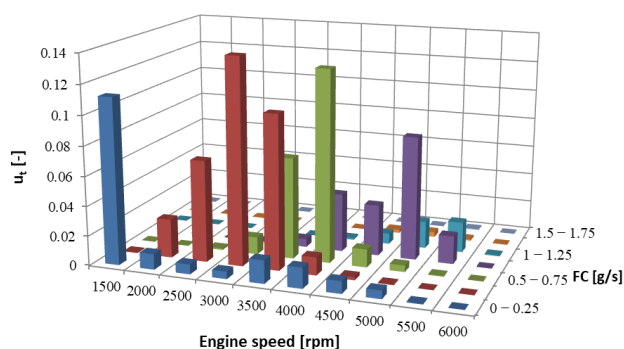


Fig. 7. Operating time density for different speed ranges and fuel consumption values

### 3.2. Analysis of the engine ecological indicators

The characteristics of the environmental performance of the tested vehicle, as in the case of the characteristics of the engine operation time density, are presented as a function of the engine rotational speed and the instantaneous engine load associated with fuel consumption. The influence of the engine operating parameters on its ecological indicators was determined for each of the substances limited by the Euro 4: CO, HC, and NO<sub>x</sub>. Due to the close relation between the carbon dioxide emissions and the fuel consumed, the characteristics for this exhaust component were omitted.

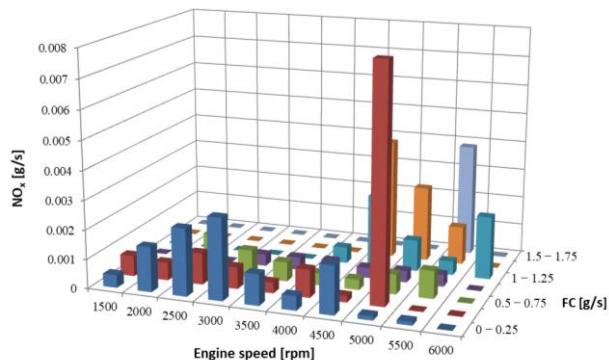


Fig. 8. NO<sub>x</sub> emission per second as a function of engine speed and fuel consumption ranges

The time emission of NO<sub>x</sub> depends both on engine speed and engine load (Fig. 8). For the tested motorcycle, the maximum value of NO<sub>x</sub> emissions (0.008 g/s) was registered for the speed range 4500–5000 rpm and the load of 0.25–0.5 g/s of fuel consumed. The average emission for this compound was 0.0067 g/s.

Although NO<sub>x</sub> emission was determined for a wide range of engine speeds and loads, the highest values were registered for the high rotational speeds range of 4000–5500 rpm and fuel consumption of 0.25–0.5 g/s. High engine speeds generate a higher temperature in the cylinder, which directly favors the formation of nitrogen oxides.

The characteristics of CO<sub>2</sub> emissions as a function of rotational speed and load are shown in figure 9. This figure indicates that the highest emission values were in the high engine speed range from 4500–5000 rpm and fuel consumption in the range 0.5–1.75 g/s. The high engine speed, and hence the high doses of fuel supplied, cause global and local oxygen deficiencies, which is closely related to the formation of CO<sub>2</sub>. What is more, their formation was also influenced by the high temperature in the cylinder, which was conducive to CO<sub>2</sub> dissociation. The highest value, 0.05 g/s, was recorded for speeds in the range of 5000–5500 rpm and fuel consumption of 1.5–1.75 g/s.

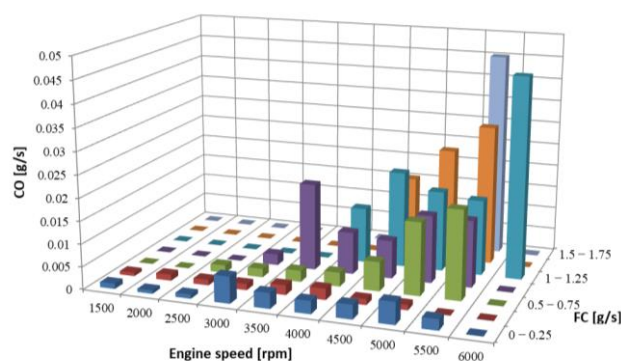


Fig. 9. CO emission per second as a function of engine speed and fuel consumption ranges

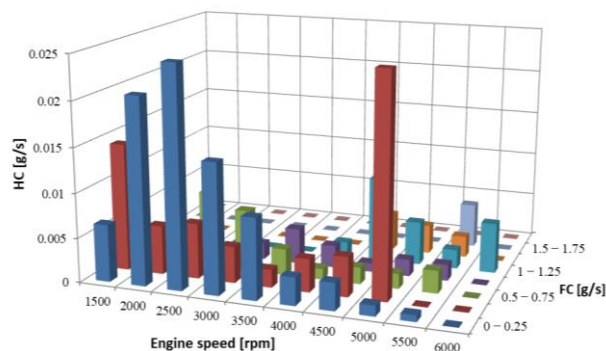


Fig. 10. HC emission per second as a function of engine speed and fuel consumption ranges

The characteristics of the HC emission per second as a function of engine rotational speed and fuel consumption (Fig. 10) showed that the largest hydrocarbon emission



values were in the range of low loads and average rotational speeds of 1000–2500 rpm with fuel consumption in the range of 0–0.5 g/s.

Another significant range of the existing HC emission values is for the rotational speeds of 4000–5500 rpm and a load of 0.25–1.75 g/s. In this value range the highest HC emission value was recorded, which amounted to 0.005 g/s. The reason for this is the fact that at high rotational speeds the injected fuel dose did not mix thoroughly resulting in incomplete combustion.

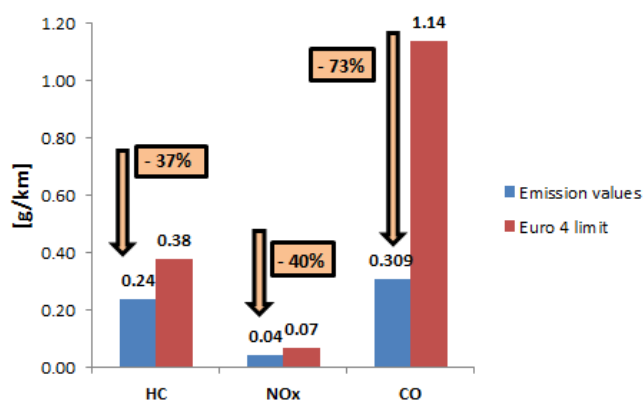


Fig. 11 Comparison of the determined road emission with the Euro 4 emission standard

Using the determined mass emissions of individual gas compounds and the distance traveled during the whole test, the road emission of each compound was calculated. The obtained emission values were compared with the admissible values specified for the Euro 4 standard (Fig. 11). The set emission value limits were not exceeded. For CO, an emission value was 73% lower than the limit value, for HC and NO<sub>x</sub> it was lower by almost 40%, which was associated with high efficiency of the engine exhaust aftertreatment system, which comprised of a three-way catalytic reactor (allowing oxidation of carbon monoxide and hydrocarbons at simultaneous reduction of nitrogen oxides). Meeting the emission standards was also the result of the fact that the vehicle was still fairly new.

## 4. Conclusions

The tests performed on a two-wheel vehicle chassis dynamometer and analysis of their results allowed to formulate conclusions regarding the work indicators and ecological characteristics of the test vehicle. The analysis did not find any exceedances of the emission limit imposed by the legislators, which confirms the validity of the current directions of motorcycle engines development. The main development tendency (as in the case of car engines) is to meet ever more stringent emission standards by using engine exhaust aftertreatment systems. The test vehicle was equipped with a three-way catalytic reactor. The fact that both the vehicle and the aftertreatment system were not deteriorated through heavy exploitation lead to a positive impact on the final road emission results for all harmful compounds limited by the Euro 4 standard.

The WMTC test is characterized by high engine speed variability, which is extremely difficult to accurately reproduce on a chassis dynamometer. Differences of several dozen percent between the final obtained results and the emission limits prove that the vehicle meets the established standards at the lower end of their range. This is very advantageous in the aspect of long-term operation of the engine and the exhaust aftertreatment systems, because over time their wear will adversely affect the engine's ecological indicators.

Numerous studies have shown that emissions in real operating conditions are significantly different from those obtained under laboratory conditions when using type approval tests (this is described in more detail in the introduction). Therefore, the research done in this article is the basis for further research by the authors, which will be focused on measurements of engine operating parameters and emissions in real driving conditions. The measurements will be made on the same test vehicle using the same measuring apparatus, in order to enable a reliable comparison of the obtained results. The development of measurement technology for the emission of toxic and harmful components (lower weight and dimensions of the exhaust gas analyzers, and the ability to measure gaseous compounds and particulates using only one device) makes it possible to test even two-wheeled vehicles in real operating conditions. Such research is new, both on a national and global scale.

## Bibliography

- [1] Asian Development Bank. Integrated Vehicle Emission Reduction Strategy for Greater Jakarta, Indonesia, 2002.
- [2] HIESMAYR, J., SCHMIDT, S., HAUSBERGER, S., KIRCHBERGER, R. et al. Results, assessment and legislative relevance of RDE and fuel consumption measurements of two-wheeler-applications. *SAE International*. 2017, **32**(0042).
- [3] ICCT, The International Council on Clean Transportation, Where we work/India, <http://www.theicct.org/india>.
- [4] MARTINI, G., MANFREDI, U., DE GENNARO, M. Gaseous emissions from Euro 3 motorcycles and Euro 5 passenger cars measured over different driving cycles. *SAE International*. 2013, **01**(2619).
- [5] SALEH, W., KUMAR, R., KIRBY, H., KUMAR, P. Real world driving cycle for motorcycles in Edinburgh. *Transportation Research*. 2009, **14**, 326-333.
- [6] TONG, H.Y., TUNG, H.D., HUNG, W.T., NGUYEN, H.V. Development of driving cycles for motorcycles and light-duty vehicles in Vietnam. *Atmospheric Environment*. 2011, **45**, 5191-5199.
- [7] TSAI, J.H., CHIANG, H.L., HSU, Y.C., PENG, B.J et al. Development of a local real world driving cycle for motorcycles for emission factor measurements. *Atmospheric Environment*. 2005, **39**, 6631-6641.
- [8] TSAI, J.H., HUNAG, P.H., CHIANG, H.L. Air pollutants and toxic emissions of various mileage motorcycles for ECE driving cycles. *Atmospheric Environment*. 2017, **153**, 126-134.



- [9] YUDIOSON, A., REKSOWARDOJO, I.K., SULAEMAN, A., Motorcycle emission profiles in Bandung City, Indonesia. *SAE International*. 2017, **32**(0076).
- [10] Worldwide Emissions Standards. Passenger Cars & Light Duty Vehicles. Delphi brochure 2016/2017.
- [11] [www.asphaltandrubber.com](http://www.asphaltandrubber.com)
- [12] [www.ec.europa.eu](http://www.ec.europa.eu)
- [13] [www.globalmrv.com](http://www.globalmrv.com)
- [14] [www.soft-engine.org](http://www.soft-engine.org)
- [15] [statistica.com](http://statistica.com)

Natalia Szymlet, MEng. – Faculty of Machines and Transport, Poznan University of Technology.

e-mail: [Natalia.R.Szymlet@doctorate.put.poznan.pl](mailto:Natalia.R.Szymlet@doctorate.put.poznan.pl)



Łukasz Rymaniak, DEng. – Faculty of Machines and Transport, Poznan University of Technology.

e-mail: [Lukasz.Rymaniak@put.poznan.pl](mailto:Lukasz.Rymaniak@put.poznan.pl)



Piotr Lijewski, DSc., DEng. – Faculty of Machines and Transport, Poznan University of Technology.

e-mail: [Piotr.Lijewski@put.poznan.pl](mailto:Piotr.Lijewski@put.poznan.pl)



Maciej Siedlecki, MEng. – Faculty of Machines and Transport, Poznan University of Technology.

e-mail: [Maciej.S.Siedlecki@doctorate.put.poznan.pl](mailto:Maciej.S.Siedlecki@doctorate.put.poznan.pl)



Barbara Sokolnicka, MEng. – Faculty of Machines, Transport at Poznan University of Technology.

e-mail: [Barbara.D.Sokolnicka@doctorate.put.poznan.pl](mailto:Barbara.D.Sokolnicka@doctorate.put.poznan.pl)



## Optical analysis of the gas flame development in a RCM using a high-power ignition system

*The combustion process quality is determined by several factors: the composition of the fuel-air mixture in the vicinity of the spark plug and the discharge conditions on the spark plug. This article assesses a high-power ignition system using optical gas flame propagation analyzes. The tests were carried out in a rapid compression machine, using a fast camera for filming. The spark plug discharge quality assessment was determined indirectly by the flame propagation conditions after the ignition of the mixture (during methane combustion). The size of the flame surface and the rate of its change were assumed as a comparative criterion. It has been found that when using an ignition system with high discharge power the rate of flame development is 14% higher with respect to conventional ignition systems. In addition, the shorter development time of the early flame phase after discharge when using the new ignition system was confirmed. Based on the obtained test results and analyzes, modifications of engine operation settings were indicated, resulting from the use of a high discharge power system.*

Key words: spark ignition, plasma ignition, optical tests, combustion process diagnostics, ignition systems

### 1. Introduction

The combustion process in a conventional spark-ignition engine is triggered by the external thermal energy generated by the electric arc. Its value and the nature of the transfer of this energy have a fundamental impact on the development of the flame front, and thus on the combustion process parameters (flame development speed, heat release rate, combustion efficiency) and the ability of the mixture to ignite.

There are solutions in the form of an increased number of spark plugs in the combustion chamber (Twin Spark engine or DTSI system – Digital Twin Spark Ignition) to increase the ignition energy and multiply the number of ignition points in the combustion chamber volume. Thanks to these solutions, it is possible to shorten the duration of combustion to a minimum [3, 6]. The disadvantage of this type of ignition systems is the necessity to use a minimum of two spark plugs, which is not always possible due to the space restrictions in the engine head. In addition, such systems have a greater risk of failure.

An alternative method of initiating the ignition using a spark plug discharge is a laser system. It is characterized by the multiple times greater energy supplied and has the capacity of focusing it in a central point of the combustion chamber [9]. In addition, it is possible to ignite the mixture in several points at the same time using one "spark plug". Unfortunately, this system is limited by the large laser costs and the need for frequent repair of optical elements. This results in it being used only in laboratory conditions and prototype engines.

Camilli et al. [2] pointed out the possibility of non-invasive modification of a conventional ignition system using a capacitor system to increase the efficiency of the mixture combustion process. Improved engine performance indicators in the form of specific fuel consumption, power, CO<sub>2</sub> and NO<sub>x</sub> emissions, as well as the repeatability of the engine operation cycles. Such a modernized system, in combination with a low-resistance spark plug, allows increasing the efficiency of energy transfer from 1% with

a standard solution up to 50% using a system with a larger electrical capacity [7].

The use of capacitors contributes to the increase of the peak current in the breakdown phase reaching a value of up to 1000 A for 5 ns. At the same time, the power released in the system reaches up to 5 MW. A conventional ignition system, with the same engine operating conditions, reaches a value of up to 100 mA, producing 0.125 W of power [8].

Jacobs et al. [4] in collaboration with a certified AVL research center used optical analysis to demonstrate that using a spark plug with increased peak power improves ignition initiation and flame development, resulting in faster combustion of the mixture compared to a conventional spark plug. This is explained by the formation of a large volume plasma between the spark plug electrodes in the first breakdown phase [10].

### 2. Aim of research

Optical flame development analysis using the ignition systems with a large, impulse delivered maximum power, is limited in the modern literature only to the initial phase of mixture ignition. In addition, it mainly concerns engines powered by a stoichiometric gasoline-air mixture. The current state of knowledge does not allow an unambiguous assessment of the flame development during the combustion of gas mixtures.

The authors of this article proposed the assessment and comparative optical analysis of flame development during the combustion of a stoichiometric mixture of natural gas and air using a conventional ignition system and a system with an increased electrical capacity.

The analysis of the results of such tests will allow to supplement the current state of knowledge with information on the high power maximum ignition system. These works can significantly contribute to improving the combustion process control, and thus obtaining more favorable operational and emission indicators for the operation of spark-ignition engines fueled with natural gas.

### 3. Research method

#### 3.1. Test object

Experimental research was performed on a rapid compression machine (RCM) that performs a piston cycle of an internal combustion engine at defined thermodynamic conditions. The choice of the test object was dictated by the possibility of full optical access to the combustion chamber (Fig. 1). The RCM technical parameters are shown in Table 1.

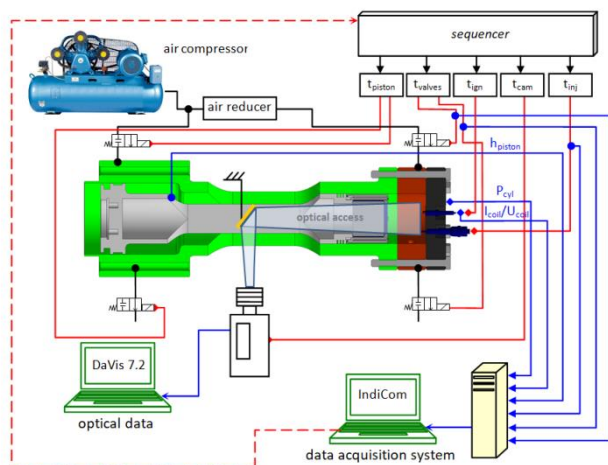


Fig. 1. Diagram of the RCM setup [5]

Table 1. Characteristics of a rapid compression machine

Parameter	Unit	Value
Bore × stroke	mm	80 × 90
Compression ratio	–	14.7
Simulated engine speed	rpm	up to 500
Ignition system	–	spark ignition
Valves system	–	electromagnetic
Fuel system	–	direct gas-injection (electromagnetic injector)
Air system	–	naturally aspirated

The air supply system for the piston enables obtaining the average piston rod linear speed corresponding to the average linear velocity of the piston of the internal combustion engine (at its rotational speed of 500 rpm). Compressed air is supplied to the chamber under the piston rod, which expands the piston rod towards the combustion chamber. The solenoid valves used for controlling the air inlet and exhaust gas outlet in the RCM combustion chamber ensure the required reaction time. The special design of the piston rod in conjunction with a mirror and a transparent piston crown (quartz glass) allows the phenomena occurring in the combustion chamber to be observed.

The natural gas-air mixture is prepared using direct injection with Bosch injectors. It is ignited by a spark plug placed centrally in the combustion chamber. The ignition controller (produced by Mechatronics Kędzia) enables setting the ignition advance angle and the energy discharge value with the specified charging time of the coil. A high-voltage ceramic capacitor connected in parallel was used to execute the high-power ignition (Fig. 2). The order of devices activating along with the time of their activation is

controlled by the microcontroller (sequencer) with the trigger uncertainty equal to 1 ns.

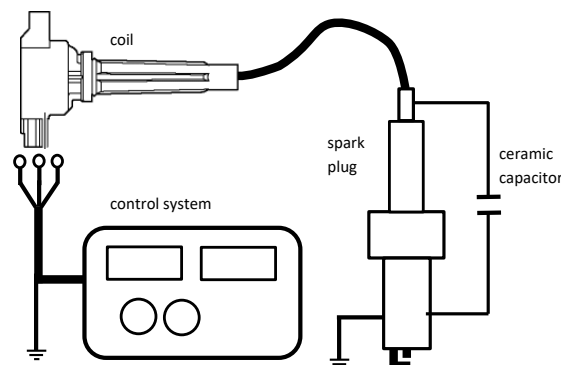


Fig. 2. Setup diagram of a high power ignition system

#### 3.2. Measurement apparatus

To determine the phenomena occurring in the combustion chamber and to compare the ignition systems used, an engine indication system, necessary sensors and a camera for fast filming were used.

A LaVision camera model HSS5 that allows recording images at a maximum frequency of 250,000 Hz was used. The monochrome CMOS sensor used allows to record images at a maximum resolution of  $1024 \times 1024$  pixels. The tests used a 5 kHz filming speed with an image size of  $1024 \times 624$  pixels (the active filming area was  $510 \times 510$  pixels). The camera was controlled by an external computer with the manufacturer's software (DaVis 7.2) allowing advanced image processing.

A piezoelectric AVL GH14D pressure sensor with a measuring range of 0–250 bar was used to record pressure in the RCM combustion chamber. The linear position of the RCM piston was determined using the Megatron LSR 150 ST R5k linear potentiometer. The charging current of the primary ignition coil as well as the discharge voltage on the spark plug was measured using the current clamp (Pico Technology) and the high voltage probe (Chauvin Arnoux SHT40kV), respectively. The above signals were recorded using the induction system – AVL IndiCom with data acquisition software – AVL Concerto.

#### 3.3. Test conditions

A comparison of the proposed methods of spark ignition, i.e. a conventional solution and a high-power ignition required the adoption of a comparative criterion. Thus, the area of the flame in relation to the combustion chamber volume was taken as an indicator. The second indicator used was the flame surface increase rate over time. Due to the method of obtaining research data (access to the combustion chamber from the bottom of the piston – Fig. 1), the flame area is understood as a flat exposure of the image (in contrast to the spatial distribution of the flame in the combustion chamber). Image analysis was performed with 15 repetitions of the combustion process carried out by a rapid compression machine for both ignition systems.

The stoichiometric fuel mixture in the cylinder was determined based on the previously performed characteristics of the injector fuel outflow and the total volume of the

RCM chamber. Before the next cycle, the volume of the cylinder was flushed with fresh air to remove the remaining exhaust gases. The injected gas dose was kept at  $q_0 = 32$  mg. The obtained average linear velocity corresponded to the average linear velocity of the piston of an internal combustion engine with the rotational speed equal to  $n = 360$  rpm.

The maximum charging current of the primary winding of the ignition coil ( $I_{\max \text{ av}}$ ) was 7 A, which resulted in an average maximum voltage on the secondary winding ( $U_{\max \text{ av}}$ ) of 4.3 kV (where the distance between electrodes was  $d = 0.4$  mm). The discharge on the spark plug was on average 10 ms before TDC ( $t_{\text{av}}$ ). The remaining test conditions are shown in Table 2.

Table 2. Test conditions

Ignition type	conventional ignition	high discharge energy ignition
$n_{\text{sr}}$ [rpm]	360	
$q_0$ [mg]	32	
$I_{\max \text{ sr}}$ [A]	7	
$U_{\max \text{ sr}}$ [kV]	4.6	3.9
$t_{\text{sr}}$ [ms before TDC]	10.6	9.6
$C$ [pF]	0	480
$R$ [k $\Omega$ ]	1.6	
$d$ [mm]	0.4	
camera	$f = 5$ kHz $1024 \times 624$ px	

#### 4. Data selection criteria

Initial analysis of indicated data, in the form of indicated pressure, showed a high non-repeatability of the RCM work cycles. The issue of the non-repeatability of RCM's work is presented in [1]. The reasons for such operating conditions of RCM are seen in the injection system (injec-

tion of gas into the combustion chamber) and the nature of fuel injection.

Further analysis of the cylinder pressure characteristics and the piston position allowed to determine the linear velocity, which was characterized by a very low repeatability between cycles. This was probably due to the instability of the air pressure supplied to the chamber under the piston rod, the limited air tightness of this chamber and the solenoid valves. The linear velocity of the piston, different for each cycle, contributed to the differentiation in the moment of ignition, which was performed as a function of time alone. In addition, each ignition was carried out under different thermodynamic conditions (pressure, temperature) due to different piston positions.

In the next stage of research work, a criterion allowing the elimination of incorrect cycles was adopted. The criterion was the standard deviation of pressure to the time when the combustion took place so that the thermodynamic conditions during the discharge were similar.

Standard deviation values for conventional and high-power ignition were 1.61 and 1.21 bar, respectively (Fig. 3). The pressure characteristics were considered abnormal if their absolute value exceeded the average pressure set for all cycles by 1.21 bar (standard deviation value for high power ignition – see the three-sigma rule). As a result of such criterion, 6 out of 15 cycles for each ignition system were eliminated as unreliable. Standard deviation pressure value for the remaining operating cycles was 0.57 for conventional ignition and 0.83 for ignition with a high maximum discharge power. Differences between mean values of pressure at the moment of ignition for both solutions including selected cycles did not exceed 8%.

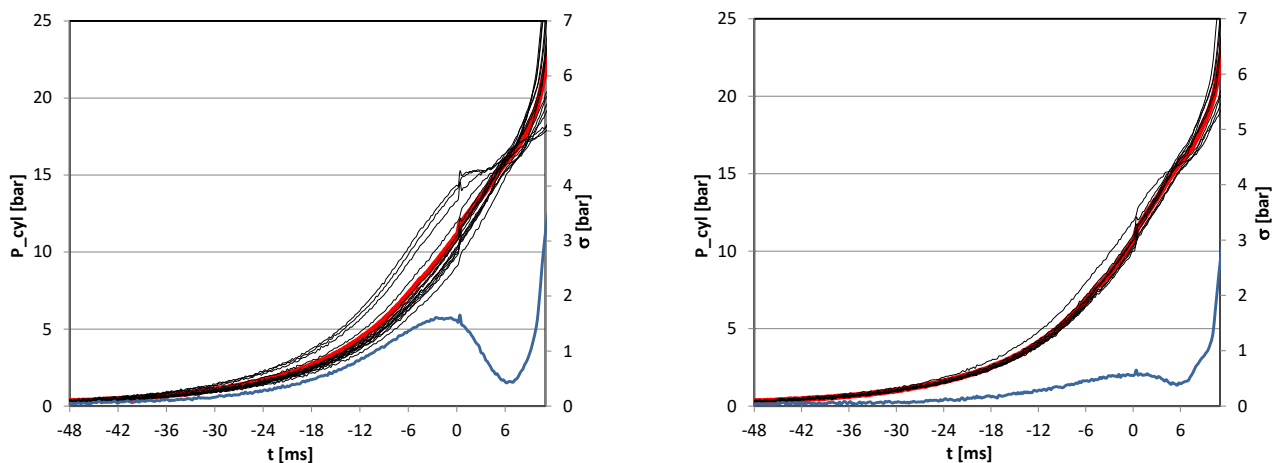


Fig. 3. Sequences of indicated pressure  $P_{\text{cyl}}$  (black), mean value (red) and standard deviation (blue) for the compression curve using conventional ignition. On the left before the selection, on the right after the exclusion of incorrect RCM work cycles; the characteristic peak on the pressure curve was caused by interferences from the ignition system ( $t = 0$  ms)

#### 5. Optical analysis algorithms

Pictures taken using the HSS5 camera included more than 140 ms of the RCM work cycle at 5000 fps. Such a long recording time resulted from the uncertainty of the moment of ignition. In order to achieve the desired results, further processing of the photos was necessary. For this

purpose, the camera manufacturer software LaVision – DaVis 7.2 was used. The algorithm for optical analysis is shown in Fig. 4.

In the first stage, the number of photos was limited to the minimum value, containing only the necessary information. The analysis was limited to approximately 300



consecutive images. Then, the background was subtracted (the so-called reference image – a black frame). This procedure was used to eliminate noises and reflections on other pictures.

In the next stage, a mask was used to limit the analyzed area. The circle-shaped mask was the same size as the combustion chamber and insulated the remaining area outside the chamber (the bottom of the piston, cylinder walls).

The last stage of the analysis was to calculate the flame area in the RCM combustion chamber. A program was written in the internal language of the DaVis software by the article authors. For its operation it was necessary to:

1) determine the minimum luminance value attributed to the analyzed pixel (above the given luminance value the pixel was treated as the flame surface);

2) determine the cylinder diameter expressed in pixels.

Images showing the beginning of an electric discharge with different discharge powers are shown in Fig. 5.

The image sequences processed using the algorithm shown in Figure 4 are depicted in Fig. 6.

The obtained values of the flame surface and their analysis are presented in Chapter 6.

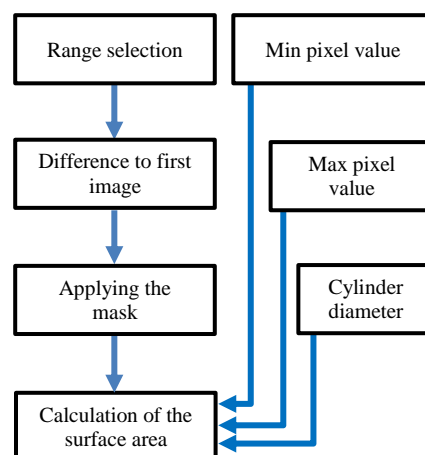


Fig. 4. Optical analysis algorithm using DaVis 7.2

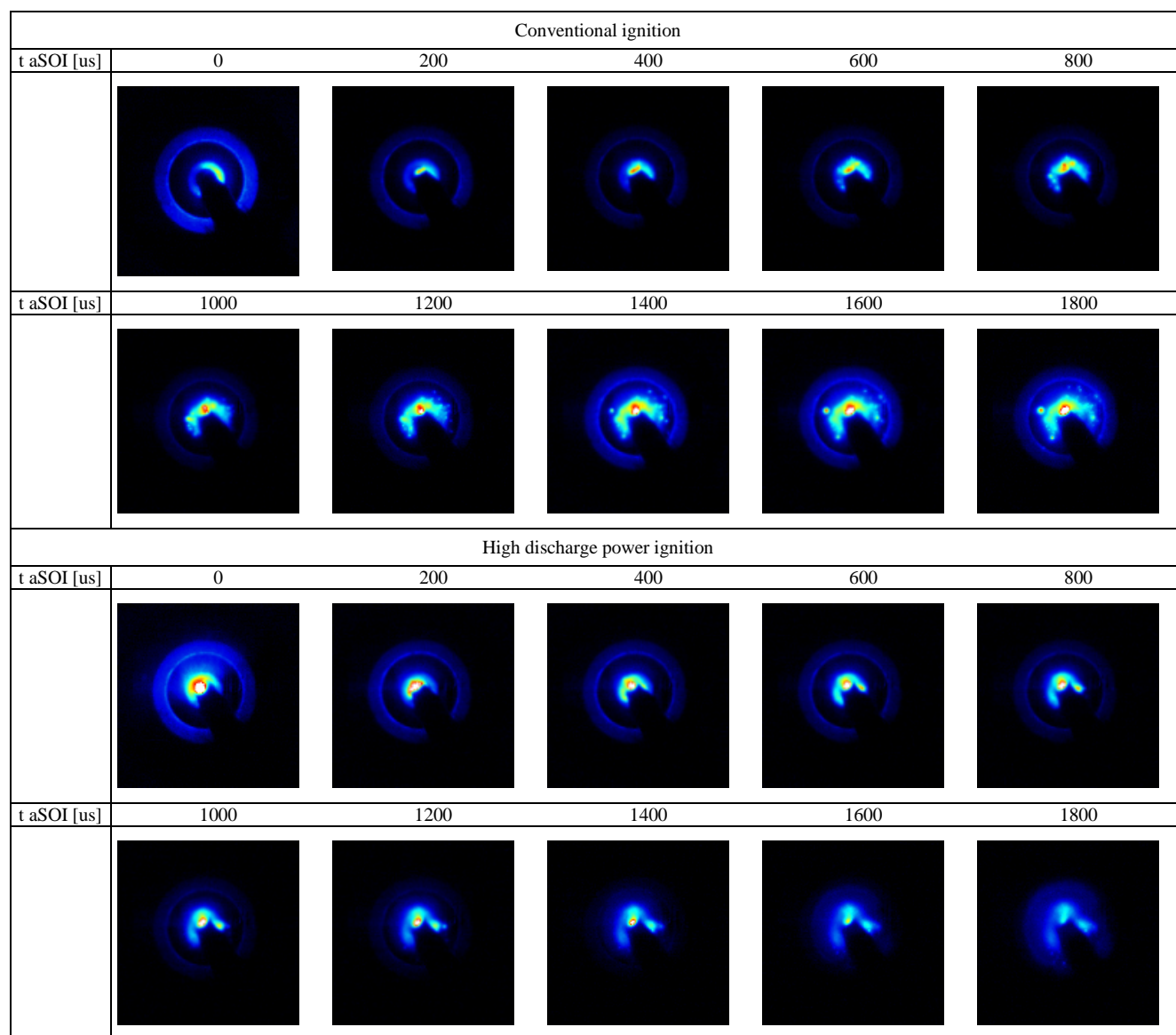


Fig. 5. Images of the ignition phase start ( $f = 5$  kHz, the first image represents SOI – start of ignition)

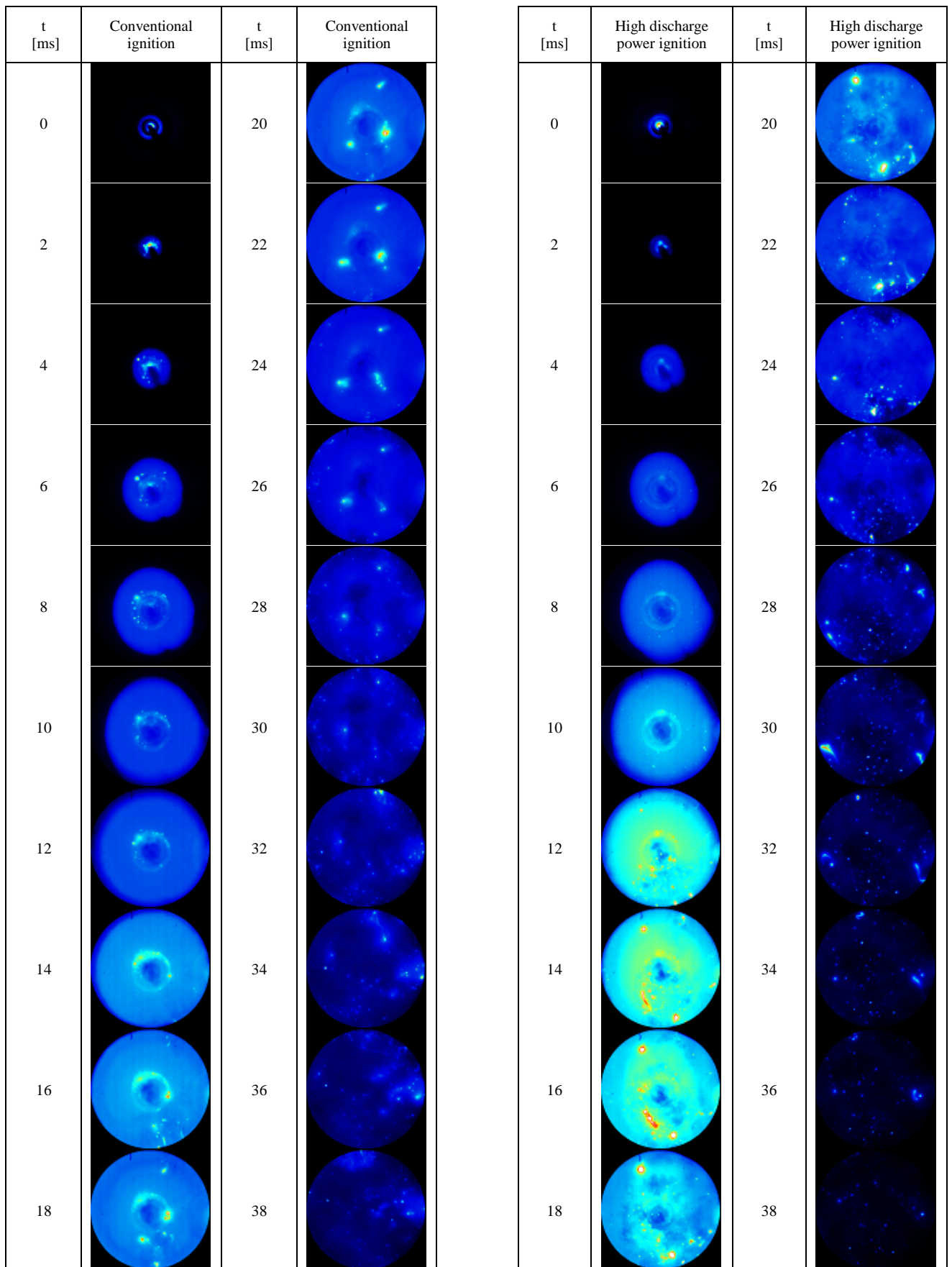


Fig. 6. Selected images of the combustion process using conventional ignition and high discharge power ignition ( $f = 5$  kHz, the first image represents SOI – start of ignition)

## 6. Results

The flame area values in the RCM combustion chamber were determined as a result of image analysis using the DaVis software. The specific nature of the optical access to the combustion chamber and the software application of image masking made it possible to analyze over 1800 mm<sup>2</sup> of the filmed combustion chamber area. The results of analyzes of all selected cycles along with the standard deviation value are shown in Fig. 7. The moment of the electric discharge between the spark plugs was taken as the point where time = 0.

Standard deviation values of the surface area in the flame development phase (up to 10 ms) and in the decay phase (from 25 ms) for conventional ignition exceed the values of this deviation when using a high-capacity ignition. Alternative ignition is characterized by greater stability and process repeatability, which is probably due to the higher value of current flowing in the breakdown phase, in

which the ignition is initiated. In the case of a conventional solution, the ignition may be initiated at random during one of three stages of ignition: breakdown, arc or glow. In addition, a shorter time gap is observed between breakdown point and the development of the flame (Fig. 8) with a mixture ignited with high power ignition. The greater flame surface area value in the combustion chamber using conventional ignition in the first period after the start of the process (up to 2 ms) result from the constraints of the created program. The high luminance value attributed to the pixels at the time of the electric breakdown was treated as the flame surface. Although, in reality the higher brightness (luminance of pixels) was caused by the visible light emitted by the electric arc. Nevertheless, on Fig. 8, it is possible to notice a greater emission of visible light during a standard ignition, which causes additional energy losses in the system.

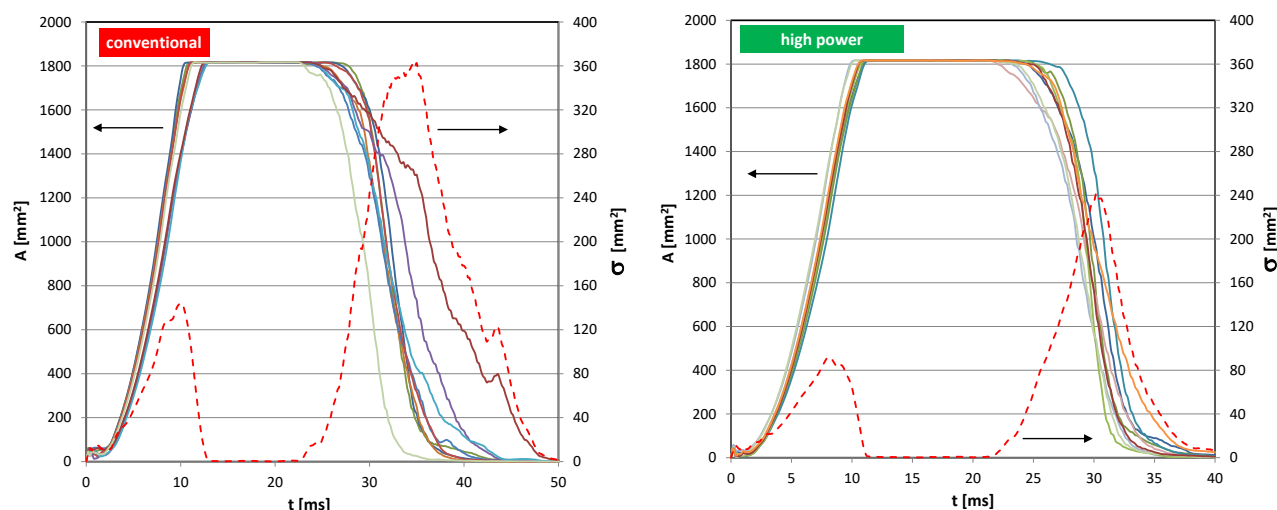


Fig. 7. Flame surface area as a function of time (solid line) and its standard deviation (dashed line); on the left – conventional ignition, on the right – high-power ignition

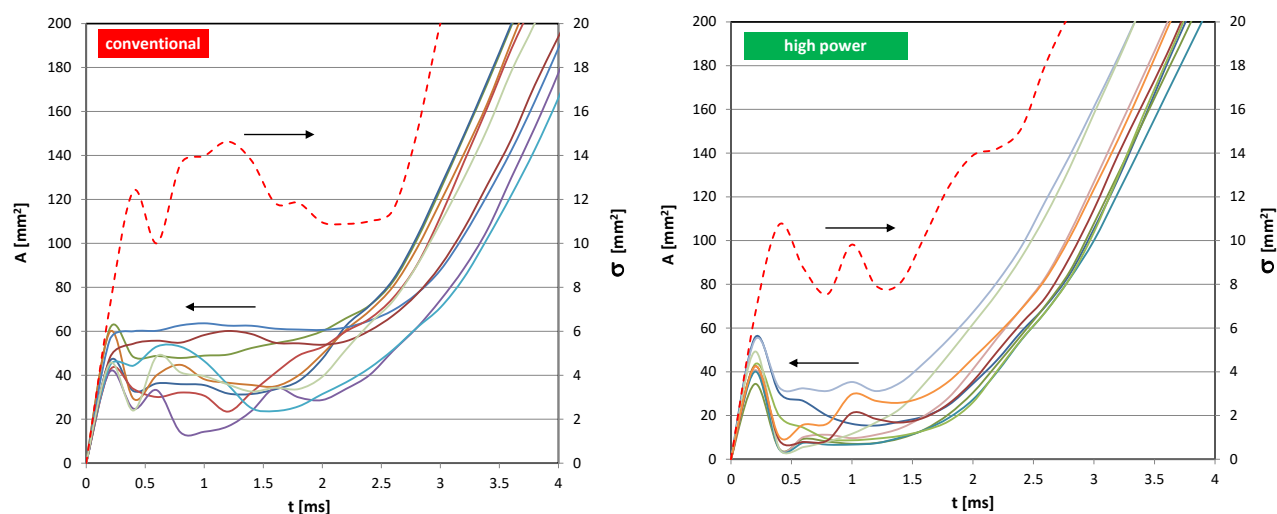


Fig. 8. Flame surface area as a function of time (solid line) and its standard deviation (dashed line) for the early stage of flame development; on the left - conventional ignition, on the right - high-power ignition

The mean values of the flame surface area and the time derivative of this field inform indirectly about the flame development rate. The results of these analyzes are presented in Fig. 9. From the mean value analyzes it was found, that the flame presence duration in the combustion chamber for high-power ignition was reduced by about 20% in relation to the conventional ignition. In addition, the maximum flame velocity, expressed as a derivative of the surface area of the flame, was found to be 14% higher. These values indicate the possibility of increasing the thermal efficiency of the engine using a high-power ignition.

The analysis of the initial flame development phase in a short time after the electric breakdown allowed to determine the average time delay from the electric breakdown to the moment when the flame front begins developing. This time was approximately 2 ms for standard ignition and 1.5 ms for high-power ignition. These values are directly referenced in the voltage values on the secondary winding of the ignition coil, where the voltage value after this time drops to zero, thus ending the glow stage in the discharge process. With regard to the second solution, its use in an internal combustion engine may require correction of the ignition advance angle.

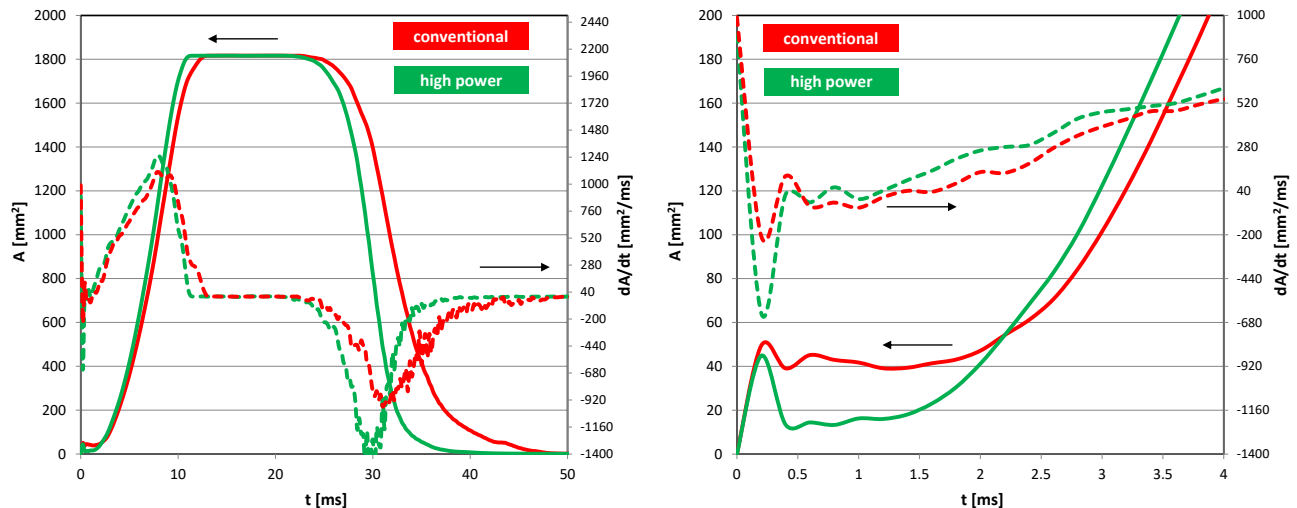


Fig. 9. Average flame area in the combustion chamber as a function of time (solid line) and its derivative (dashed line) for the entire combustion process (left), and early stage of flame development (right)

## 7. Conclusions

The analysis presented in the article concerned the optical evaluation of flame development using two ignition methods: conventional and high discharge power, when burning gaseous fuel (methane) using a stoichiometric mixture.

Based on the specific comparative criteria, which were: the flame surface area and its rate of change, the following conclusions were formulated for ignition systems (classical and high ignition power):

1. Based on the mean values analysis of the flame surface averaged over many cycles, the flame duration in the combustion chamber was found to be reduced by about 20% when using high-power ignition relative to the conventional ignition.

2. The maximum flame velocity expressed as a derivative of the surface area of the flame was determined to be approximately 14% greater.
3. During the analysis of the initial flame development phase, the average time delay between the electric breakdown and the development of the flame front was determined (the value of the secondary voltage in the system was used as a confirmation). This time was approximately 2 ms for standard ignition and 1.5 ms for high-power ignition.

The values indicated above show the possibility of increasing the thermal efficiency of the engine with the use of a high-capacity ignition.

*The research presented in the article was conducted as part of the statutory work no 05/52/DSPB/0261.*

## Nomenclature

A flame area  
f frequency  
RCM rapid compression machine  
P<sub>cyl</sub> cylinder indicating pressure  
 $\sigma$  standard deviation  
t time  
SOI start of ignition

U voltage  
I current  
q<sub>0</sub> fuel dose  
n engine speed  
TDC top dead centre  
DTSI Digital Twin Spark Ignition



## Bibliography

- [1] BOROWSKI, P., CIESLIK, W., PIELECHA, I., WISŁOCKI, K. Evaluation of the repeatability of combustion process in rapid compression machine using optical research. *XXII International Symposium on Combustion Processes*. 22-25.9.2015, Poland.
- [2] CAMILLI, L.S., GONNELLA, J.E. Improvement in spark-ignition engine fuel consumption and cyclic variability with pulsed energy spark plug. *SAE Technical Paper*. 2012; DOI: 10.4271/2012-01-1151.
- [3] FORTE, C., BIANCHI, G.M., CORTI, E., FANTONI, S. Evaluation of the effects of a Twin Spark Ignition System on combustion stability of a high performance PFI engine. *Energy Procedia*. 2015, **81**, DOI: 10.1016/j.egypro.2015.12.143.
- [4] JACOBS, T.J., CAMILLI, L., NEUBAUER, M. High power discharge combustion effects on fuel consumption, emissions, and catalyst heating. *SAE Technical Paper*. 2014, DOI: 10.4271/2014-01-2626.
- [5] PIELECHA, I. Optyczne metody diagnostyki wtrysku i spalania benzyny. *Wydawnictwo Politechniki Poznańskiej*. Poznań, 2017.
- [6] RAMTILAK, A., JOSEPH, A., SIVAKUMAR, G., BHAT, S.S. Digital Twin Spark Ignition for improved fuel economy and emissions on four stroke engines. *SAE Technical Paper*. 2005; DOI: 10.4271/2005-26-008.
- [7] ROHWEIN, G.J. An efficient, power-enhanced ignition system. *IEEE Transactions on Plasma Science*. 1997, **25**, 2.
- [8] ROHWEIN, G.J., CAMILLI, L.S. Automotive ignition transfer efficiency. *SAE Technical Paper*. 2002; DOI: 10.4271/2002-01-2839.
- [9] TSUNEKANE, M., INOHARA, T., KANEHARA, K., TAIRA, T. Micro-solid-state laser for ignition of automobile engines. *Advances in Solid State Lasers Development and Applications*. 2010.
- [10] <http://pulstarnatgas.com/testing/existence-of-plasma>

Łukasz Fiedkiewicz, MEng. – Faculty of Machines and Transport, Poznan University of Technology.

e-mail: [Lukasz.M.Fiedkiewicz@doctorate.put.poznan.pl](mailto:Lukasz.M.Fiedkiewicz@doctorate.put.poznan.pl)



Prof. Ireneusz Pielecha, DSc., DEng. – Faculty of Machines and Transport, Poznan University of Technology.

e-mail: [Ireneusz.Pielecha@put.poznan.pl](mailto:Ireneusz.Pielecha@put.poznan.pl)



## Analysis of wind impact on emission of selected exhaust compounds in jet engines of a business jet aircraft in cruise phase

*Among the most important problems currently faced by air transport, we can distinguish the adverse impact of aircrafts on the natural environment, as well as the rising costs of transport. One of the possibilities to improve this situation is better adjustment of aircraft characteristics to the performed transport tasks, taking into account all the requirements and limitations that exist in air traffic and the adverse impact of air transport on the natural environment. It is reflected in the research tasks conducted under the SESAR program. The aspiration to minimize the adverse impact of aircrafts on the environment is executed, among others, through determining such trajectories that are characterized by minimal fuel consumption or minimal emission of harmful substances in the engines exhausts. These goals are corresponding with the research conducted and described in the paper. The main aim of the work was to analyse the impact of wind speed and direction on the emission of harmful substances of a jet aircraft performing a flight on a given route. For research purposes, the route between two Polish cities Gdansk and Rzeszow was considered. The distance between the two airports was divided into sections for which wind direction and strength were determined (read from the windy.com website). Next, the aircraft performance was determined and the fuel consumption and the amount of harmful compounds ( $\text{CO}_2$ ,  $\text{NO}_x$ ,  $\text{CO}$  and  $\text{HC}$ ), emitted in the engines exhausts were determined for the route from Gdansk to Rzeszow (under favourable wind conditions) and on the return route – from Rzeszow to Gdansk (under unfavourable wind conditions). For comparative purposes, emission of these substances for windless conditions was also determined. The results are presented in tables and depicted in the graph, as well as discussed in the conclusions of the paper.*

Key words: jet engine, emission, exhausts, fuel consumption, cruise phase, ATM, SESAR

### 1. Introduction

As a result of the intensive development of air transport, there is observed a continuous increase in emissions of harmful substances in jet engines exhausts, influencing the air quality and deepening the greenhouse effect, which in turn leads to irreversible global climate change. In 1988 there was established the Intergovernmental Panel on Climate Change (IPCC) to monitor negative climate changes resulting from the economic activities [1, 8].

According to the IPCC reports, if preventive measures are not taken, the temperature in the current century will increase more than in the last 10,000 years, which in turn will affect the entire ecosystem. To increase environmental protection, the United Nations Framework Convention on Climate Change (UNFCCC) was adopted, under which the Kyoto Protocol was signed. This is the most important agreement in the field of climate protection, the objective of which is to reduce greenhouse gas emissions through pro-ecological activities undertaken mainly in highly developed countries. The European Union is a party to the Kyoto Protocol with the main objective of reducing emissions in all the EU countries (reduction of greenhouse gas emissions by 8% compared to 1990 levels), and individual emission targets for each EU Member State. The basis of the EU climate policy is the European Climate Change Program (ECCP), initiated in 2000, which is a combination of voluntary activities, good practices, market mechanisms and information programs.

The activities aimed at reducing the negative impact of air transport and aviation industry on the environment match the above goals. They are reflected in two largest aviation programs implemented by the European Union.

The first one is SESAR 2020 [12], which is a continuation of the SESAR program, while the second one is the Clean Sky 2 [3], which is a continuation of the Clean Sky program. The SESAR 2020 program focuses on searching for new solutions in the field of Air Traffic Control (ATC) and Air Traffic Management (ATM). It is assumed that the solutions developed under this program will lead to a ten-fold increase in the level of safety, a triple increase in airspace capacity, a 50% reduction in air traffic management costs and a 10% reduction in the negative impact of air transport on the natural environment. The Clean Sky 2 program focuses on developing new technical and technological solutions that are more environmentally friendly (new aircraft, new power units and on-board systems, etc.).

One of the ways to reduce the negative impact of aircraft on the natural environment is the appropriate shaping of flight paths to minimize the emission of harmful substances. This requires proper flight planning, taking into account the limitations resulting from the airspace structure and applicable regulations, as well as the current weather conditions. The weather is one of the most important factors affecting the fuel consumption, flight time and costs. The algorithm determining the fuel consumption, flight time and finally aircraft emission, at the stage of flight planning should be based on the best weather forecasts. This will enable to minimize uncertainty of the parameters and optimize the flight path taking into account the most favourable conditions for a given flight. In addition to typical parameters, such as pressure and air density, special attention must be paid to the correct determination of the temperature, speed and wind direction. The speed of sound depends on the temperature, which allows to determine

correctly the Mach number for an aircraft flying at a given true airspeed (TAS). The wind speed and direction influence the aircraft groundspeed (VOG).

Planning a flight that minimizes emissions or fuel consumption is a difficult and demanding task, due to the complexity of the conditions that have to be taken into account (airspace structure, restrictions, location of prohibited zones, traffic conditions and weather forecast). It can be done only with the use of an appropriate computing system. The flight planning system must include appropriate computing models: aircraft, airspace, flight path, air traffic and weather [9]. In addition, it must have access to current weather conditions and information on current and planned air traffic and the airspace structure. All these elements will be used by the appropriate computation algorithm, which will be able to determine the optimal flight profile for a given criterion (cost, fuel consumption, emission of harmful compounds in the exhausts, etc.), taking into account the current flight conditions and existing restrictions and boundaries.

The development of a flight planning algorithm for different flight modes, i.e. on fixed routes or in FRA (Free Route Airspace), is one of the research and development tasks performed by the authors of the paper under the SESAR 2020 program. One of the optimization criterion is the emission of harmful compounds in the exhausts.

In the process of developing computational models that will determine the optimal aircraft's trajectory, it is very important to know how sensitive is the solution to the change of the optimization parameters or the change of external parameters. Based on this information, it will be possible to select the parameters of the used models, which will allow to obtain results with satisfactory accuracy, with the lowest calculation costs. It will also enable to determine appropriate weights at the edges of the graph modelling the airspace, appropriate for the implementation of the assumed task objectives. The purpose of the presented work is to determine the impact of wind speed and direction on the emission of harmful compounds in the aircrafts engines on a fixed route. It will enable to determine an aircraft trajectory in terms of the minimization of emissions resulting from fuel combustion by a jet aircraft's engines and determine the sensitivity of the solution to the impact of external conditions.

## 2. Problem statement and research methodology

This paper describes the impact of wind on the emissions of pollutants in the exhausts of a passenger aircraft, on the example of a business jet aircraft (Gulfstream IV, equipped with two Rolls Royce Tay 611C engines) on the exemplary route. The presented research methodology is universal and can be applied to any other jet aircraft – passenger and transport one. The research was focused only on the cruise phase, because it is usually the longest part of the journey. For most commercial passenger aircrafts, most of the fuel is consumed in this phase of flight. It takes place between the stages of ascent and descent. It ends when the plane approaches the destination, and the descent phase begins, and the plane prepares to land. During a cruise phase, for operational reasons or due to Air Traffic Control (ATC) instructions, planes can change a given flight level –

they can climb to a higher level or descent to a lower one. During very long flights, planes are able to fly higher when the value of the thrust required for flight decreases, which results from the decreasing weight of the aircraft along with the decreasing weight of fuel consumed during the flight. Usually, pilots ask ATC to allow them to fly at the optimum flight level for the aircraft they operate. This optimal level of flight depends, for example, on the type of aircraft, its operating mass and flight length. ATC generally accepts this request if it does not compromise safety.

In the research there was adopted an exemplary mission of the aircraft on the route between two Polish cities – Gdansk and Rzeszow, for which the cruise phase was 384 km long. In this phase, the cruising speed was assumed to be 0.8 Ma at the altitude of 10,000 m, as shown in Fig. 1.

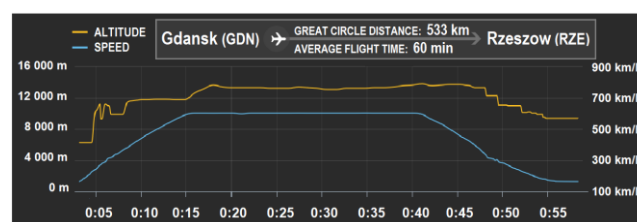


Fig. 1. Trajectory of Gulfstream IV, equipped with two Rolls Royce Tay 611C engines (based on [5])

Assuming no wind conditions, the aircraft reaches a cruising altitude of 10,000 m 15 minutes after the take-off and a relatively constant speed of 0.8 Ma (about 860 km/h). It descends for the last 18 minutes of the flight. In the analysed case, the research on  $\text{NO}_x$ , HC, CO and  $\text{CO}_2$  emission concerns 27 minutes of a steady flight (from 15th to 42nd minute of the flight), which corresponds to the flight trajectory of 384 km. However, in the research it was important to study the impact of wind on emission, so the time of flight on the route shown in Fig. 1 will change (shorten or lengthen).

On the basis of real meteorological data obtained via windy.com, the wind distribution on the considered route was analysed on the altitude from 10,000 m, taking into account its direction and velocity. The distance covered by the aircraft in the cruise phase was divided into 16 sections of the length of 24 km each, as shown in Fig. 2.

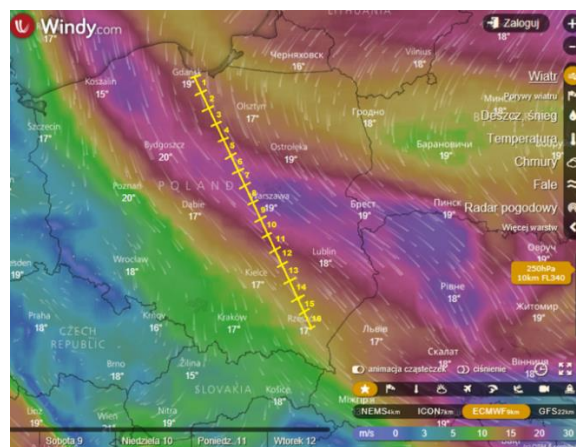


Fig. 2. Map of meteorological conditions (wind direction and velocity) at the time of conducted research on the trajectory of Gulfstream between Gdansk and Rzeszow at the altitude of 10,000 m (based on [10])

Based on meteorological data, for each of these sections the wind velocity and its direction in relation to the flight trajectory were determined. The component of wind velocity  $V_x$ , affecting the velocity of the aircraft's flight over ground VOG was also determined (Fig. 3).

Depending on the wind direction (from the head or the tail of the aircraft), the component of the wind velocity  $V_x$  will be added or subtracted from the velocity vector of the aircraft. By dividing the obtained value by the length of the route that the aircraft covered in the cruise phase, the flight time is computed, which is required to determine the emission of pollutants in the exhausts.

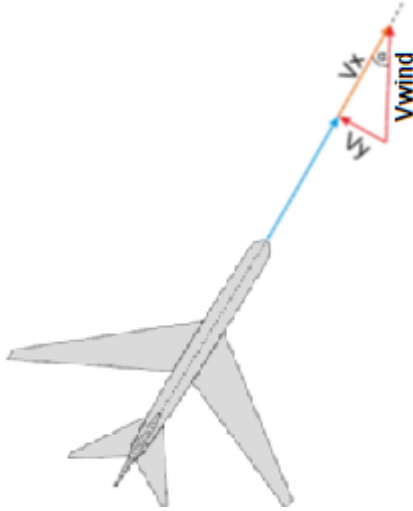


Fig. 3. Distribution of a wind vector  $V_{wind}$  on  $V_x$  and  $V_y$  components

$$V_x = V_{wind} \cdot \cos \alpha_{wind} \quad (1)$$

where:  $V_x$  – axial component of wind velocity,  $V_{wind}$  – wind velocity,  $\alpha_{wind}$  – angle between the velocity of the aircraft and the direction of the wind,

$$V_{OG} = V_{flight} \mp V_x \quad (2)$$

where:  $V_{OG}$  – velocity of the aircraft over ground,  $V_{flight}$  – velocity of the aircraft relative to air,

$$t = \frac{L}{V_{OG}} \quad (3)$$

where:  $t$  – flight time of the aircraft in the cruise phase,  $L$  – distance covered by the plane in the cruise phase.

### 3. Analysis of the results of conducted research

The purpose of many studies and projects aimed at increasing the efficiency of using air transport is to optimize the trajectory of the flight.

The flight path is implemented through fragments of the airspace. The optimal trajectory will run through fragments of space with the best parameters defined for the flight being performed. In this work, the focus will be on optimizing the trajectory of the flight in terms of minimizing emissions of pollutants in the jet engines exhausts. The ambient conditions in particular fragments of the airspace were taken into account (wind velocity and wind directions at different flight levels). The results of these computations are given in Table 1.

Table 1. Data on the wind speed and its wind direction relative to the trajectory of the flight

Section number	$V_{wind}$ [m/s]	$\alpha$ [°]
1	16	25
2	16	30
3	16	20
4	16	5
5	20	10
6	20	10
7	20	20
8	20	30
9	20	20
10	18	20
11	18	20
12	16	20
13	16	30
14	18	35
15	15	35
16	12	35

To perform a flight at a given altitude at a given velocity, a given thrust is required. This thrust can be determined using the following formulas (4)–(6). For the given flight parameters (altitude and flight speed) and aircraft parameters (mass, weight and lifting surface), the drag and lift coefficients can be assigned. With these coefficients ( $C_z$  and  $C_x$ ), it is possible to determine the power and thrust required for the flight [5]:

$$N_n = \frac{C_x}{C_z} \cdot Q \cdot V \quad (4)$$

$$P_n = \frac{N_n}{V} \quad (5)$$

where:  $N_n$  – power required for the flight,  $P_n$  – thrust required for the flight,  $C_x$  – drag coefficient,  $C_z$  – lift coefficient (depend on mass and velocity airplane),  $V$  – flight velocity,  $Q$  – airplane weight determined from the formula:

$$Q = m \cdot g \quad (6)$$

where:  $m$  – mass of the plane,  $g$  – acceleration of gravity.

For the computed value of thrust required for the flight there can be read the appropriate value of the engine thrust from the altitude-speed characteristics to ensure safe flight parameters and also the specific fuel consumption corresponding to that thrust value. Based on available data bases, e.g. [6], for this value of the thrust, it is possible then to determine the  $CO_2$ ,  $NO_x$ , HC, CO emission indexes (EI), which constitutes the first step in further computations of emissions of these compounds in jet engines exhausts. Emission indexes depend on the design of the engine, its load and the flight altitude. Knowing the emission indexes, it is possible to determine the emission of CO,  $NO_x$  and HC on a given section of the aircraft's cruise phase. For this reason the formulas (7)–(9) can be applied [11].

$$E_{NO_x} = EI_{NO_x} \cdot 10^{-3} \cdot K \cdot SFC \cdot t \cdot l \quad [kg] \quad (7)$$

$$E_{CO} = EI_{CO} \cdot 10^{-3} \cdot K \cdot SFC \cdot t \cdot l \quad [kg] \quad (8)$$

$$E_{HC} = EI_{HC} \cdot 10^{-3} \cdot K \cdot SFC \cdot t \cdot l \quad [kg] \quad (9)$$

where:  $E_{NO_x}/E_{CO}/E_{HC}$  – emission of particular compounds in exhausts [kg],  $EI_{NO_x}/EI_{CO}/EI_{HC}$  – emission factors for particular substances, depended on the type of engine and



the range of its run [g/kg],  $K$  – engine thrust [N], SFC – specific fuel consumption [kg/(N·h)],  $t$  – engine run time at a given thrust [h],  $l$  – number of engines.

Emission of  $\text{CO}_2$  depends only on fuel consumption. The formula of the carbon dioxide emission is as follows [11]:

$$E_{\text{CO}_2} = 3.15 \cdot K \cdot \text{SFC} \cdot t \cdot l \quad [\text{kg}] \quad (10)$$

The emission of  $\text{NO}_x$ , CO, HC and  $\text{CO}_2$  in the exhausts of Gulfstream IV in each section of the cruise phase of the journey from Gdansk to Rzeszow for the assumed flight conditions is presented in Table 2.

Table 2. Emission of  $\text{NO}_x$ , CO, HC and  $\text{CO}_2$  in the exhausts of Gulfstream IV in each section of the flight from Gdansk to Rzeszow with the time given

Section number	Time [min]	$E_{\text{NO}_x}$ [kg]	$E_{\text{CO}}$ [kg]	$E_{\text{HC}}$ [kg]	$E_{\text{CO}_2}$ [kg]
1	1.574637905	1.582999	0.105986	0.013626	145.2866
2	1.578639338	1.587022	0.106256	0.013660	145.6558
3	1.571337020	1.579681	0.105764	0.013597	144.9820
4	1.565781952	1.574096	0.105390	0.013549	144.4695
5	1.543086659	1.551280	0.103863	0.013353	142.3755
6	1.543086659	1.551280	0.103863	0.013353	142.3755
7	1.548471227	1.556694	0.104225	0.013399	142.8723
8	1.557344963	1.565614	0.104822	0.013476	143.6910
9	1.548471227	1.556694	0.104225	0.013399	142.8723
10	1.559820329	1.568103	0.104989	0.013498	143.9194
11	1.559820329	1.568103	0.104989	0.013498	143.9194
12	1.571337020	1.579681	0.105764	0.013597	144.9820
13	1.578639338	1.587022	0.106256	0.013660	145.6558
14	1.573117508	1.581471	0.105884	0.013613	145.1463
15	1.588472899	1.596908	0.106917	0.013746	146.5631
16	1.604131018	1.612649	0.107971	0.013881	148.0078
Total	25.06619539	25.1993	1.687164	0.216906	2312.774

Table 3. Emission of  $\text{NO}_x$ , CO, HC and  $\text{CO}_2$  in the exhausts of Gulfstream IV in each section of the flight from Rzeszow to Gdansk with the time given

Section number	Time [min]	$E_{\text{NO}_x}$ [kg]	$E_{\text{CO}}$ [kg]	$E_{\text{HC}}$ [kg]	$E_{\text{CO}_2}$ [kg]
1	1.777605428	1.787045	0.119648	0.015382	164.0137
2	1.772533398	1.781946	0.119306	0.015338	163.5457
3	1.781830968	1.791292	0.119932	0.015419	164.4036
4	1.789028314	1.798528	0.120417	0.015481	165.0677
5	1.819606298	1.829268	0.122475	0.015746	167.8890
6	1.819606298	1.829268	0.122475	0.015746	167.8890
7	1.812175506	1.821798	0.121975	0.015681	167.2034
8	1.800171323	1.809730	0.121167	0.015577	166.0958
9	1.812175506	1.821798	0.121975	0.015681	167.2034
10	1.796875136	1.806417	0.120945	0.015549	165.7917
11	1.796875136	1.806417	0.120945	0.015549	165.7917
12	1.781830968	1.791292	0.119932	0.015419	164.4036
13	1.772533398	1.781946	0.119306	0.015338	163.5457
14	1.779547029	1.788996	0.119778	0.015399	164.1929
15	1.760297703	1.769645	0.118483	0.015232	162.4168
16	1.74146036	1.750708	0.117215	0.015069	160.6787
Total	28.61415277	28.76609	1.925971	0.247608	2640.132

For comparative purposes, assuming identical external conditions, in Table 3 there are presented the obtained results of the amount of pollutants emitted in the exhaust

gases on the return journey (i.e. at the unfavourable wind component vector in this case).

For reference purposes, the results presented in Table 4 were obtained for unreal no wind conditions at the altitude of 10 km.

Table 4. Emission of  $\text{NO}_x$ , CO, HC and  $\text{CO}_2$  in the exhausts of Gulfstream IV in each section of the flight from Gdansk to Rzeszow with the time given assuming no wind NO WIND

Section number	Time [min]	$E_{\text{NO}_x}$ [kg]	$E_{\text{CO}}$ [kg]	$E_{\text{HC}}$ [kg]	$E_{\text{CO}_2}$ [kg]
1	1.7	1.67884473	0.112403379	0.014450869	154.0832252
2	1.7	1.67884473	0.112403379	0.014450869	154.0832252
3	1.7	1.67884473	0.112403379	0.014450869	154.0832252
4	1.7	1.67884473	0.112403379	0.014450869	154.0832252
5	1.7	1.67884473	0.112403379	0.014450869	154.0832252
6	1.7	1.67884473	0.112403379	0.014450869	154.0832252
7	1.7	1.67884473	0.112403379	0.014450869	154.0832252
8	1.7	1.67884473	0.112403379	0.014450869	154.0832252
9	1.7	1.67884473	0.112403379	0.014450869	154.0832252
10	1.7	1.67884473	0.112403379	0.014450869	154.0832252
11	1.7	1.67884473	0.112403379	0.014450869	154.0832252
12	1.7	1.67884473	0.112403379	0.014450869	154.0832252
13	1.7	1.67884473	0.112403379	0.014450869	154.0832252
14	1.7	1.67884473	0.112403379	0.014450869	154.0832252
15	1.7	1.67884473	0.112403379	0.014450869	154.0832252
16	1.7	1.67884473	0.112403379	0.014450869	154.0832252
Total	27	26.86151569	1.798454061	0.231213903	2465.331603

## 4. Conclusions

The aim of the conducted research is to determine the impact of wind on fuel consumption by a passenger jet aircraft during the cruise phase and on emission of pollutants in its engines exhausts. For that purpose, there was assumed a journey between two cities Gdansk and Rzeszow covered by a business jet Gulfstream IV with the velocity of 0.8 Ma at the altitude of 10,000 m.

Based on available real meteorological data, it was possible to take into account the external conditions at the altitude of 10 km – the wind speed and its direction in relation to the trajectory of the aircraft.

For comparative purposes, to see to what extent the emission of the analysed pollutants is wind dependent, there were considered three scenarios:

- I. journey from Gdansk to Rzeszow at the meteorological parameters read from the map presented in Fig. 2;
- II. journey from Rzeszow to Gdansk at the meteorological parameters read from the map presented in Fig. 2;
- III. journey from Gdansk to Rzeszow at no wind conditions – just to obtain reference results.

The analysis carried out for those scenarios led to the following observations:

- 1) In general, the higher the headwinds speed, the longer the journey (duration of the flight), and thus the higher the  $\text{NO}_x$ , CO, HC and  $\text{CO}_2$  emission values. In the case of tailwind (pushing) winds, the situation is reversed. In the analysed case, the journey from Gdansk to Rzeszow in cruise phase lasted for 25 minutes (Table 2), whereas from Rzeszow to Gdansk – for 29 minutes (Table 3). Such a journey in reference conditions (no wind) would last for 27 minutes (Table 4).

2) The total emission on a given trajectory is strongly wind dependent:

▪ In case of the journey from Gdansk to Rzeszow (with favourable winds), the total emission of:

- NO<sub>x</sub> was 25.1993 kg,
- CO was 1.687164 kg,
- HC was 0.216906 kg,
- CO<sub>2</sub> was 2312.774 kg.

▪ However, on the return trip – from Rzeszow to Gdansk (upwind), the total emission of:

- NO<sub>x</sub> was 28.76609 kg,
- CO was 1.925971 kg,
- HC was 0.247608 kg,
- CO<sub>2</sub> was 2640.132 kg.

▪ It means that on the analysed route of 384 km the difference in those emissions depending on the direction of wind impact on the aircraft ( $V_x$ ), in case of:

- NO<sub>x</sub> was 3.6 kg,
- CO was 0.3 kg,
- HC was 0.03 kg,
- CO<sub>2</sub> was 327.36 kg.

▪ The difference in CO<sub>2</sub> emissions results from the fact that on the return journey the aircraft consumed about 100 kg of fuel more, assuming identical meteorological conditions.

▪ It can also be noticed an increase in the emission of other pollutants. This results from different emission indexes depended from the engine's operating range (when the engine is running at high load, the EINO<sub>x</sub> emission index is high whereas the EICO and EIHC emission indexes are low).

▪ It is also worth noting that the percentage differences in emission of all these pollutants in the case of a tailwind flight vs. headwind flight are similar (about 15%), however, mass differences are significant (e.g. the amount of CO<sub>2</sub> emitted compared to the amount of HC emitted).

Another observation is that in the case of a flight with favourable winds, the total emission is lower compared to the windless variant. In the case of unfavourable winds, which is logical, this emission is higher. It is worth noting that the differences on these 'plus' and 'minus' emissions are not the same (although the wind adopted for analysis has the same value in a given route section but interacts on the aircraft in the opposite direction in relation to its trajectory). These observations are shown in Table 5 and Fig. 4.

Table 5. Total emission of NO<sub>x</sub>, CO, HC and CO<sub>2</sub> in the exhausts of Gulfstream IV in each scenario of the journey

Journey scenario	ENO <sub>x</sub> [kg]	ECO [kg]	EHC [kg]	ECO <sub>2</sub> [kg]
Headwinds (Gdansk –Rzeszow journey)	28.7661	1.925971	0.247608	2640.132
No wind (Gdansk –Rzeszow or Rzeszow –Gdansk journey)	26.8615	1.798454	0.231214	2465.332
Tailwinds (Rzeszow –Gdansk journey)	25.1993	1.687164	0.216906	2312.774

The described research methodology is universal. In the paper it is presented on the example of the Gulfstream IV aircraft due to the access to its technical data, but nothing prevents us from using it for similar analyses for other jet aircraft.

In order to minimize emission of pollutants in the aircraft engines, it may be worth considering to conduct the research on the optimization of the aircraft's flight trajectory, so that it is covered with the most preferable wind direction.

*This project has received funding from the SESAR Joint Undertaking under the European Union's Horizon 2020 research and innovation programme under grant agreement No 734129.*

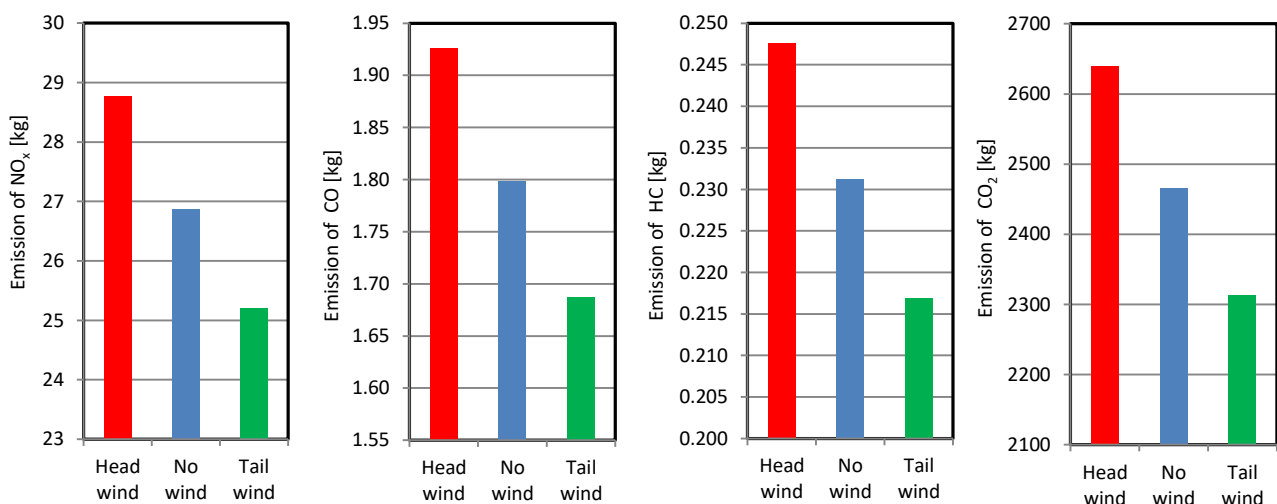


Fig. 4. Total emission of NO<sub>x</sub>, CO, HC and CO<sub>2</sub> in the exhausts of Gulfstream IV in each scenario of the journey

## Bibliography

- [1] BALMORI, M.A. The effects of microwave radiation on the wildlife. Preliminary results, Valladolid (Spain), 2003.
- [2] BRUSOW, W., KLEPACKI, Z., MAJKA, A. Airports and facilities data base. *EPATS technical report*, Project no. ASA6-CT-2006-044549, 2007.
- [3] Clean Sky website. <http://www.cleansky.eu>
- [4] FISZDON, W. Flight mechanics (Mechanika lotu), PWN, Warszawa (in Polish). 1964.
- [5] Flightradar website, <https://www.flightradar24.com>
- [6] ICAO aircraft engine emission databank, <https://www.easa.europa.eu/easa-and-you/environment/icao-aircraft-engine-emissions-databank>
- [7] International Civil Aviation Organization (ICAO), International Standards and Recommended Practices, Environmental Protection. Annex 16, Volume II Aircraft Engine Emissions (third edition), ICAO, July 2008.
- [8] IPCC, Revised 1996 Guidelines for National Greenhouse Gas Inventories, Volume 3, Greenhouse Gas Inventory Reference Manual, Intergovernmental Panel on Climate Change, WGI Technical Support Unit, Hadley Centre, Meteorological Office, Bracknell, UK, 1997.
- [9] KOPECKI, G., PĘCZKOWSKI, M., ROGALSKI, T. Przykładowy algorytm wyznaczania trasy przelotu w przestrzeni lotów swobodnych. *Autobusy*. 2017, 6.
- [10] Maps of meteorological conditions, <https://www.windy.com>
- [11] SCHAEFER, M., BARTOSCH, S. Overview on fuel flow correlation methods for the calculation of NO<sub>x</sub>, CO and HC emissions and their implementation into aircraft performance software, *Interner Bericht Deutsches Zentrum für Luft- und Raumfahrt (DLR)*. Institut für Antriebstechnik, Köln. 2013.
- [12] SESAR JU website, <https://www.sesarju.eu>

Małgorzata Pawlak, DEng. – Faculty of Navigation, Department of Ship Operation, Gdynia Maritime University.

e-mail: [M.Pawlak@wn.am.gdynia.pl](mailto:M.Pawlak@wn.am.gdynia.pl)



Andrzej Majka, DEng. – Faculty of Mechanical Engineering and Aeronautics, Rzeszow University of Technology.

e-mail: [Andrzej.Majka@prz.edu.pl](mailto:Andrzej.Majka@prz.edu.pl)



Michał Kuźniar, MEng. – Faculty of Mechanical Engineering and Aeronautics, Rzeszow University of Technology.

e-mail: [MKuzniar@prz.edu.pl](mailto:MKuzniar@prz.edu.pl)



Jowita Pawluczy, MEng. – Faculty of Mechanical Engineering and Aeronautics, Rzeszow University of Technology.

e-mail: [Jowita.Pawluczy@prz.edu.pl](mailto:Jowita.Pawluczy@prz.edu.pl)



## Solving the problem of air quality in Indian cities by retrofitting the EGR

This paper touches problem of transportation pollution focusing on  $\text{NO}_x$  reducing in the India. There were India country chosen for study as the second populated country and most polluted cities in the world. As from statistics, it is known that more than 65% of Indian cars are old and they are the main reason of air pollution. Most of the old cars do not have any control measures for eliminating deadliest gases. Dumping the old cars is not possible, as the poor owns most of the old cars. For eliminating the pollution from old cars, the possible remedy is to control the emission of pollutants. Comparing to all gases in exhaust, nitrogen oxides are the dangerous one. It can may cause up to death. The best method to control the  $\text{NO}_x$  gas is EGR (Exhaust Gas Recirculation) valves. This research mainly focuses on the possible ways of installing EGR in old engines and fabricate an EGR in one of the Indian cars. Maruti Suzuki 800 is best of for fabricating EGR, as it is a base model and most sold Indian car. As the result, there tremendous decreasing in  $\text{NO}_x$  emission also the emission  $\text{CO}_2$  was reduced. The investigation about fabricating EGR in old vehicle results a positive output after calculated the cost of the fabrication, time consumption, work challenges and other facts. As Indian government adopt this concept, they can reduce the pollution from all types of vehicles to a great extend in few years of time with low investment.

Key words: engine pollution, retrofitting, EGR

### 1. Introduction

Nitrogen oxides ( $\text{NO}_x$ ) is common name for the chemical compounds group of oxides of nitrogen, which are highly reactive. Nitrous acids and nitric acid are also belonging to this group. Combustion of transportation fuel is the main reason for  $\text{NO}_x$  formation. All types of cars, power plants and off-road equipment have a major role in  $\text{NO}_x$  formation. There are a lot of harmful effects on human health as well as entire environment.  $\text{NO}_x$  responds with ammonia, moisture and different mixes to shape nitric corrosive vapor and related particles. Little particles can infiltrate profoundly into delicate lung tissue and harm it causing sudden death in outrageous cases. Inward breath of these particles might cause or decline respiratory illnesses as bronchitis for example.  $\text{NO}_x$  responds with volatile organic compounds with the vision of sunlight to frame and to obliterate ozone. Ozone can cause unfavorable impacts, for example, harm to lung tissue and diminishment in lung work for the most part in week persons (kids, elderly, and asthmatics).  $\text{NO}_x$  additionally promptly responds with common organic chemicals to frame a wide assortment of dangerous items: nitroarenes, nitrosamines and furthermore, some of the nitrate radical may cause DNA mutation. As of late, another pathway, by means of  $\text{NO}_x$ , to ozone discovered that prevalently happens in beachfront regions through development of nitryl chloride when  $\text{NO}_x$  encounters salt mist.  $\text{NO}_x$  emissions likewise cause worldwide cooling through the arrangement of OH radicals that devastate methane atoms, countering the impact of ozone harming substances. The impact can be critical. The extreme goal of maximum  $\text{NO}_x$  is to wind up in the soil as nitrate or nitrite, which are valuable to developing plants.

$\text{NO}_x$  and other  $\text{NO}_x$  associate with water, oxygen and different synthetic compounds in the atmosphere to shape acid rain. Acid rain hurts delicate biological systems, for example, lakes and backwoods. Acid rain comes about when sulfur dioxide ( $\text{SO}_2$ ) and nitrogen oxides ( $\text{NO}_x$ ) are discharged into the atmosphere and transported by wind

and air streams. The  $\text{SO}_2$  and  $\text{NO}_x$  respond with water, oxygen and different synthetic substances to frame sulfuric and nitric acids. These then blend with water and different materials previously tumbling to the ground. The nitrate particles that outcome from  $\text{NO}_x$  make the air cloudy and hard to see however. Haze is caused when daylight experiences small pollution particles noticeable all around, which decrease the clearness and shade of what we see, particularly humid conditions [7, 9, 11, 16, 18].

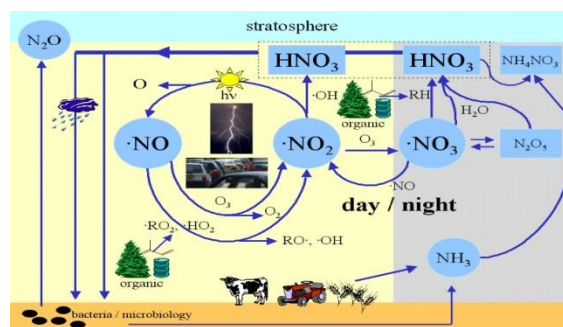


Fig. 1. Environmental effects of  $\text{NO}_x$  [12]

When world zones be studied due to  $\text{NO}_x$  contamination it can be observed some differences in level of it – see Fig. 2.

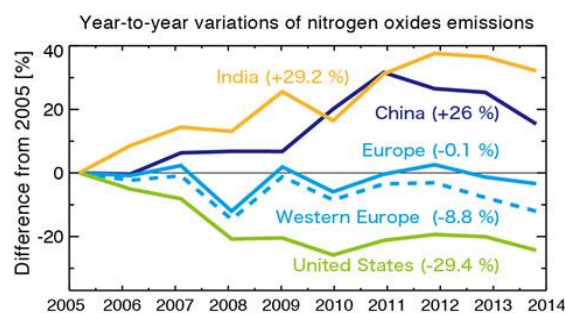


Fig. 2. Year-to-year variations of  $\text{NO}_x$  [19]



Focusing on European Union countries it can be found that for example during 2011 road transport and energy production are the prime sources of  $\text{NO}_x$  emissions – Fig. 3.

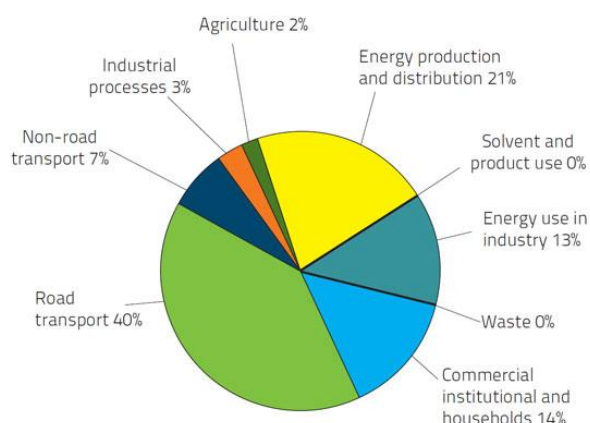


Fig. 3.  $\text{NO}_x$  emissions in the EU during 2011 [5]

Similar situation was in USA, when during 2010 road transport and energy production are the prime sources for emission of  $\text{NO}_x$  – Fig. 4.

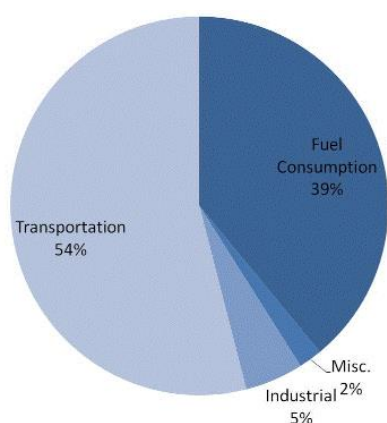


Fig. 4.  $\text{NO}_x$  emissions in the USA during 2010 [4]

And in India, the quantity of urban cities where the guidelines of nitrogen oxides ( $\text{NO}_x$ ) surpassed standards expanded from 18% to 29% out of 10 years, as indicated by the Center for Science and Environment – Fig. 5.

In 2007, none of the Indian urban cities was in the basic class — that is 1.5 times as far as possible. In 2016, 12% of the urban communities where  $\text{NO}_x$  was being checked entered the basic rundown [8, 14, 15].

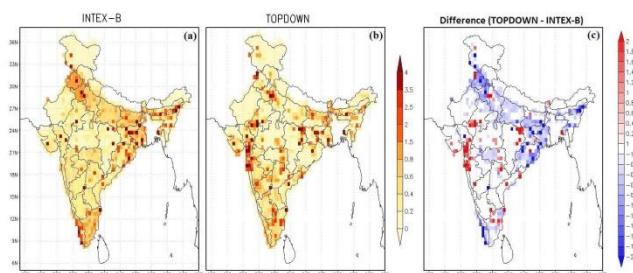


Fig. 5. Satellite constraints of  $\text{NO}_x$  emissions in India [8]

As mentioned above, around 50% of  $\text{NO}_x$  emission is from road transportation. As per the studies from Minister of Road Transport, Highways and Shipping in India, old commercial vehicles are responsible for biggest part of the vehicular pollution – Fig. 6 [10, 14, 16].

HOW POLLUTING ARE THEY?					
Emission by more-than-10-year-old vehicles in 2011					
Vehicle	% of fleet	% of emissions in each category			
		PM2.5	SO2	NOX	CO
2-wheelers	17	30	21	32	51
3-wheelers	18	42	22	41	54
4-wheelers	17	58	21	33	45
Buses	12	26	14	18	21
Heavy-duty trucks	16	39	20	30	39
Light-duty trucks	13	46	16	25	33

Source: Study on re-fuelling road transport for better air quality in India

Fig. 6.  $\text{NO}_x$  emissions by old vehicles [10]

## 2. Some methods of reducing $\text{NO}_x$ emissions

There are some methods to reduce  $\text{NO}_x$ , as follow:

- Humid Air Method – in this technique, water vapour is blended in the air before providing it to the cylinder. Air from the turbocharger blower is gone through a cell that humidifies and chills the hot air taking moisture from the cooling water until air immersion is accomplished. This strategy can accomplish diminishment of  $\text{NO}_x$  by 70–80%,

- Exhaust Gas Recirculation (EGR) – as the name recommends, some measure of exhaust gases is sent back to the search space to stir up with the air to be provided to cylinder for combustion. This lessens the oxygen substance of the air and subsequently decreases development of  $\text{NO}_x$  by 50% even [1, 2, 15],

- Water Injection and Water emulsion – in this strategy, water is added to lessen the temperature of ignition prompting low  $\text{NO}_x$  emanation. In water emulsion, fuel is mixed with water and in water infusion; a different fresh water injector is mounted in the cylinder head that infuses water. This technique has a disadvantage of expanding the specific fuel oil burning with lessening in  $\text{NO}_x$  by just 20–45%,

- High scavenge pressure and compression ratio – with high rummage weight and compression ratio, substantial measure of air can be acquainted inside the cylinder with bring down burning temperature and  $\text{NO}_x$  outflow by 25%,

- Selective Catalytic Reduction (SCR) – is the most productive technique to diminish  $\text{NO}_x$  outflows from exhaust gases up to 90–95%. In this technique the exhaust gas is blended by water arrangement of urea and after that it is gone through catalytic convertor. The main drawback of SCR is its cost of installation and working expense.

A generally embraced course to reduce  $\text{NO}_x$  outflows is Exhaust Gas Recirculation (EGR). Its includes recirculating a controllable extent of the engine exhaust again into the intake air. For controlling the flow of gas there is a valve. EGR reduces  $\text{NO}_x$  by the lowering combustion chamber temperatures. Gases represented from EGR frameworks will likewise contain near equilibrium of CO &  $\text{NO}_x$ ; the

small amount initially inside the combustion chamber represses the aggregate net generation of these and different contaminations when tested on a time average.

An appropriately working EGR can hypothetically build the effectiveness of gasoline engine through a various mechanisms:

- reduced throttling losses. There will be increase in the pressure of inlet manifold. At a given power output throttle plate must be opened further because of the inertia of inert exhaust gas to the intake manifold and this make diminishing in throttling losses,
- reduced heat rejection. Brought down peak combustion temperatures not just decreases  $\text{NO}_x$  development, it additionally diminishes the loss of thermal energy to combustion chamber surfaces, during the expansion stroke making more accessible for change to mechanical work,
- reduced chemical dissociation. The lower top temperatures result in a greater amount of the discharged energy staying as sensible energy close TDC (Top Dead Centre), instead of being bound up in the dissociation of combustion items. This impact is minor compared with the initial two.

EGR valves are differentiated by the way working or with the working principle. The main types are:

- mechanical controlled,
- electronic controlled,
- working with vacuum,
- combination of vacuum & pressure.

EGR valve designs also differ from petrol powered and diesel powered. Nowadays, the modern vehicles use different type valves configuration with electronic one as dominant. But in old engines, a vacuum hose is connected to carburettor or throttle body to the valve.

### 3. Fabricating and implementing EGR

As going through the surveys and statistics, found that old cars are the main source of  $\text{NO}_x$  emission. For reducing  $\text{NO}_x$ , fabricating EGR in old vehicle is the best solution.

For fabricating an EGR in old engine, the first and main task is selection of a car. Its confusing task to select a particular as far so much brands are there. So, came to solution of selecting a base model, means an engine had only basic specifications. As far we can make alterations depends upon engine specification. However, by selecting base model engine's EGR mechanism will be suite for all engines.

During the period from 1983 to 2014, a city car ruled Indian streets called Maruti 800 is a produced by Maruti Suzuki. With more than 30 long periods of generation, this became the second longest creation auto in India, next just to Ambassador by Hindustan motors. It is reverently called as "The Car that put India on Wheels". The first generation (SS80) had an 800cc F8B engine and depended on the 1979 Suzuki Fronte. A modernized aerodynamic version utilizing the shape of the second generation (SB308) was displayed in late 1986.

Generally viewed as the most leading car in India, Maruti sold around 2.66 million in India itself out of 2.87 million 800s manufactured. Before the entry of Maruti Alto at 2004, Maruti 800 persist as top of the line auto in India. It was likewise sent out to various Asian countries includ-

ing, Bangladesh, Sri Lanka and Nepal and was additionally accessible in Morocco and sold in European markets as the Maruti Suzuki.

Table 1. Maruti 800 engine specification

Cylinders	3
Displacement	796 cm <sup>3</sup>
Type	Water Cooled SOHC Petrol
Valve train	2 valves
Bore & Stroke	68.5 × 72.0 mm
Max Power	37 BHP@5000 rpm
Max Torque	59 Nm@2500 rpm

To fabricate a fully functioning EGR system in a chosen engine the EGR line was design with all necessary components. So, there were made:

- recognition of fluid flow using Bernoulli equation, giving information about the balance between elevation, velocity and pressure in duct of EGR line,
- electronics platform with Arduino Open Source to manage signals from various sensors and actuators. This project uses an Arduino Leonardo microcontroller board to take sensor readings for calibration and for control of servo using various sensor inputs [3],
- time-financial analyses

The design of the EGR line (Fig. 7) is simply based on the fact that the design must be simple, purposeful and efficient. The conventional EGR valve is 2 input 2 output 4-way valve, which is situated between the two manifolds the valve operates and opens the separation between intake and exhaust manifolds causing a part of the exhaust gas to mix with the intake air. Normally this valve is operated mechanically owing the temperature of the gases. The mechanical system consists of valve that operates based on exhaust manifold pressure and intake manifold pressure. However later electronically operated EGE valves are introduced. But the conventional EGR valve cannot serve our purpose, so we introduced a two-way valve operated between on and off in 90-degree angle. The valve is operated using a servomotor, which rotates according to the signal of the controller.

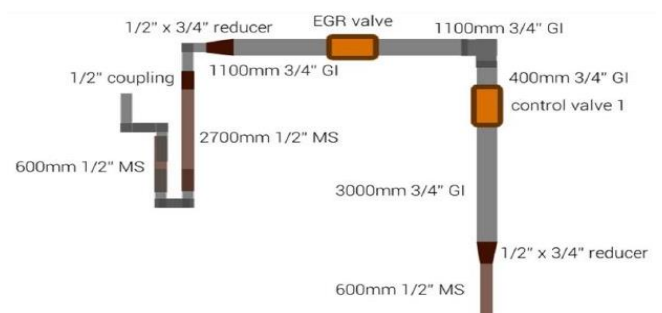


Fig. 7. Design of EGR line for Maruti 800 engine

The sensors characteristic curves were obtained by analysing their signal output values using the Arduino Leonardo microcontroller board. So, there were tested and analysed sensor characteristics:



- throttle position sensor (TPS)

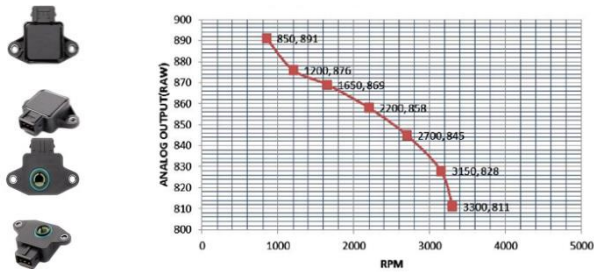


Fig. 8. Throttle Position Sensors with analog output vs. rpm

- manifold absolute pressure sensor (MAPS)

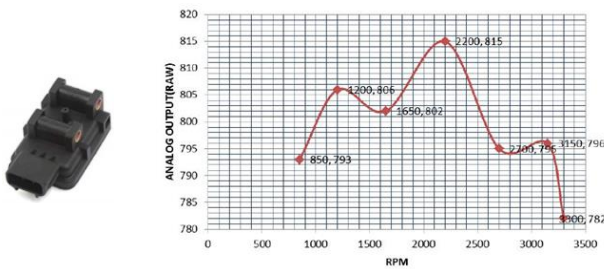


Fig. 9. Manifold Absolute Pressure Sensors with analog output vs. rpm

- oxygen sensor/lambda sensor

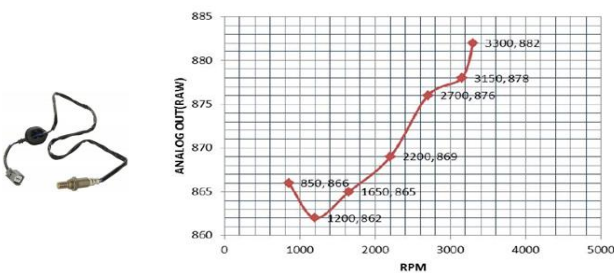


Fig. 10. Oxygen / Lambda Sensors with analog output vs. rpm

- mass air flow sensor (MAF)

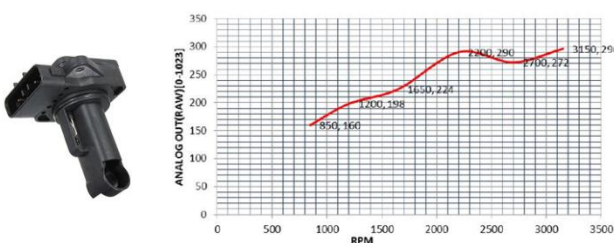


Fig. 11. Mass Air Flow Sensors with analog output vs. rpm

- EGR valve control and electronics



Fig. 12. EGR valve with Arduino code for motor control

EGR valve is a simple modified globe valve (open when parallel), i.e. for a 90-degree sweep, the valve is fully open. Since approximate flow through the EGR line is about 30% (approximately one-third the flow from the main exhaust pipe), a 45 degree sweep is enough to obtain the 15% flow rate [17].

The control algorithm was developed after careful study of the sensor characteristics of throttle position sensor, manifold absolute pressure sensor and the lambda sensor and then carefully fixing the range of operation of the servo motor [3, 6].

The final circuit – the all in one data logging and control module enables simultaneous data logging from all four sensors along with the control of the servo while comparing these values. The final circuit is a combination of the calibration and servo control circuits, with the addition of a dual 7-segment LCD display connected to the circuit so that the current EGR percentage may be displayed. The displays are connected in a multiplexed manner due to the fact that only a limited number of input/output digital pins are available in the Arduino Leonardo microcontroller board. The MAF sensor requires an additional 12 V supply, which may be taken directly from the engine battery. Due to safety reasons, the supply is taken from a 12 V, 1 A, SMPS, DC adapter so that the components on the breadboard are saved from high values of current.

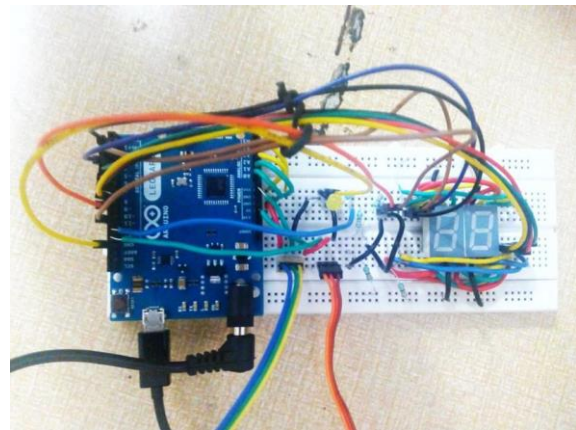


Fig. 13. Breadboard implementation of the final circuit

#### 4. Estimating the cost and time period for fabricating EGR to all old cars in India

India is a big country having 29 states and 7 union territories. So the cost of materials & labour cost is differs from state to state. So taking the average of from all state.

To counting fabricating cost it was taken Indian Rupees (INR) to European Currency (Euro) exchange stock as given on August 15<sup>th</sup>, 2018: 1 Euro = 79.30 INR.

##### COSTS

- Material cost

There were estimating the cost of materials for fabricating EGR on Maruti 800. It will change with the car. So here, also the mean price was considering.

AURDINO LEONARS board: it was used AT mega 32u4 (5v). Its input volts is 7–12 V flash memory of 32 kB with 500 INR (6.31 Euro).

INLET SECTION: the main component are:

Convergent-divergent section = 110 INR (1.39 Euro)  
 Convergent nozzle = 120 INR (1.51 Euro)  
 Total for inlet section = 230 INR (2.90 Euro)  
 EGR LINE: it needs so much nibbling, elbow pipe, reducer extra.

Item	Price (in INR)
½" MS extender	105
¾" to ½" Reducer	110
¾" GI nibbling	85
¾" GI short elbow	100
¾" GI elbow	110
¾" to ½" Reducer	110
½" MS short elbow	120
Total	740 (9.33 Euro)

For EGR valve, Techno 2W-200-20-3/4". It costs 1810 INR (22.82 Euro) [17].

Manual Over Ride Valve of Aira Euro Automation's costs 700 INR (8.83 Euro).

At last, for brass nozzle is 310 INR (3.91 Euro).

Therefore, for making EGR line the total price is 3560 INR (44.98 Euro).

### SENSORS

Sensors mentioned above have got process as follow:

Name	Brand/Model	Price (in INR)
Throttle Position Sensors	Generic	2200
Manifold Absolute Pressure Sensors	Generic	1850
Oxygen/Lambda Sensors	Denso	4650
Mass Air Flow Sensors	Generic	3100
Total		9820 (123.83 Euro)

#### – miscellaneous expenses

So much of small, but important things we need. For example, electric wires, connectors, adapters, screws, bolt& nuts etc. The expense for tools also included here. We can use same tools for so many cars. Here we took as average. It's also include electricity charge, welding cost, water bills etc. So for all, as an average we count 500 INR (6.31 Euro) for one car.

#### – labour cost

For fabricating an EGR, we need a technical crew having: one Automotive Engineer, one Electronics and Communication Engineer, one Quality inspector, two Professional Welders, three Automotive Mechanic and for management level – one person should be there as supervisor or as district head. One head for a state with one assistant & one main head for all country with three assistant. The salary structure for the District, State & National heads we don't need to hire new person, can give extra duty to: Regional Transport Officer (District Level, State Transport Commissioner (State Level), Transport Research Advisor (National Level).

Designation	Salary (in INR)
Automotive Engineer	1000/car
E & C Engineer	55,000/month
Quality Inspector	650/car
Professional Welder	350/car
Automotive Mechanic	350/car
State level Assistant	35,000/month
National level Assistant	50,000/month

### TIME

In India, maximum period of one car according to tax payment is 15 years. After that, they need re-registration and that time they should have to follow the current emission standard. In addition, the Bharat stage 4 emission standard was introduced in 2010.

Now it is 2018, so we considering the cars and taxis between 2004 and 2010.

Number of cars from 2004 to 2010 = 71,911,501

Number of taxis from 2004 to 2010 = 10,048,572

Total number of cars = 81,960,073 vs. more than 210 mln grand total (including buses, two-wheelers, jeeps, goods vehicle etc.).

As result of research, we are cutting 50% of cars from this because in some of taxis are heavy vehicles, and in cars some are dumber, were destroyed in accident, some are unusable. Therefore, the final count of cars are 40,980,037.

India have 718 districts. For the speedy output opening seven station in a district is the better number, so,  $718 \cdot 7 = 5,026$ . However, the big cities like Mumbai, Delhi, Ahmedabad, Pune, Chennai, Vizag, Hyderabad, Lucknow, Jaipur, Kolkata, Kochi, Amritsar have enormous amount of cars. We have to open more than one station in all cities. Therefore, we came to decision for 7,200 total stations. An average of eight cars can be fabricate in one station. Total 57,600 cars per day. So number of days we need to fabricate all cars  $40,980,037/57,600 = 711.45$  days. In years (including weekends and holidays)  $711.45/216 = 3.3$  years to retrofitting all old cars in India.

### 5. Conclusions

Citizens of India as others aimed to make India unpolluted. Initiated a research for it and results in a finding that NO<sub>x</sub> is the most deadliest pollutant from cars especially from old cars. As a solution decided to reduce NO<sub>x</sub> emission from old cars by retrofitting EGR system in it, which is considered as the best remedy for NO<sub>x</sub> emission. It was done for base model and a most popular car Maruti 800. The fabrication was very successful with very cost.

The total cost for implementing an EGR in a car is 14,850 INR (188 Euro) without the labour charge. Government of India can implies a subsidy scene to poor car owners and take surcharge from the owners having high annual income. This make the cost of fabrication in a tally. We need total 5026 working station for 40.9 million cars. By fabricating 57,600 cars per day, we can implement EGR in all cars within 3.3 years, but of course, another portion of old vehicles comes every year.

As a conclusion, we can say within 2 years we can control the NO<sub>x</sub> emission to a great extent. As the results of this, the air pollution of India will reduce and Indian cities



shall be eliminated from the list of most polluted cities in world. Before 50 years, India was the one of the country

with good air quality, as per my research we can make it again.

## Bibliography

- [1] ABD-ALLA, G.H., Using exhaust gas recirculation in internal combustion engines: a review, *Energy Conversion and Management*. **43**, 2002.
- [2] ALGER, T. Clean-and-cool: cooled EGR improves fuel economy and emissions in gasoline engines. *Technology Today*. Summer 2010.
- [3] Arduino and coding, [www.arduino.cc](http://www.arduino.cc)
- [4] DUTTON, J.A., Products of combustion, energy conservation and environmental protection, [www.e-education.psu.edu/egge102/node/1951](http://www.e-education.psu.edu/egge102/node/1951).
- [5] European Union emission inventory report 1990-2016, [www.eea.europa.eu/publications/european-union-emission-inventory-report-1](http://www.eea.europa.eu/publications/european-union-emission-inventory-report-1).
- [6] Exhaust gas mass flow sensor for applications in commercial Diesel engines: the system for optimizing the emission characteristics. *Kolbenschmidt Pierburg Group*. [www.powerparts.it/eger\\_valves.pdf](http://www.powerparts.it/eger_valves.pdf)
- [7] GAMBLE, E., TERRELL, D., DEFRANCESCO, R. Nozzle selection and design criteria. 40th AIAA/ASME/SAE/ASEE Joint Propulsion Conference and Exhibit Fort Lauderdale. 2004, DOI:10.2514/6.2004-3923. [arc.aiaa.org/doi/10.2514/6.2004-3923](http://arc.aiaa.org/doi/10.2514/6.2004-3923).
- [8] GHUDE, S.D., PFISTER, G.G., JENA, C.K. et al. Satellite constraints of nitrogen oxide (NO<sub>x</sub>) emissions from India based on OMI observations and WRF-Chem simulations. *Geophysical Research Letters*. 2013, **40**, 423-428, DOI: 10.1029/2012GL053926.
- [9] GRISSO, R., HIPKINS, P., SHAWN, D. et al. Nozzles: selection and sizing. Virginia Cooperative Extension. Publication 442-032. 2013.
- [10] GUTTIKUNDA, S.K., MOHAN, D., Re-fueling road transport for better air quality in India. *Energy Policy*. 2014, **68**, 556-561, DOI: 10.1016/j.enpol.2013.12.067.
- [11] KECH, J., SCHMIDT, G., PHILIPP, G. et al. Exhaust gas recirculation: internal engine technology for reducing nitrogen oxide emissions. *Engine technology*, [www.mtu-online.com](http://www.mtu-online.com).
- [12] Nitrous Oxide Cycle Diagram, [www.airpollution411.blogspot.com](http://www.airpollution411.blogspot.com).
- [13] OO, T., OT, T., Effect of exhaust gas recirculation on performance of petrol engine. *Research&Reviews: Journal of Engineering and Technology*. 2017, **6**(2), 14-17.
- [14] Road Transport Year Book. Statics and details of vehicles registration in India <https://data.gov.in/catalog/road-transport-year-book-2013-14-and-2014-15>.
- [15] SHAHADAT, M.M.Z., NABI, M.N., AKHTER, M.S. et al. Combined effect of EGR and inlet air preheating on engine performance in Diesel engine. *International Energy Journal*. 2008, **9**, 109-116.
- [16] Survey and statics for air pollution & fatalities from World Health Organization, [www.who.int/airpollution/en/](http://www.who.int/airpollution/en/)
- [17] Types of EGR valves and sensors. [documents.tips/documents/hyundai-motor-company-new.html&www.egrsensors.com.au](http://documents.tips/documents/hyundai-motor-company-new.html&www.egrsensors.com.au)
- [18] WALKE, P.V., DESHPANDE, N.V., BODKHE, R.G. Impact of exhaust gas recirculation on the performances of Diesel engine. *Proceedings of the World Congress on Engineering*. 2008, **II**.
- [19] World's first estimation of long-term variations in global atmospheric pollutant emissions based on data assimilation. Nagoya University, 27.01.2017, [www.jamstec.go.jp/e/about/press\\_release/20170127](http://www.jamstec.go.jp/e/about/press_release/20170127).

Zbigniew J. Sroka, DSc., DEng. – Faculty of Mechanical Engineering, Wrocław University of Science and Technology.

e-mail: [Zbigniew.Sroka@pwr.edu.pl](mailto:Zbigniew.Sroka@pwr.edu.pl)



Wojciech Walkowiak, DEng. – Faculty of Mechanical Engineering, Wrocław University of Science and Technology.

e-mail: [Wojciech.Walkowiak@pwr.edu.pl](mailto:Wojciech.Walkowiak@pwr.edu.pl)



Marek Reksa, DEng. – Faculty of Mechanical Engineering, Wrocław University of Science and Technology.

e-mail: [Marek.Reksa@pwr.edu.pl](mailto:Marek.Reksa@pwr.edu.pl)



Czesław Kolanek, DEng. – Faculty of Mechanical Engineering, Wrocław University of Science and Technology.

e-mail: [Czeslaw.Kolanek@pwr.edu.pl](mailto:Czeslaw.Kolanek@pwr.edu.pl)



Chandu Valuvila Thulasidharan Pillai, MEng. – Faculty of Mechanical Engineering, Wrocław University of Science and Technology.

e-mail: [Chandu.T.Pillai@gmail.com](mailto:Chandu.T.Pillai@gmail.com)



Małgorzata PAWLAK

Andrzej MAJKA

Michał KUŹNIAR

Jowita PAWLUCZY

CE-2018-211

## Emission of selected exhaust compounds in jet engines of a jet aircraft in cruise phase

Nowadays, air transport is in an intense development phase. In order to optimize air communication and make it even more economical and environmentally friendly, attempts are made to undertake such activities as, e.g., SESAR project, which aims to develop and implement a modern ATM system. One of the parts of this project is the research on minimizing fuel consumption and emissions of pollutants in the engine exhausts. In the paper there is therefore presented the methodology for determining emission of those pollutants for the longest stage of the flight – the cruise phase. First, the value of the thrust required for the flight of an exemplary aircraft was determined, and then the values of the engines thrust and specific fuel consumption were computed. Additionally, it was necessary to determine the Emission Indexes (EI) of CO, NO<sub>x</sub>, HC and CO<sub>2</sub> for the cruise phase, based on known such indexes for the LTO. Total emissions of these pollutants for the mission adopted to conduct research – a 1000 km long cruise – were determined. These emissions were computed for the exemplary aircraft per one kilometre, as well as per one hour of flight for various cruising altitudes and flight speeds.

Key words: jet engine, emission, fuel consumption, cruise phase, ATM, SESAR

### 1. Introduction

Air transport is the most modern and the most dynamically developing branch of transport. Unfortunately, it also brings a negative impact on the natural environment and the population living in areas of high traffic intensity. This impact is mainly caused by the emission of noise and harmful substances, resulting from the combustion of fossil fuels by aircrafts engines.

The negative impact of air transport is the stronger the more intensive air traffic occurs in a given area. Europe is a unique region on Earth because of to the very high population density and high intensity of flights performed on its territory. In 2015, more than 9.9 million IFR operations were carried out in Europe and forecasts predict their growth by 16 percent by 2022 (Fig. 1) [3]. Currently, around 27,000 controlled flights take place in the European airspace every day. Europe is facing an airspace capacity crisis, as it is predicted that the number of flights will increase by as much as 50% in the next 10–20 years [3].

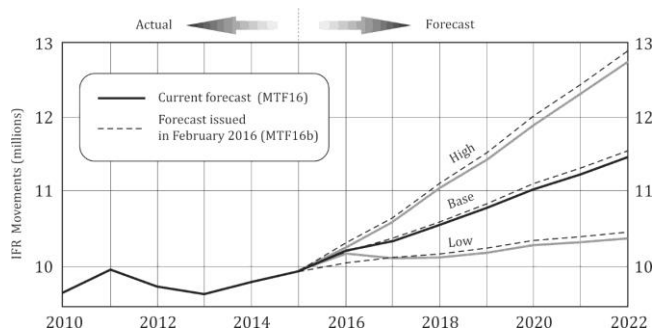


Fig. 1. A seven-year forecast for total Europe flight movements [3]

Historically, Europe consisted of a number of countries that did not create uniform political, economic or demographic systems. Along with the development of closer political and economic cooperation within the European Union, the efforts have been made to harmonize the rules of

Air Traffic Control (ATC) and Air Traffic Management (ATM), which has led to creation of a Single European Sky (SES) over Europe. Despite those activities, the ATC and ATM systems in Europe are fragmented and dominated by local ANSP (Air Navigation Service Providers) that have a monopoly for the running the ATC and ATM services. The border division of the airspace has made the European ATC and ATM system a kind of a mosaic of national ATC and ATM systems [9, 10, 11, 15].

The answer to these problems was the launch of the SESAR program (Single European Sky ATM Research), which is a technological pillar of the SES. The aim of this program is to improve ATM system performance by its modernising and harmonising in order to increase the capacity of the ATM network to cope with the ever-increasing number of flight operations while improving economic and security indicators [2, 14].

The current level of technical development of ATC and ATM systems has created the possibility of implementing a new way of flight planning method, leading to the abandonment of airways (Airways, AWY), and using only Waypoints (WP) to define the flight path. The airspace in the area where it will be possible to plan such a route is called the Free Route Airspace (FRA) [4]. The FRA concept will enable to match the path to aircraft performance better by optimising and minimising the differences between planned and operationally performed paths. It will also allow to improve the predictability of air traffic, which will reduce delays and consequently increase airspace capacity and improve air traffic efficiency indicators. The Polish Air Navigation Services Agency (PANSa) plans to launch the FRA airspace called POLFRA in the Polish airspace (FIR Warsaw) on February 28<sup>th</sup>, 2019 [12].

Preparing an appropriate flight plan has always been a difficult and demanding task due to the complexity of the airspace and the need to take into account the conditions and restrictions of different types. Path optimization is desirable and constitutes an added value. Currently, there

are few companies on the market that have been involved in the development of computer flight planning systems (CFSPs) to meet the demand of airlines and other commercial users. However, CFSP systems are not widely available, mainly due to the high cost of their purchase. Therefore, there is a need to develop a simpler, widely available flight planning system, dedicated for non-commercial users (General Aviation, GA) and small commercial companies (Business Aviation, BA) as well as for flight planning of unmanned systems (Remotely Piloted Aircraft Systems, RPAS) [2, 14].

An essential part of the newly developed CFSP system will be the algorithm that can find the optimal path for an aircraft in the FRA for the given optimization criterion, taking into account the required restrictions and flight conditions.

The proper work of the algorithm will be possible if the proper set of input data and calculation models are available. Till today, the following minimum set of computational models has been identified: airspace model, trajectory model, aircraft model and model of the surrounding environment.

Currently there are no consistent models defining the emission of harmful substances in the aircrafts engines exhausts during the whole flight. There are relatively well-developed models that are capable of determining the emission of the aircraft in the take-off and landing phases (LTO). But there are no advanced models available for the full flight phase, which could be a standard. The need to determine flight paths characterized by the minimum emission of pollutants in the exhausts requires precise determination of aircraft emissions in all phases of the flight.

## 2. Problem statement and research methodology

In this paper the method of determination of harmful compounds present in exhaust gases emitted by a passenger aircraft engines is described – the proposed computational method is universal, i.e. it can be used for any jet communication and transport aircraft, if suitable technical data is available. The solution to the problem is illustrated on the example of the Gulfstream IV (Rolls-Royce Tay 611C) business jet aircraft.

The flight consists of 9 main successive stages:

- 1) taxi-out – means controlled movement of the aircraft on the apron, using its own propulsion, between the stopping point and the point from which the take-off will take place.
- 2) start – is the flight phase in which the airplane moves from the point of run-up on the runway and rises into the air.
- 3) departure from the airport and climb – includes the climb of the aircraft after take-off to the contractual moment when the aircraft reaches the altitude of 915 m (3000 ft).
- 4) climb-out to the cruising altitude – is the phase of the flight, during which the aircraft climbs from 915 m to a fixed cruising altitude.
- 5) cruise – takes place between the stages of ascent and descent and is usually the longest stage of the journey. It ends when the plane approaches the destination, and the descent phase begins, and the plane prepares to

land. During a cruise phase, for operational reasons or Air Traffic Control (ATC), planes can climb or descend from one flight level to a higher or a lower one. During very long flights, aircrafts are able to fly higher with the lower thrust required for flight, when the weight of fuel on board decreases. Usually, pilots ask ATC to allow them to fly at the optimum flight level for the aircraft they operate. This optimal level of flight depends, for example, on the type of aircraft, its operating mass and flight length. ATC generally accepts this request if it does not compromise safety. For most commercial passenger airplanes, most of the fuel is used in this phase of the flight.

- 6) descent – is the flight stage during which the airplane decreases its altitude during preparations to landing and is the opposite of the climb phase. Like climb, descent can be continuous or graduated for operational reasons or ATC; the continuous descent is the most fuel-efficient option. This phase lasts until the aircraft reaches a height of 915 m.
- 7) approach to landing – is the final stage of the approach to the landing of the aircraft, occurs when the aircraft descends below 915 m and is in line with the runway and approaches the landing.
- 8) landing at the destination airport – is the flight stage when the plane returns to earth and continues until the plane is at the point where taxiing begins.
- 9) taxi-in – covers the movement of the aircraft on the ground, using its own propulsion, which takes place from the moment when the aircraft ends the run-out and runs to the stopping place from the runway and switches off the engines.

In the research, the Landing and Take-off Operations (LTO) were omitted, and the main attention was paid to the cruise stage. For the flight at a certain altitude and with certain velocity, the aircraft has a certain thrust requirements. This thrust depends on the altitude and velocity of the aircraft, its mass, aerodynamic parameters and lifting surface. The method of determining the thrust required for the flight was taken from [5]. The ambient parameters ( $T, p, \rho$ ) at a given altitude  $H$  can be computed from the dependences for the International Standard Atmosphere (ISA), where:

$$T = T_0 \cdot \left(1 - \frac{H}{44300}\right) \quad (1)$$

$$p = p_0 \cdot \left(1 - \frac{H}{44300}\right)^{5.356} \quad (2)$$

$$\rho = \frac{p_0}{T_0 \cdot R} \quad (3)$$

where:  $T_0, p_0$  – temperature and ambient pressure at the level of  $H = 0$  [m] for the ISA ( $T_0 = 288.15$  [K] and  $p_0 = 101325$  [Pa]),  $R$  – individual gas constant for air ( $R = 287.2$  [J/(kg·K)]),  $\rho$  – air density [kg/m<sup>3</sup>].

In the next step, the lift coefficient for the known flight velocity is determined:

$$C_z = \frac{2 \cdot Q}{v^2 \cdot \rho \cdot S} \quad (4)$$

where:  $Q$  – aircraft weight determined from the formula:

$$Q = m \cdot g \quad (5)$$

$m$  – mass of the plane [kg],  $g$  – acceleration of gravity [ $\text{m/s}^2$ ],  $V$  – flight velocity [ $\text{m/s}$ ],  $S$  – lifting surface [ $\text{m}^2$ ],  $C_z$  – lift coefficient [-].

Then, the drag coefficient is determined:

$$C_x = 0.015 + 0.08 \cdot C_z^2 \quad (6)$$

With the coefficients  $C_z$  and  $C_x$ , it is possible to determine the approximate value of power and thrust required for the flight:

$$P_n = \frac{C_x}{C_z} \cdot Q \cdot V \quad (7)$$

$$P_n = \frac{N_n}{V} \quad (8)$$

where:  $P_n$  – thrust required for the flight [N],  $N_n$  – power required for the flight [W].

For the described methodology of computations and formulas given above the technical data of the Gulfstream IV aircraft was used and the results of the calculations are presented in the further part of the work. The following chart (Fig. 2) shows the thrust required for the flight as a function of the flight velocity [Ma] determined for the Gulfstream IV aircraft (for the altitude of 11,000 m).

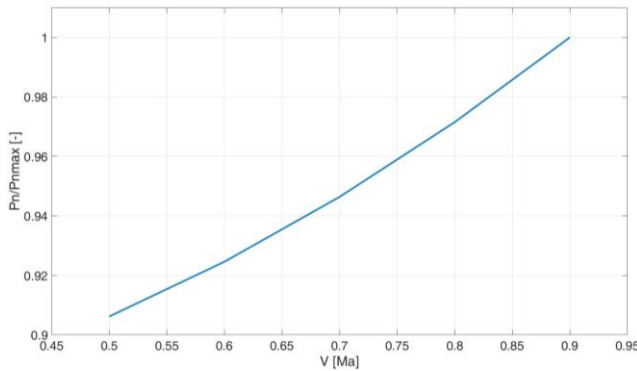


Fig. 2. Thrust required for the flight as a function of the flight velocity [Ma] determined for the Gulfstream IV aircraft (for the altitude of 11,000 m)

The range of engine run is selected in such a way to ensure a safe value of thrust for the flight. On the basis of the speed and altitude characteristics of the jet engine, the specific fuel consumption corresponding to a given thrust value can be given. These characteristics are determined experimentally (test bed aircrafts) or approximated in an analytical (computational) way.

Based on the available literature – manuals, engine catalogues, websites (e.g. [8]), the engine performance in the phase of LTO operation on the ground was read (Table 1). At the selected points, the thrust and the corresponding SFC were read and then a function between these points was approximated using a program written in the Matlab environment. The ground (rotational) characteristics of the engine was obtained, i.e. thrust and SFC as a function of rotations of the high pressure rotor. These characteristics are determined experimentally on the test benches (which are most often used and thus the analysis was based on such data) or by tedious and labour-intensive gas-dynamic com-

putations, which give the results with an accuracy of up to  $\pm 10\%$  in relation to the actual engine run.

The methodology developed by the authors of the paper can be used to determine the engine thrust and SFC during the flight. The correct determination of engine performance during the flight is very important when determining the emission of pollutants in the engine exhausts, it is however often treated in a vague or imprecise way in some articles.

To determine the speed-altitude characteristics of the engine based on its rotational characteristics, it is necessary to reduce the engine performance parameters at ground level. The formula for the engine thrust is as follows [1]:

$$K = m' \cdot c_5 - \dot{m} \cdot V \quad (9)$$

where:  $m'$  – exhausts mass flow [ $\text{kg/s}$ ],  $\dot{m}$  – mass flow of the air intake by the engine [ $\text{kg/s}$ ],  $c_5$  – exhaust gas velocity in the nozzle [ $\text{m/s}$ ],  $V$  – aircraft flight velocity [ $\text{m/s}$ ].

For ground characteristics, where  $V = 0$  [ $\text{km/h}$ ] the thrust is described by the formula [1]:

$$K_0 = m' \cdot c_5 \quad (10)$$

The first thing to determine are the parameters of the environment at a given flight velocity and flight altitude. To determine total temperature and total pressure at a given flight altitude and velocity, there can be used the following formulas:

$$T_c = T_0 \cdot (1 + 0.2 \cdot \text{Ma}^2) \quad (11)$$

$$p_c = p_0 \cdot (1 + 0.2 \cdot \text{Ma}^2)^{3.5} \quad (12)$$

where:  $T_c$ ,  $p_c$  – total temperature [K] and total pressure (dynamic pressure and temperature) [Pa],  $T_0$ ,  $p_0$  – ambient temperature [K] and ambient pressure [Pa] at a given flight altitude (according to the ISA),  $\text{Ma}$  – velocity of the plane [in Mach].

Having the value of a thrust at sea level, it is possible to determine a thrust for a known flight altitude and flight velocity [1]:

$$K = K_0 \cdot \frac{p_c}{101325 [\text{Pa}]} - \dot{m}_c \cdot V \quad (13)$$

where:  $\dot{m}_c$  – reduced mass air flow, determined from the formula:

$$\dot{m}_c = \dot{m}_0 \cdot \left( \frac{101325 [\text{Pa}]}{p_c} \cdot \sqrt{\frac{T_c}{288.15 [\text{K}]}} \right)^{-1} \quad (14)$$

where:  $\dot{m}_0$  – mass flow at  $H = 0$  [m] and  $V = 0$  [m/s].

The specific fuel consumption can be computed from:

$$\text{SFC} = \text{SFC}_0 \cdot \sqrt{\frac{288.15 [\text{K}]}{T_c}} \quad (15)$$

where:  $\text{SFC}_0$  – specific fuel consumption [ $\text{kg}/(\text{N} \cdot \text{h})$ ] at  $H = 0$  [m] and  $V = 0$  [m/s].

The chart below (Fig. 3) shows the approximated speed and altitude characteristic of the Rolls-Royce Tay 611C jet engine determined at 11,000 m by the authors of this paper, applying the universal methodology described in the paper.



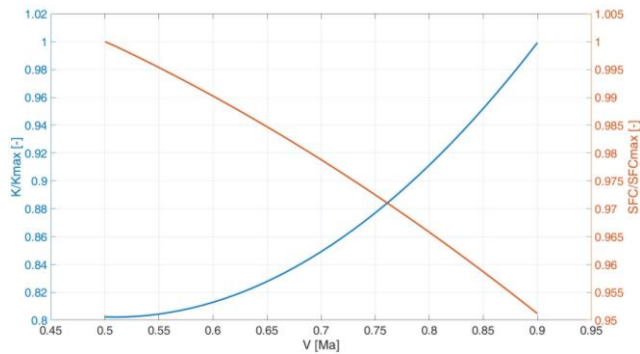


Fig. 3. Approximated speed and altitude characteristic of the Rolls-Royce Tay 611C jet engine (determined for the altitude of 11,000 m)

The next chart (Fig. 4) shows the thrust curve of the two Rolls-Royce engines and a curve of the thrust required for the flight. The range between these curves is the manoeuvring range (it is possible to make adjustments to the thrust of the engines and use a higher engine power for the flight).

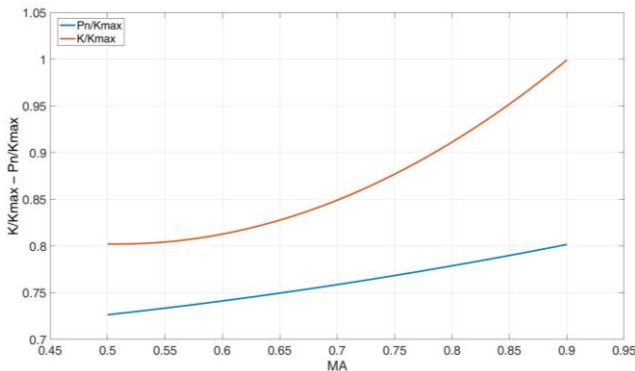


Fig. 4. A curve of thrust of two Rolls-Royce Tay 611C jet engines and a curve of the thrust required for the flight

Knowing the engines performance corresponding to the given flight stage, the emission of harmful compounds in exhausts of jet engines (e.g.  $\text{NO}_x$ , HC, CO) can be determined. To determine these emission, there can be used the following formulas:

$$E_{\text{CO}} = EI_{\text{CO}} \cdot 10^{-3} \cdot K \cdot \text{SFC} \cdot t \cdot l \quad (16)$$

$$E_{\text{NO}_x} = EI_{\text{NO}_x} \cdot 10^{-3} \cdot K \cdot \text{SFC} \cdot t \cdot l \quad (17)$$

$$E_{\text{HC}} = EI_{\text{HC}} \cdot 10^{-3} \cdot K \cdot \text{SFC} \cdot t \cdot l \quad (18)$$

where:  $E_{\text{CO}}/E_{\text{NO}_x}/E_{\text{HC}}$  – emission of particular compounds in exhausts [kg],  $EI_{\text{CO}}/EI_{\text{NO}_x}/EI_{\text{HC}}$  – emission factors for particular substances, depended on the type of engine and the range of its run [g/kg],  $K$  – engine thrust [N],  $\text{SFC}$  – specific fuel consumption [kg/(N·h)],  $t$  – engine run time at a given thrust [h],  $l$  – number of engines.

Due to the fact that the formation of some compounds ( $\text{CO}_2$ ,  $\text{H}_2\text{O}$  and  $\text{SO}_2$ ) as a result of fuel combustion by aircraft engines is directly proportional to the amount of fuel consumed, modelling emissions of these compounds requires only the knowledge of the fuel consumption and emission factors for a given fuel. The formula of the carbon dioxide emission [kg] is as follows:

$$E_{\text{CO}_2} = 3.15 \cdot K \cdot \text{SFC} \cdot t \cdot l \quad (19)$$

The problem in determination of emission during cruise stage is the lack of information concerning emission factors (EI) for toxic compounds in jet engine exhausts. These coefficients are determined experimentally for landing and take-off operations (LTO) and depend on the engine construction, as well as its load (range of cruising power). Engine power settings and times-in-mode for a given LTO cycle are specified by ICAO [6], as shown in Table 1.

Table 1. Engine power settings and times-in-mode for the LTO cycle specified by ICAO [6]

LTO cycle	Thrust range [%Foo*]	Cycle time [min]
Take-off (T/O)	100	0.7
Climb-out (C/O)	85	2.2
Approaching (App)	30	4.0
Taxi (Idle)	7	26

\*Foo – rated thrust

Each engine has different emission factors. The values of these emission factors can be found in the available ICAO databases. For example, for the Rolls Royce Tay 611C engine, EI of emitted pollutants for LTO determined for the engine power settings and times-in-mode, are shown in Table 2.

Table 2. Emission factors for RR Tay 611C

	T/O	C/O	App	Idle
$EI_{\text{NO}_x\text{LTO}}$ [g/kg]	9.93	9.79	5.23	1.08
$EI_{\text{HCLTO}}$ [g/kg]	0	0.67	16.0	96.67
$EI_{\text{COLTO}}$ [g/kg]	2.52	4.18	49.24	124.60

It is worth noticing that no EI coefficients are given for the remaining flight stages. The authors of the paper, based on the literature [7, 13], have determined these emission factors for a given moment of flight, i.e., for the engine thrust and external conditions affecting the engine run. Emission indexes corresponding to the appropriate range of engine run during the LTO cycle must be reduced taking into account the change in ambient pressure and ambient temperature due to higher altitude and flight velocity. These formulas for the reduced emission indexes are as follows [13]:

$$EI_{\text{CO}} = EI_{\text{COLTO}} \cdot \frac{\theta^{3.3}}{\delta^{1.02}} \quad (20)$$

$$EI_{\text{HC}} = EI_{\text{HCLTO}} \cdot \frac{\theta^{3.3}}{\delta^{1.02}} \quad (21)$$

$$EI_{\text{NO}_x} = EI_{\text{NO}_x\text{LTO}} \cdot \sqrt{\frac{\delta^{1.02}}{\theta^{3.3}}} \cdot e^h \quad (22)$$

where:  $EI_{\text{CO}}$ ,  $EI_{\text{HC}}$ ,  $EI_{\text{NO}_x}$  –  $\text{CO}$ ,  $\text{HC}$  and  $\text{NO}_x$  emission indexes at a given altitude [g/kg],  $EI_{\text{COLTO}}$ ,  $EI_{\text{HCLTO}}$ ,  $EI_{\text{NO}_x\text{LTO}}$  –  $\text{CO}$ ,  $\text{HC}$  and  $\text{NO}_x$  emission indexes measured for LTO parameters [g/kg],  $\theta$  – temperature change coefficient [-]:

$$\theta = \frac{T_c}{288.15 \text{ K}} \quad (23)$$

$\delta$  – pressure change coefficient [-]:

$$\delta = \frac{p_c}{101325 \text{ Pa}} \quad (24)$$

$e$  – Euler number ( $e = 2.72$ ),  $h$  – air humidity factor depended on the altitude [-],

$$h = -19 \cdot (\omega - 0.00634) \quad (25)$$

$\omega$  – specific humidity, where

$\omega = 10^{-3} \cdot e^{-0.0001426 \cdot (H-12900)}$  for ISA,

where  $H$  – is the cruising altitude given in feet.

In the last step, the obtained emission factors for the cruise phase should be substituted to the formulas (16)–(18). In this way, knowing the flight duration, there can be determined the emission of CO, HC and NO<sub>x</sub> for a given altitude and flight velocity, as well as the mean mass of the emitted pollutants at a given route section, e.g. 1 km, and mean emission intensity of a given pollutant, as shown in Tables 3 and 4.

### 3. Results and discussion

In Table 3 there are shown the obtained results of the average emission intensity [kg/h] of selected harmful compounds emitted in exhausts during the cruise phase on a route of 1000 km for the studied aircraft (Gulfstream IV) at known altitude and flight velocity.

It is worth noting that the presented methodology for determining the aircraft's performance and emission of pollutants in the exhausts of its engines is universal and can be used for any other jet aircraft.

Table 3. Emission intensity [in kg of CO, HC, NO<sub>x</sub>, CO<sub>2</sub> per 1 hour of flight]

Cruising altitude	Ma	$\dot{E}_{CO} \left[ \frac{\text{kg}}{\text{h}} \right]$	$\dot{E}_{HC} \left[ \frac{\text{kg}}{\text{h}} \right]$	$\dot{E}_{NOx} \left[ \frac{\text{kg}}{\text{h}} \right]$	$\dot{E}_{CO2} \left[ \frac{\text{kg}}{\text{h}} \right]$
9000 m	0.7	3.7750	0.4854	60.9380	5452
	0.8	3.8397	0.4937	62.6622	5586
	0.9	4.0309	0.5183	66.5783	5912
10,000 m	0.7	3.9646	0.5097	58.5721	5395
	0.8	4.0385	0.5192	60.3186	5536
	0.9	4.2509	0.5465	64.2582	5874
11,000 m	0.7	2.9772	0.2977	62.9360	5335
	0.8	3.0375	0.3037	64.9165	5483
	0.9	3.0876	0.3088	66.7853	5618

When considering changes in emission of the selected pollutants with regard to the changes of cruising velocity and cruising altitude, it can be noted that the higher the cruising velocity, the lower the CO<sub>2</sub> emission, which is caused by the lower fuel consumption.

At the cruising altitudes of 9 and 10 km, the engine works at a similar load, but gives different thrust values (with the increasing altitude the thrust decreases) at different emission factors. This results in lower NO<sub>x</sub> emission and higher CO and HC emission at 10 km compared to the one at 9 km. However, at the height of 11 km, the engine load increases, which leads to the change in EI, thrust and SFC values (as the altitude increases, the thrust decreases, the SFC increases but fuel consumption decreases). This in turn means that despite the reduction of CO<sub>2</sub> emissions (which results from the lower fuel consumption), as well as

the reduction of CO and HC emissions, the NO<sub>x</sub> emission increases.

It can also be noted that higher cruising velocity of the aircraft at a given cruising altitude results in higher emission intensity of all pollutants considered.

In Table 4 there are shown the obtained results of the average emission [kg/km] of selected harmful compounds emitted in exhausts during the cruise phase on a route of 1000 km for the studied aircraft (Gulfstream IV) at known altitude and flight velocity.

Table 4. Emission [in kg of CO, HC, NO<sub>x</sub>, CO<sub>2</sub> per 1 km of flight]

Cruising altitude	Ma	$E_{CO} \left[ \frac{\text{kg}}{\text{km}} \right]$	$E_{HC} \left[ \frac{\text{kg}}{\text{km}} \right]$	$E_{NOx} \left[ \frac{\text{kg}}{\text{km}} \right]$	$E_{CO2} \left[ \frac{\text{kg}}{\text{km}} \right]$
9000 m	0.7	0.004931927	0.000634161	0.079613715	7.122878538
	0.8	0.004389399	0.000564379	0.071633040	6.385702416
	0.9	0.004095975	0.000526667	0.067653135	6.007442843
10,000 m	0.7	0.005254596	0.000675546	0.077630213	7.150418042
	0.8	0.004683474	0.000602120	0.069951864	6.420134383
	0.9	0.004382041	0.000563360	0.066240571	6.055213450
11,000 m	0.7	0.004004727	0.000400446	0.084657232	7.176279599
	0.8	0.003575109	0.000357452	0.076406108	6.453439253
	0.9	0.003230290	0.000323071	0.069871705	5.877629314

Considering changes in emissions of tested pollutants depending on the change in cruising altitude, it can be noted that CO and HC emissions at 11 km reach lower values than those at 9 and 10 km. However, as the altitude increases, the engine load increases, which leads to an increase in NO<sub>x</sub> emissions. In turn, with the increase of cruising altitude, CO<sub>2</sub> emissions decrease, which is caused by lower fuel consumption.

It can also be noted that as the flight velocity increases, emissions per one kilometre of all harmful substances are reduced – flight velocity is of great importance. With the increase of cruising velocity, the time to cover the same route (e.g. 100 km) is significantly shortened.

The engine load increases by several percent in line with the increase of the cruising velocity (from 0.7 to 0.9 Ma) which, combined with the shorter flight time on a given route, means that the average emission per kilometre is lower.

### 4. Conclusions

The paper describes an effective method of determination of pollutants emitted in a passenger aircraft engines exhausts during the cruise phase. For the research purposes, the Gulfstream IV (Rolls-Royce Tay 611C) business jet aircraft was taken. However, this computational method is universal and can be used for any jet communication and transport aircraft (for which suitable technical data is available) in order to compute the emission of different pollutants in the exhausts of its engines, generated on a given route (in cruise phase).

The obtained results indicate that any change in the ambient conditions during engine operation (caused by a change in altitude and flight speed) significantly affects the emission of pollutants in the engine exhausts. It can be noticed that with the increase in cruising altitude, the emission of CO, HC and CO<sub>2</sub> decreases, while the NO<sub>x</sub> emission increases. However, when the same flight level is considered, there can be noticed that with the increase of the flight

speed, the emission of harmful compounds in the exhaust increases. The developed method can be used for similar analyses for other jet passenger aircrafts.

This project has received funding from the SESAR Joint Undertaking under the European Union's Horizon 2020 research and innovation programme under grant agreement No 734129.

## Bibliography

- [1] BALMORI, M.A. The effects of microwave radiation on the wildlife. Preliminary results, Valladolid (Spain), 2003.
- [2] BRUSOW, W., KLEPACKI, Z., MAJKA, A. Airports and facilities data base. *EPATS technical report*, Project no. ASA6-CT-2006-044549, 2007.
- [3] Clean Sky website, [www.cleansky.eu](http://www.cleansky.eu)
- [4] FISZDON, W. Flight mechanics (Mechanika lotu), PWN, Warszawa (in Polish). 1964.
- [5] Flightradar website, [www.flightradar24.com](http://www.flightradar24.com)
- [6] ICAO aircraft engine emission databank, [www.easa.europa.eu/easa-and-you/environment/icao-aircraft-engine-emissions-databank](http://www.easa.europa.eu/easa-and-you/environment/icao-aircraft-engine-emissions-databank)
- [7] International Civil Aviation Organization (ICAO), International Standards and Recommended Practices, Environmental Protection. Annex 16, Volume II Aircraft Engine Emissions (third edition), ICAO, July 2008.
- [8] IPCC, Revised 1996 Guidelines for National Greenhouse Gas Inventories, Volume 3, Greenhouse Gas Inventory Reference Manual, Intergovernmental Panel on Climate Change, WGI Technical Support Unit, Hadley Centre, Meteorological Office, Bracknell, UK, 1997.
- [9] KOPECKI, G., PĘCZKOWSKI, M., ROGALSKI, T. Przykładowy algorytm wyznaczania trasy przelotu w przestrzeni lotów swobodnych. *Autobusy*. 2017, 6.
- [10] Maps of meteorological conditions, [www.windy.com](http://www.windy.com)
- [11] SCHAEFER, M., BARTOSCH, S. Overview on fuel flow correlation methods for the calculation of NO<sub>x</sub>, CO and HC emissions and their implementation into aircraft performance software, *Interner Bericht Deutsches Zentrum für Luft- und Raumfahrt (DLR). Institut für Antriebstechnik*, Köln. 2013.
- [12] SESAR JU website, [www.sesarju.eu](http://www.sesarju.eu)
- [1] CICHOSZ, E., KORDZIŃSKI, W., ŁYŻWIŃSKI, M., SZCZECIŃSKI, S. Charakterystyka i zastosowanie napędów – napędy lotnicze. *Wydawnictwa Komunikacji i Łączności*, Warszawa 1980.
- [2] EUROCONTROL webpage, [www.eurocontrol.int](http://www.eurocontrol.int)
- [3] EUROCONTROL, Flight movements and service units 2016-2022, EUROCONTROL Seven-Year Forecast, European organisation for the Safety of Air Navigation, February 2016.
- [4] EUROCONTROL, Free route airspace developments. For a route-free European network, European Organisation for the Safety of Air Navigation, 2016.
- [5] FISZDON, W. Mechanika lotu, PWN, Warszawa, 1964.
- [6] ICAO, Convention on International Civil Aviation, Annex 16 : Environmental Aviation, Volume II: Aircraft Engine Emissions, International Civil Aviation Organization, Third Edition, July 2008.
- [7] ICAO emission databank, <https://www.easa.europa.eu/easa-and-you/environment/icao-aircraft-engine-emissions-databank>
- [8] Jet Engine specification database, [jet-engine.net](http://jet-engine.net)
- [9] KOPECKI, G., PĘCZKOWSKI, M., ROGALSKI, T. Przykładowy algorytm wyznaczania trasy przelotu w przestrzeni lotów swobodnych. *Autobusy*. 2017, 6.
- [10] KRZYŻANOWSKI, M. Conflict free and efficient flight routes planning in free route airspace. *Prace Naukowe Politechniki Warszawskiej*, Transport, z. 95, Warszawa 2013.
- [11] MALARSKI, M. Inżynieria ruchu lotniczego, *Oficyna Wydawnicza Politechniki Warszawskiej*, Warszawa 2006.
- [12] Polska Agencja Żeglugi Powietrznej, PAŻP webpage, [www.pansa.pl](http://www.pansa.pl)
- [13] SCHAEFER, M., BARTOSCH, S. Overview on fuel flow correlation methods for the calculation of NO<sub>x</sub>, CO and HC emissions and their implementation into aircraft performance software, *Interner Bericht Deutsches Zentrum für Luft- und Raumfahrt (DLR). Institut für Antriebstechnik*, Köln, 2013.
- [14] SESAR JU webpage, [www.sesarju.eu](http://www.sesarju.eu)
- [15] SKORUPSKI, J. Współczesne problemy inżynierii ruchu lotniczego. Modele i metody. Praca zbiorowa. *Oficyna Wydawnicza Politechniki Warszawskiej*, Warszawa 2014.

Małgorzata Pawlak, DEng. – Faculty of Navigation, Department of Ship Operation, Gdynia Maritime University.

e-mail: [M.Pawlak@wn.am.gdynia.pl](mailto:M.Pawlak@wn.am.gdynia.pl)



Andrzej Majka, DEng. – Faculty of Mechanical Engineering and Aeronautics, Rzeszow University of Technology.

e-mail: [Andrzej.Majka@prz.edu.pl](mailto:Andrzej.Majka@prz.edu.pl)



Michał Kuźniar, MEng. – Faculty of Mechanical Engineering and Aeronautics, Rzeszow University of Technology.

e-mail: [MKuzniar@prz.edu.pl](mailto:MKuzniar@prz.edu.pl)



Jowita Pawlucz, MEng. – Faculty of Mechanical Engineering and Aeronautics, Rzeszow University of Technology.

e-mail: [Jowita.Pawlucz@prz.edu.pl](mailto:Jowita.Pawlucz@prz.edu.pl)





# VIII INTERNATIONAL CONGRESS ON COMBUSTION ENGINES

POLISH SCIENTIFIC SOCIETY  
OF COMBUSTION ENGINES

**17<sup>th</sup>-18<sup>th</sup> June 2019**

## Invitation and call for papers

### DEADLINES

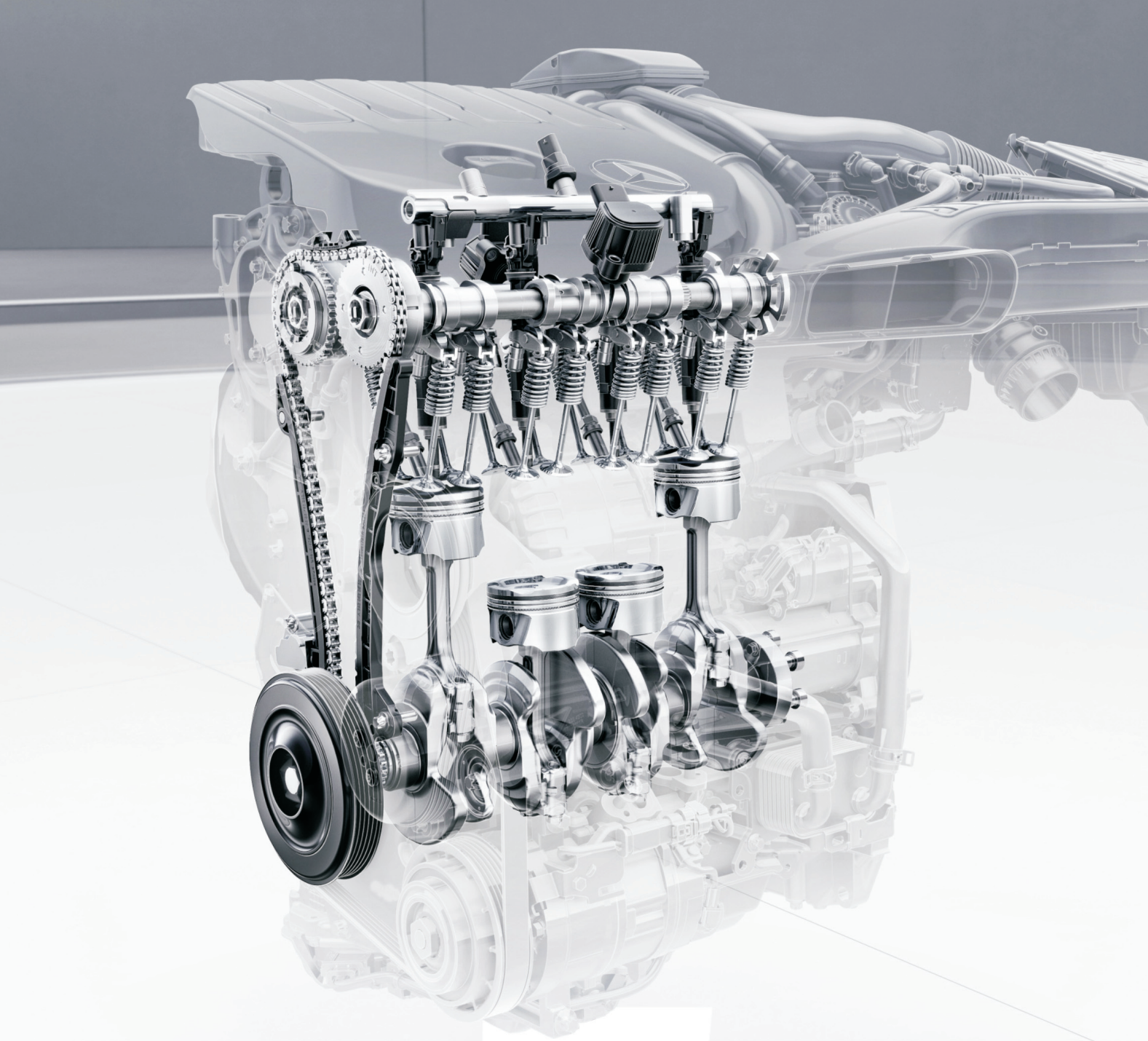
January 31, 2019	–	Abstract submission
February 15, 2019	–	Notification of abstract acceptance
March 31, 2019	–	Papers submission
April 30, 2019	–	Notification of paper acceptance
<b>June 17-18, 2019</b>	–	<b>CONGRESS PTNSS 2019</b>

**[www.congress.ptnss.pl](http://www.congress.ptnss.pl)**

**CRACOW University of Technology**

**31-155 CRACOW, Warszawska 24 street, POLAND**





**Publisher:**

**Polish  
Scientific  
Society  
of Combustion  
Engines**



**ISSN: 2300-9896**

# Combustion Engines

Polskie Towarzystwo Naukowe Silników Spalinowych



**[www.combustion-engines.eu](http://www.combustion-engines.eu)**